Patient-Derived Pancreatic Ductal Adenocarcinoma Organoids: A Strategy for Precision Medicine and Therapy Improvement

Dissertation

zur Erlangung des akademischen Grades

Doctor rerum naturalium

(Dr. rer. nat.)

vorgelegt

dem Bereich Mathematik und Naturwissenschaften

der Technischen Universität Dresden

von

Alexander Hennig

geboren am 09.04.1987 in Cottbus

Eingereicht am 29.04.2022

Diese Dissertation wurde im Zeitraum vom Dezember 2016 bis November 2021 in der Klinik und Poliklinik für Viszeral-, Thorax- und Gefäßchirurgie am Universitätsklinikum Carl Gustav Carus Dresden angefertigt

List of publications

CFTR Expression Analysis for Subtyping of Human Pancreatic Cancer Organoids.
Hennig A, Wolf L, Jahnke B, Polster H, Seidlitz T, Werner K, Aust DE, Hampe J, Distler M, Weitz J, Stange DE, Welsch T. *Stem Cells Int. 2019 May 2;2019:1024614. doi: 10.1155/2019/1024614. eCollection 2019.*

Detecting drug resistance in pancreatic cancer organoids guides optimized chemotherapy treatment.
Hennig A, Baenke F, Klimova A, Drukewitz S, Jahnke B, Brückmann S, Secci R, Winter C, Schmäche T, Seidlitz T, Bereuter JP, Polster H, Eckhardt L, Schneider SA, Brückner S, Schmelz R, Babatz J, Kahlert C, Distler M, Hampe J, Reichert M, Zeißig S, Folprecht G, Weitz J, Aust D, Welsch T, Stange DE. *Journal of Pathology*. *2022 April 3; doi: 10.1002/path.5906*

Implementing cell-free DNA of pancreatic cancer patient-derived organoids for personalized oncology.
Dantes Z, Yen HY, Pfarr N, Winter C, Steiger K, Muckenhuber A, **Hennig A**, Lange S, Engleitner T, Öllinger R, Maresch R, Orben F, Heid I, Kaissis G, Shi K, Topping G, Stögbauer F, Wirth M, Peschke K, Papargyriou A, Rezaee-Oghazi M, Feldmann K, Schäfer AP, Ranjan R, Lubeseder-Martellato C, Stange DE, Welsch T, Martignoni M, Ceyhan GO, Friess H, Herner A, Liotta L, Treiber M, von Figura G, Abdelhafez M, Klare P, Schlag C, Algül H, Siveke J, Braren R, Weirich G, Weichert W, Saur D, Rad R, Schmid RM, Schneider G, Reichert M. JCI *Insight. 2020 Aug 6;5(15):e137809. doi: 10.1172/jci.insight.137809.*

Universal and Efficient Electroporation Protocol for Genetic Engineering of Gastrointestinal Organoids.
Gaebler AM, **Hennig A**, Buczolich K, Weitz J, Welsch T, Stange DE, Pape K. *J Vis Exp. 2020 Feb 18;(156). doi: 10.3791/60704.*

Mouse Models of Human Gastric Cancer Subtypes with Stomach-Specific CreERT2-Mediated Pathway Alterations.
Seidlitz T, Chen YT, Uhlemann H, Schölch S, Kochall S, Merker SR, Klimova A, **Hennig A**, Schweitzer C, Pape K, Baretton GB, Welsch T, Aust DE, Weitz J, Koo BK, Stange DE. *Gastroenterology. 2019 Dec;157(6):1599-1614.e2. doi: 10.1053/j.gastro.2019.09.026. Epub 2019 Oct 1. PMID: 31585123*

Role of miR-203 in estrogen receptor-mediated signaling in the rat uterus and endometrial carcinoma.
Zierau O, Helle J, Schadyew S, Morgenroth Y, Bentler M, **Hennig A**, Chittur S, Tenniswood M, Kretzschmar G. *J Cell Biochem. 2018 Jul;119(7):5359-5372. doi: 10.1002/jcb.26675. Epub 2018 Mar 14. PMID: 29331043*

Table of Contents

List of Figures

List of Tables

List of Abbreviations

5-FU	5-Fluorouracil
ABC	ATP-binding cassette
ABEX	Aberrantly differentiated endocrine exocrine
ADM	Acinar-to-ductal metaplasia
ASC	Adult stem cells
ASCO	American Society of Clinical Oncology
AUC	Area under the curve
BER	Base excision repair
BMI	Body mass index
BR	Borderline
CAF	Cancer associated fibroblast
cDNA	Complementary DNA
CP	Chronic pancreatitis
CRISPR	Clustered regularly interspaced short palindromic repeats
CT	Computed tomography
ctDNA	Circulating cell free tumor DNA
CTx	Chemotherapy
ECM	Extracellular matrix
ECOG	Eastern Cooperative Oncology Group
EGFR	Epithelial growth factor receptor
EMT	Epithelial to mesenchymal transition
ESMO	European Society for Medical Oncology
EUS	Endoscopic ultrasonography
FGFR	Fibroblast growth factor receptor
FNA	Fine-needle aspiration
Gem/nab-Pac	Gemcitabine + nanoparticle albumin-bound paclitaxel
IPMN	Intraductal papillary mucinous neoplasms
LA PDAC	locally advanced pancreatic ductal adenocarcinoma
MET	Mesenchymal to epithelial transition

miRNA	MicroRNA
nab-Pac	Nanoparticle albumin-bound paclitaxel
neoCTx	Neoadjuvant chemotherapy
NF	Normalization factor
ORR	Objective response rate
OS	Overall survival
PanCa	Pancreatic cancer
PanIn	Pancreatic intraepithelial neoplasia
PDAC	Pancreatic ductal adenocarcinoma
PDO	Patient derived organoid
PFS	Progression free survival
PS	Performance status
PSC	Pancreatic stellate cell
QM	Quasi-mesenchymal
qRT-PCR	Quantitative real-time PCR
RDI	Relative dose intensity
RECIST	Response evaluation criteria in solid tumors
relAUC	Relative area under the curve
ROS	Reactive oxygen species
RQ	Relative quantity
RR	Relative risk
SDCC	Severely degenerative cancer cell
SMA	Superior mesenteric artery
SMV	Superior mesenteric vein
TIC	Tumor inducing cell
TRG	Tumor regression grade
UICC	Union for International Cancer Control

Gene and Protein Notations

The official nomenclature according to the Human Gene Nomenclature Committee was used for human gene and protein notations. Names of human genes were written in italic and capital letters. Human protein names were written in capital letters.

ACTB1b	Actin Beta
BRAF	V-Raf Murine Sarcoma Viral Oncogene Homolog B
BRCA1	Breast Cancer Type 1 Susceptibility Protein
BRCA2	Breast Cancer Type 2 Susceptibility Protein
CA19-9	Carbohydrate antigen 19-9
CDKN2A	Cyclin-dependent kinase inhibitor 2A
CFTR	Cystic Fibrosis Transmembrane Conductance Regulator
Deoxycytidine kinase	DCK
EGF	Epidermal Growth Factor
FGF10	Fibroblast growth factor 10
GAPDH	Glyceraldehyde 3-phosphate dehydrogenase
GPC1	Glypican 1
HER2/neu or ERBB2	Human epidermal growth factor receptor 2
HNF1A	Hepatocyte nuclear factor 1A
IGF-1	Insulin-like growth receptor 1
KRAS	Kirsten rat sarcoma viral oncogene homolog
KRT81	Cytokeratin-81
LGR5	Leucine-rich repeat containing G protein-coupled receptor 5
multidrug resistance protein	MRP
OPN	Osteoponin
PGE2	Prostaglandin E2
SMAD	Mothers against decapentaplegic homologue 4
TGFB	Transforming Growth Factor Beta-1 Proprotein
Timp-1	TIMP metallopeptidase inhibitor 1
TP53	Tumor suppressor protein 53

Introduction

6.1 The human pancreas – anatomy and function

The pancreas, an elongated and slender organ, weighs between 82 g and 117 g, and has an approximate size of 17-20 cm. It is located in the retroperitoneal space of the abdominal cavity and is connected to organs such as the stomach, omental bursa, transverse mesocolon, the left kidney, spleen and the duodenum[1].

The pancreas is structured into five parts: the head, uncinate process, neck, body and tail. The parts are not clearly delineated. The head, located against the C-shaped duodenum, is narrow to the superior mesenteric artery (SMA) and the superior mesenteric vein (SMV). Duodenal obstructions are observed in up to 25 % of all patients with pancreatic cancers located in the head[2]. The uncinate process extends towards the SMA posteriorly. The pancreas head and body are connected by the short pancreas neck, which contacts the SMA, SMV and hepatic portal vein. The body resembles the largest part of the pancreas and is associated with the aorta, SMA, renal vessels, splenic vein and artery as well as the common hepatic artery. The tail lies in close proximity to the splenic hilum and is connected to splenic vessels. The pancreas is adhered to multiple larger vessels which explains the low rate of resectable pancreatic tumors as surgical intervention is very limited when vessel infiltration by cancerous cells is observed.

The biological role of the pancreas serves as exocrine and endocrine gland which is unique in the human body. The exocrine function of the pancreas is the production of up to 1.5 l of pancreatic juice, a colorless and odorless alkaline liquid, every day. The pancreas juice mainly consists of digestive enzymes and bicarbonates. Acinar cells are synthesizing and secreting the digestive enzymes which are involved in sugar (amylase), protein (e.g. trypsin, chymotrypsin, aminopeptidase and elastase) and fatty acid (pancreatic lipase and phospholipase) digestion. The bicarbonates, produced by small ductal cells, neutralize the gastric acid entering the duodenum. Furthermore, ductal cells play a structural key role by forming small channels as well as the main pancreatic duct that transports the pancreatic juice to the duodenum after fusing with the bile duct. The endocrine function of the pancreas is maintained by pancreatic islets so called islets of Langerhans, which in turn contain alpha-, beta-, delta- and rare PP cells. PP cells are very few in number and secrete polypeptides which can inhibit gastrointestinal movement and the secretion of pancreatic juice. Specifically, alpha cells secrete glucagon, beta cells insulin and delta cells somatostatin.

6.2 Malignant diseases of the pancreas

6.2.1 Epidemiology, survival and risk factors of pancreatic cancer

With approximately 500.000 incidences in 2020, pancreatic cancer (PanCa) is the 14th most common malignant disease and accounts for 2.6% of all cancer cases globally. In parallel, PanCa was the cause for 466.000 mortalities in 2020, reflecting the poor prognosis of disease. PanCa is the seventh leading cause of cancer related deaths[3]. The 5-year survival rate is, among 46 cancer entities, the lowest (7%) in Europe[4]. It is predicted that PanCa will become the third leading cause of cancer associated deaths by 2025 in Europe, which might be explained by increasing rates of obesity, diabetes and alcohol consumption, as well as improved treatments in other cancer types such as breast cancer[5]. Patients presenting with early stage disease (only 10%) have a much higher 5-year survival rate of more than 30%. However, more than 50% of cases present with distant metastasis at time point of diagnosis which is associated with worse prognosis of 3% (American Cancer Society, www.cancer.net). As for nearly all solid tumors, the PanCa incidence increases with age resulting in a median age at diagnosis of 72 and 76 for men and woman respectively[3].

Several studies showed that smoking is the most important environmental risk factor for developing PanCa. The relative risk (RR) correlates with accumulated cigarette package years, duration and intensity of cigarette smoking and has been estimated to be elevated up to 3.06[6]. It is suspected that tobacco-specific carcinogens such as polycyclic aromatic hydrocarbons and N-nitroso compounds enter pancreatic tissue and promote the formation of PanCa[6]. Furthermore, 10-15 years of smoking cessation are necessary to lower the risk to the level of never-smokers. For obesity (BMI ≥ 30), RR values of 1.81 and 2.08 have been reported after analyzing data from 83.000 & 145.000 individuals, respectively[6,7]. Increased bodyweight is often associated with the development of an insulin resistance, which leads to an elevated secretion of insulin from beta-cells. Hyperinsulinemia, however, promotes cell proliferation of pancreatic cells through several mechanisms of action, e.g. binding to insulin-like growth receptor (IGF-1)[8]. Diabetes mellitus increase the risk of PanCa nearly by two-fold (RR = 1.94)[9], which also can be explained with disease associated increased levels of IGF-1 in pancreatic tissues. Consumption of animal fat, red meat, sugar and alcohol correlate with PanCa incidences, whilst the intake of folate, cereals, fiber and fruits showed a negative association to morbidity[10]. In spite of many studies, the role of diet is not fully understood whether it impacts PanCa incidence and morbidity. Recent studies also suggested that adipocytes in close proximity to pancreatic tissue can promote tumorigenesis by inducing inflammatory processes[11]. There is a genetic link that affects up to 10% of PanCa cases when at least one first-degree relative has been diagnosed with PanCa[12]. In addition, patients with chronic pancreatitis (CP) have an increased risk of PanCa development which has not been fully investigated. However, 1.1% of CP patients have been diagnosed with PanCa[13].

6.2.2 Pancreatic ductal adenocarcinoma

Within the malignant diseases of the pancreas, pancreatic ductal adenocarcinoma (PDAC) accounts for more than 90% of cases. Other malignant types that are not as common are neuroendocrine carcinoma, acinar carcinoma and pancreaticoblastoma[14].

6.2.2.1 Carcinogenesis of PDAC

The onset of PDAC cannot be explained to arise from a defined stem cell compared to other cancers of the gastrointestinal tract[15]. It is assumed, that acinar cells transdifferentiate to ductal cells, which gives them progenitor like cell properties to maintain pancreatic cell homeostasis. This process is termed as acinar-to-ductal metaplasia (ADM) and can be induced by inflammatory processes, tissue damage or other stress signals[16,17]. During ADM, acinar cells are exceedingly susceptible to activating mutations in proto-oncogenes such as the Kirsten rat sarcoma viral oncogene homolog (*KRAS*) gene. *KRAS* is mutated in more than 90% of all PDAC. Furthermore, 98% of all missense mutations in *KRAS* can be found at the three hot spots of glycin-12 (G12), glycin-13 (G13) and glutamine-61 (Q61), all of which lead to a constantly activated KRAS protein, promoting proliferation and inhibiting apoptosis[18]. In some cases, the altered allele is amplified which can drive tumorigenesis additionally. Due to the nearly universal presence of mutated *KRAS* in PDAC, it therefore can be concluded to be the initiating gene alteration of this disease. PDAC is also associated with pancreatic intraepithelial neoplasia (PanINs) and other non-invasive pre-neoplastic lesions such as intraductal papillary mucinous neoplasms (IPMNs)[19]. PanINs can be classified into three different stages depending on the degree of cellular and nuclear atypia. PanIN1 exhibit *KRAS* mutations in up to 40% of cases, but rarely other alterations, whilst PanIN3 frequently harbors additional alterations such as mutations in tumor suppressor protein 53 (*TP53*), cyclin-dependent kinase inhibitor 2A (*CDKN2A*) and mothers against decapentaplegic homologue 4 (*SMAD4*) lesions[20]. During carcinogenesis, PanIN and IPMN precursor lesions can give rise to PDAC by accumulating mutations which allow uncontrolled growth, survival advantages and other hallmarks of cancer (Figure 1)[21,22].

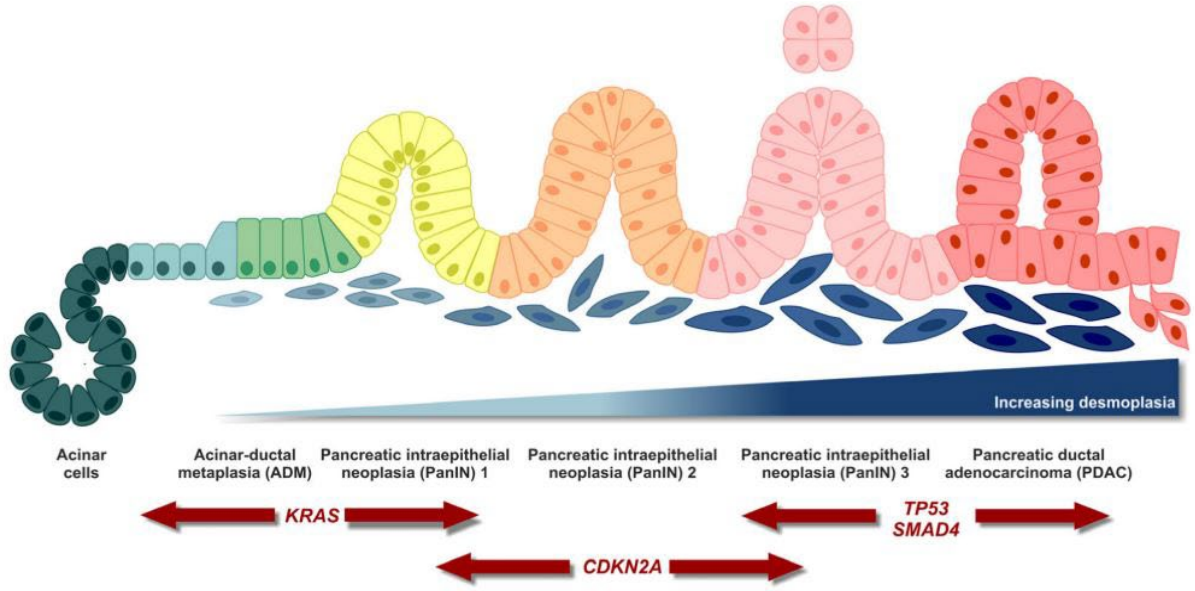

Figure 1 – Mutations in the *KRAS* gene are the initiating event during PDAC carcinogenesis. Constitutively active altered KRAS in acinar cells undergoing ADM can induce formation of PanIN1 lesions. Subsequently, acquisition of additional mutations in tumor suppressor genes such as *TP53*, *CDKN2A* or *SMAD4* support desmoplasia (grade 2 & 3 PanIN) and might result in the onset of PDAC. Modified from Orth et al.[15].

Common for PDAC is the frequent formation of metastasis at early stages of disease[23]. The underlying mechanism still needs to be discovered that contribute to the invasion of distant organs such as liver, lung, peritoneum and in rare cases also kidney and bladder, particularly since metastasis and primary tumors share genetically alterations to a very high extent[24]. It is thought that epithelial-to-mesenchymal transition (EMT) is a major driver of formation of distant metastasis, as well as mesenchymal to epithelial transition (MET)[25].

6.2.2.2 PDAC diagnosis and biomarkers

The diagnosis of PDAC is difficult due to the lack of specific symptoms or biomarkers at early stage. Most patients present with advanced PDAC and exhibit symptoms such as reduced appetite, indigestion, weight loss, exocrine pancreatic insufficiency, jaundice and dark urine. The majority of PDAC (~70%) is located in the head of the pancreas causing the afore mentioned symptoms[14], and frequently can result in biliary obstructions. Tumors in the corpus or tail are associated with more unspecific symptoms including back pain or abdominal pain. Imaging techniques such as computed tomography (CT) and endoscopic ultrasonography (EUS) are commonly used for PDAC visualization. Both techniques are essential for staging of disease by assessing vascular involvement and tumor size. EUS guided fine-needle aspiration (FNA) is often performed for histological confirmation of PDAC

disease. However, in many cases repeated sampling is necessary due to insufficient material for pathological assessment.

Carbohydrate antigen 19-9 (CA19-9) is clinically used as a tumor marker, as serum levels are increased in most symptomatic PDAC patients. The preoperative CA19-9 level is also a useful parameter for prognosis prediction[26]. Yet, CA19-9 screening tests for early PDAC detection are not recommended due to low sensitivity and specificity (79-81% and 82-90%). In addition, patients that lack the Lewis antigen A cannot produce CA19-9, which accounts for 10% of the Caucasian population, thereby negatively affecting the biomarker's sensitivity[27]. Patients with pancreatitis or mucinous cysts also show increased CA19-9 serum levels[28]. No reliable biomarker has been identified for early PDAC diagnosis yet. Several potential candidate biomarkers are currently under investigation including microRNAs (miRNAs), mucin 5AC or macrophage inhibitory cytokine 1 (MIC-1) serum levels, glypican 1 (GPC1) positive exosomes, circulating cell free tumor DNA (ctDNA) for detection of mutated *KRAS*, osteoponin (OPN) levels in combination with CA19-9 and TIMP metallopeptidase inhibitor 1 (TIMP-1)[29].

6.2.2.3 Tumor staging and grading

Tumor staging after PDAC diagnosis is essential for the choice of therapeutic intervention for the patient and the patients' prognosis. Staging according to the *Union internationale contre le cancer* (UICC) criteria is commonly used and is based on the TNM classification, which describes tumors by size (T), regional lymph node involvement (N) and the occurrence of distant metastasis (M). PDACs with a size of 2 cm in diameter or smaller are defined as T1 (T1a ≤ 0.5 cm; T1b = 0.5 – 1 cm; T1c = 1 – 2 cm), T2 tumors are greater than 2 cm but smaller than 4 cm and T3 tumors have a size greater than 4 cm. If the tumor infiltrated the coeliac axis, the AMS or the common hepatic artery it is defined as T4 regardless of tumor size. Infiltration of regional lymph nodes are specified as N0 (no lymph node involved), N1 (1-3 tumor positive lymph nodes) or N2 (more than 4 infiltrated lymph nodes). If distant metastasis are present, this is defined as M1, if not M0[30]. The combined consideration of all three parameters allows a UICC classification ranging from I to IV (Table 1).

Table 1 – The UICC TNM classification of PDAC. The TNM based classification is conducted based on the three tumor parameters of size (T), lymph node involvement (N) and the presence/absence of distant metastasis (M).

	M0			M1
	N0	N1	N2	
T1	IA	IIB	III	IV
T2	IB	IIB	III	IV
T3	IIA	IIB	III	IV
T4	III	III	III	IV

More than 50% of patients present with distant metastasis (UICC IV) which is associated with the dismal prognosis of less than 5% 5-year survival rate. In case of early disease diagnosis, which occurs in only 10-20% of PDAC patients, the 5-years survival rate is with 30-35% significantly higher [14].

The microscopic assessment of tumor tissue samples allows additional tumor grading, ranging from G1 to G3. Low grade PDAC (G1) exhibits well differentiated cells, which show slow growth and are unlikely to form distant metastasis. PDAC with a moderate grade (G2) have an abnormal cell morphology. The most aggressive type of PDAC is poorly differentiated (high-grade G3) and commonly forms metastasis. The grading of PDAC has prognostic value as G3 is associated with poor prognosis compared to G1[31].

6.2.2.4 Treatment

The therapeutic intervention in PDAC is very limited as surgical resection of the tumor is the only potential curative measure so far. The aim is to achieve resection with tumor free margins (R0) as it improves the prognosis significantly compared to resections with positive tumor margins (R1)[32]. However, surgical resection is only possible in about 20% of patients at time point of diagnosis, which can be explained with the silent progression of PDAC at early stages and the occurrence of symptoms at advanced stages of disease[33]. The indication of surgical resection is also not given, when PDAC tumors infiltrated major arteries (locally advanced pancreatic ductal adenocarcinoma; LA PDAC), which is observed in nearly 35% of all patients at the time of diagnosis[14,33,34]. A subgroup of patients present with borderline (BR) resectable disease can receive surgical although the tumor infiltrated vessels . A clear definition for BR PDAC does not exist, and the risk for R1 or R2 resections (macroscopically tumor infiltrated resection margins) is increased within this group of patients. In case of distant metastasis to more than one location and one metastasis, surgical intervention is also not recommended, which accounts for 50-55% of patients[35].

6.2.2.4.1 Systemic treatment of LA PADAC

Systemic chemotherapy is the standard of care to treat unresectable LA PDACs and in case of a good response to treatment by downsizing of the tumor burden, the PDAC might become resectable[33]. Administering gemcitabine as a single drug therapy was the treatment of choice for more than 10 years as it showed improved overall survival (OS) compared to 5-fluorouracil (5-FU) monotherapy (5.6 vs. 4.4 months, $p = 0.002$)[36]. Based on the results of the ACCORD11 study , gemcitabine was replaced as the standard of care measure by the multi-drug protocol FOLFIRINOX, a combination of 5-FU, leucovorin (folinic acid), irinotecan and oxaliplatin[37]. In this multicenter randomized phase 2/3 trial, patients with metastatic PDAC receiving FOLFIRINOX showed improved OS compared to the gemcitabine monotherapy cohort (11.1 vs. 6.8 moths, $p < 0.001$). Furthermore, progression free survival (PFS) was superior in the FOLFIRINOX group (6.4 vs. 3.3 months, $p < 0.001$) as well as the objective response rate (ORR; 31.6% vs. 9.4%, $p < 0.001$). Two years later, the results of the IMPACT trial, a randomized, multicenter, open-label, phase-3 study showed that the combination of gemcitabine and nanoparticle albumin-bound paclitaxel (nab-Pac) has superior efficacy compared to the gemcitabine monotherapy[38]. Gemcitabine plus nab-Pac (Gem/nab-Pac) was administered to patients with metastatic PDAC and increased OS significantly compared to patients treated with gemcitabine alone (8.5 vs. 6.7 months, $p < 0.001$). The 1-year survival rate (35% vs. 22%) and 2-year survival rate (9% vs. 4%) was improved as well as the PFS (5.5 vs. 3.7 months, $p < 0.001$). The ORR for Gem/nab-Pac was much higher compared to gemcitabine monotherapy (23% vs. 7%, $p < 0.001$). Both multi-drug regimens (FOLFIRINOX and Gem/nab-Pac) were successfully introduced in the palliative setting and current studies are evaluating patients benefits of drug combination protocols in the neoadjuvant setting.

The downside of increased efficacies of multidrug treatments are high rates of adverse events, which were observed for both treatments, FOLFIRINOX and Gem/nab-Pac[38,39]. According to a meta-analysis of 13 studies in which patients received FOLFIRINOX as first-line treatment, severe grade 3 or 4 side effects were observed in 60.4% of individuals[40]. The most frequent adverse events seen were neutropenia (19.6%), thrombocytopenia (5.9%), diarrhea (8.2%), vomiting (8.8%) and fatigue (11.7). The IMPACT trial reported grade 3 & 4 neutropenia in 153 out of 405 Gem/nab-Pac treated patients (38%), leukopenia in 31%, thrombocytopenia in 13% and anemia in 13% of cases. The most frequent non-hematologic grade 3 & 4 adverse event was fatigue (17%), peripheral neuropathy (17%) and diarrhea (6%). As a consequence, dose reduction, a delay in treatment cycles or a reduction of cycle number was often necessary resulting in a median relative dose intensity (RDI) of 81% for nab-pac and 75% for gemcitabine. Similar rates of treatment adaptation were necessary for the treatment with

FOLFIRINOX (RDI: 5-FU 82%, irinotecan 81% and oxaliplatin 78%)[39]. Of note, the consequences of RDI reduction on LA PDAC chemotherapy outcome has not been investigated yet.

Recommendations for choice of treatment with either FOLFIRINOX or Gem/nab-Pac vary between countries and their published guidelines such as the European Society for Medical Oncology (ESMO) or American Society of Clinical Oncology (ASCO). In general, co-morbidities and patients´ performance status (ECOG) are the main parameters to consider. FOLFIRINOX is mainly administered to relatively young patients with good ECOG, while Gem/nab-Pac or mono-therapies are often chosen for elderly. In accordance with that, a retrospective analysis of 167 LA PDAC patients treated with either FOLFIRINOX (n = 86) or Gem/nab-Pac (n = 81) showed significant differences in patient´s age (FOLFIRINOX = 54 years vs. Gem/nab-Pac = 65 years) and ECOG performance status (FOLFIRINOX ECOG: 0 83.7%, ECOG 1: 16.3%) vs. Gem/nab-Pac ECOG 0: 70.4%, ECOG 1: 29.6%)[41]. However, no significant differences were observed for OS, PFS and ORR. Adverse events occurred more frequently in the FOLFIRINOX group. The randomized phase 2 clinical SWOG-S1505 trial was performed in patients with resectable PDAC and showed no differences in OS between the cohorts treated with FOLFIRINOX or Gem/nab-Pac[42]. This underlines the importance to identify biomarkers that guide decision making in the systemic treatment of LA PDAC, which also accounts for adjuvant chemotherapy. Adjuvant chemotherapy, however, can only be administered to 50% of patients as many individuals suffer from a poor ECOG after surgical resection of the primary tumor[33]. RDI reduction is also often applied due to the onset of severe adverse events. Nevertheless, completion of adjuvant chemotherapy increases OS significantly[43,44]. It has been shown that completion rates of systemic chemotherapy are higher in the neoadjuvant setting (83-90% for FOLFIRINOX) and as a result many trials are currently investigating how neoadjuvant therapy can be improved[42,45]. Accordingly, BR PDAC patients benefit from neoadjuvant chemotherapy, as R0 resections with tumor free margins are significantly improved compared to surgery alone (82.4% vs. 33.3%, p = 0.01)[46]. R0 resection correlate with an improved survival in PDAC patients[47,48].

A poor response to the respective pre-surgery systemic treatment is not taken into account when choosing the adjuvant chemotherapy protocol.

6.2.2.5 Response assessment in PDAC after systemic chemotherapy

The Response Evaluation Criteria in Solid Tumors (RECIST) 1.0 and 1.1 have been used to assess the response of PDAC patients to systemic chemotherapy in clinical trials[49]. Using CT imaging, the single longest tumor diameter is measured and monitored during treatment. In clinical trials such as the aforementioned ACCORD-11 and IMPACT studies, reduction of tumor burden assessed by using RECIST

correlated well with ORR, OS and PFS. However, RECIST as a metric-based approach allows monitoring of distant PDAC metastasis but has limited value about the progression of the primary PDAC lesion. The underlying reasons for the poor visualization are the poor defined and irregular margins of PDAC resulting in a non-spherical shape, and the frequent involvement of adjacent large vessels, which makes the assessment of the tumor dimension particularly challenging[49]. In addition, in the event of good response to chemotherapy, PDAC might not show a reduction in tumor size due to the high degree of fibrosis. A retrospective study conducted by Ferrone and colleagues showed that imaging-based response prediction is not suitable in the neoadjuvant setting of LA PDAC patients treated with FOLFIRINOX[50]. In this trial, treatment outcome was assessed by CT imaging and response to FOLFIRINOX was seen in around 30% of patients. However, R0 resection was achieved in over 90% of neoadjuvant treated (neoCTx) patients, compared to 86% in the CTx naïve cohort. The authors concluded that new biomarkers are urgently needed to determine the individual LA PDAC patients´ response to systemic neoCTx.

After systemic neoadjuvant chemotherapy, the resection specimen retrieved during surgery gets evaluated by board certified pathologists to assess the R- and N-status, the tumor regression grade (TRG) and other histopathological parameters. Several TRG systems are in use all of which share the key feature of determining the amount of residual tumor tissue relative to the original tumor size or the degree of fibrosis or other regressive changes in the surrounding area[51]. The most common TRG systems are the following ones according to: Evans, White, CAP (college of American pathologists) and Le Scodan[52–55]. The evaluation of treatment response as described by Le Scodan and colleagues includes three groups of outcomes defined as minor- (TRG1), intermediate- (TRG2) and major response (TRG3). TRG1 is defined by the presence of more than 50% viable tumor cells or less than 50% of severely degenerative cancer cells (SDCCs), a type C pattern of nonviable cells within the tissue according to Ishikawa which describes a random distribution of dead tumor cells and the absence of complete necrosis[56]. The presence of 50-80% SDCCs, a type A and B distribution of nonviable cells (Ishikawa classification) and small areas of necrosis define TRG2. Characteristic for the histological type B pattern is a fibrous connective capsule with a high degree of SDCCs at the margin whilst cancer cells in the tumor core are not affected by the lesion. Fibrotic tissue is predominant in the type A pattern with only a few SDCCs detectable while non-affected cancers cells are absent. A major response (TRG3) to neoadjuvant chemotherapy is relatively rare and defined by a proportion of 80% or more of SDCCs, a type A pattern distribution of nonviable tumor cells and large areas of necrotic tissue.

A prediction of individual patients´ responses to neoCTx is not possible yet. In a retrospective study it has been shown, that reduction in CA19-9 serum level correlates with TRGs in the neoadjuvant

setting[57]. Molecular characterization of PDAC tumors might be a promising approach to stratify treatment and improve patient care.

6.2.2.6 Resistance to systemic chemotherapy in PDAC & LA PDAC

Reasons for the aggressiveness of PDAC is, despite the silent progression at early stages of disease, the resistance to chemotherapeutic substances. The underlying reasons for chemoresistance in PDAC are subject of current research. For gemcitabine, several mechanisms have been identified that reduce efficacy of treatment. One mechanism impacting the efficacy of gemcitabine is the expression of nucleoside transporters regulating the drug efflux. Overexpression of ATP-binding cassette (ABC) pumps mediate resistance to multiple chemotherapeutic drugs including gemcitabine. Drugs that specifically target these ABC transporters could bypass resistance to gemcitabine as early studies indicated[58]. Enzymes involved in the nucleoside metabolism are also associated with reduced response to gemcitabine treatment. An example is deoxycytidine kinase (dCK) which catalyzes the transformation of gemcitabine into its active form. Consequently, low levels of dCK correlate with a reduced OS of PDAC patients[59]. EMT has also been found to mediate drug resistance, although the underlying mechanism of action is unclear. The tumor microenvironment (TME) is another key factor promoting tolerance to gemcitabine. Pancreatic stellate cells (PSCs) and cancer associated fibroblasts (CAFs) which originate from PSCs can increase the chemoresistance in epithelial PDAC cells directly by changing the tumor cells physiology or indirectly by altering the TME which selects for aggressive and drug resistant transformed cells[60–62]. Other identified factors promoting gemcitabine resistance are tumor inducing cells (TICs), infiltrating macrophages and neutrophils, epigenetic factors and microvesicles[63].

No studies have been published yet identifying molecular mechanisms that are associated with resistance to nab-paclitaxel in PDAC[64]. Since taxanes are commonly used for treating other tumor entities, only general resistance mechanisms are known. ABC pumps play a key role, and alterations in the β-tubulin family members which reduces the ability of paclitaxel to stabilize microtubes[65].

Not much is known about 5-FU resistance although it has been used for more than 60 years as anti-cancer agent. In colon cancer cell lines, expression levels of thymidylate synthase correlate with 5-FU resistance. The lack of TP53, however, is associated with improved 5-FU efficacy[66].

The lack of studies revealing drug resistance in PDAC also accounts for irinotecan, which is also commonly used for the treatment of gastrointestinal cancers. As irinotecan targets topoisomerase I, mutations in the respective gene can lead to drug resistance[67]. Furthermore, the ATP-binding cassette gene multidrug resistance protein (MRP) is overexpressed in many colon tumors and actively promotes

irinotecan efflux. MRP overexpression has also been linked to oxaliplatin resistance in ovarian cancer cells[68]. Other oxaliplatin mediated resistance involved reduced drug uptake, decreased platinum accumulation in their DNA, which is linked to increased base excision repair (BER) and altered apoptosis programs[69–71].

Taken together, for most chemotherapeutic drugs commonly used in the treatment of LA PDAC the underlying mechanisms of drug resistances in PDAC are unknown.

6.2.3 Molecular subtypes of PDAC

For many cancer entities, it has been shown, that histopathological similar tumors can show differential responses to standard of care. Using next generation sequencing, substantial molecular differences between tumors of the same entities have been revealed, disrupting the ideology of organ-specific clinical management of cancer [72]. Nowadays, molecular subtyping of malignant diseases is a standard procedure for many tumor entities in the clinics. Assessment of the expression status of the human epidermal growth factor receptor 2 (HER2/neu or *ERBB2*) which is overexpressed in 20% of breast cancer is routinely performed and guides clinical decision making. Improved treatment outcome has been achieved in patients with HER2/neu positive tumors, when treated with monoclonal antibodies such as trastuzumab that binds to the HER2/neu receptor, causing an inhibition of tumor growth[73].

The main goal of molecular subtyping of PDAC tumors is to improve patient care and treatment by providing subtype specific therapies which has been shown for other cancer entities. Initially, subtyping of PDAC was sought by investigating single genetic alterations[74]. Genome wide sequencing of increasing numbers of PDAC revealed that the four genes *KRAS*, *TP53*, *SMAD4* and *CDKN2A* are mutated in more than 50% of cases, whilst most of the other detected mutations were found in less than 1% of individuals. As a result of that, subtyping in PDAC is rather challenging as biomarkers such as *ERBB2* amplifications, *BRAF* mutations or *BRCA1* and *BRCA2* mutations that have predictive properties to treatment outcome are rare[73–76]. A more promising approach is the analysis of patterns of genomic aberrations. Four different genome categories have been defined in PDAC: stable, scattered, locally rearranged and unstable genomes. Subtype specific therapies are potentially available for two out of the four categories. Tumors with locally rearranged genomes consist of large stretches of DNA that are more susceptible to amplifications of genes, such as *ERBB2* or *FGFR2*, for which targeted therapy agents are available. PDACs with unstable genomes are often characterized by loss of DNA damage response, which sensitizes them to platinum based chemotherapy or PARP inhibitor treatment[74,77].

In 2011, three new PDAC subtypes based on transcriptomic profiling were published by Collisson and colleagues. Microdissected epithelial tissue from resected tumors from CTX naïve patients was analyzed using hybridization based arrays[72]. Furthermore, expression data published earlier by Badea and colleagues were included in the analysis resulting in a gene signature of 62 genes which was termed as PDAssinger[72,78]. Based on expression data analysis according to the PDAssinger set, three molecular subtypes of PDAC have been defined: the quasi-mesenchymal (QM), exocrine-like and classical subtypes. Strikingly, these subtypes were independent predictors of OS and identified the QM subtype to be the one associated with the poorest prognosis, while the classical subtype showed the longest OS (Figure 2).

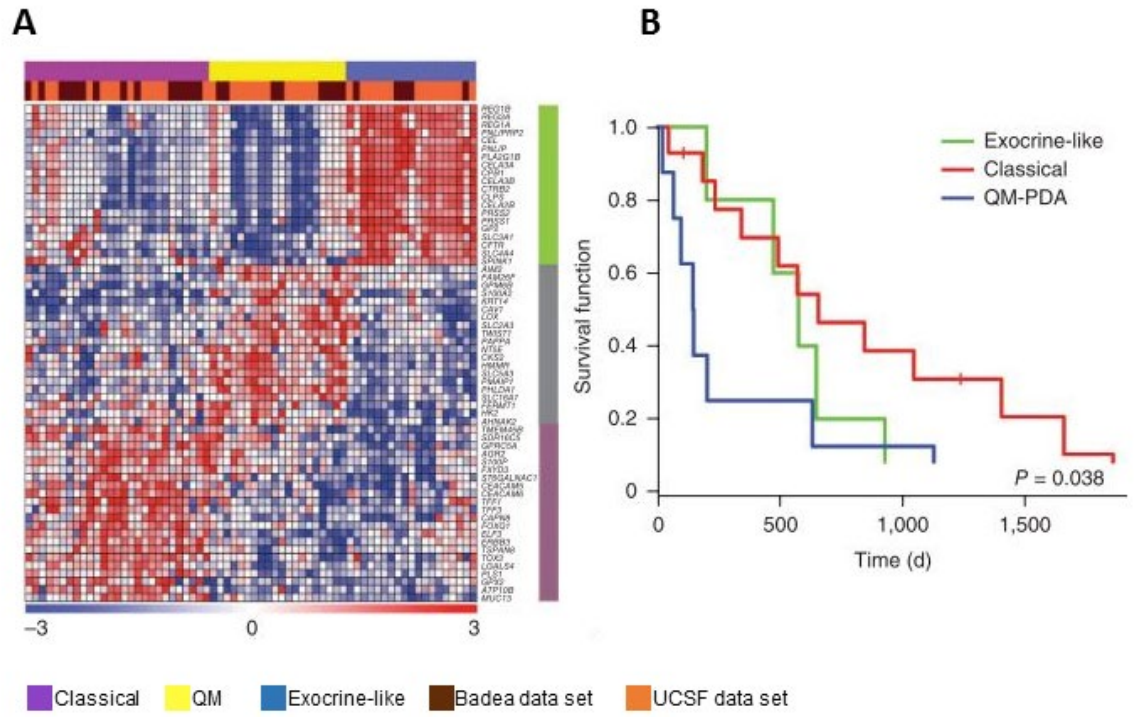

Figure 2 - Molecular subtyping of PDAC. A) The Heatmap illustrates the mRNA expression data sets from the University of California-San Francisco (UCSF), and Badea and colleagues [78] that have been merged using the distance-weighted discrimination method resulting in the identification of three subtypes of classical, quasi-mesenchymal (QM) and exocrine-like. The green, grey and violet bars on the side represent the PDAssinger genes that are upregulated in the exocrine-like, QM and classical subtype respectively. **B)** PDAC patients prognosis correlates with their respective subtype as depicted in the Kaplan-Meier diagram. Modified according to Collisson and colleagues[72].

A study by Moffitt and colleagues analyzed PDAC expression data using array technology and defined only two subtypes of basal-like and classical PDAC[79]. These subtypes overlap with the QM and classical subtype defined by Collisson. The absence of the third exocrine-like subtype was due to the algorithm that was used as transcripts of normal pancreatic tissue were subtracted in the expression analysis. As a result, Moffitt questions whether Collissons' exocrine-like subtype is a result of tissue contamination with normal pancreatic epithelia. A third study by Baily and colleagues defined four subtypes of PDAC based on transcriptome data: squamous, pancreatic progenitor, immunogenic and aberrantly differentiated endocrine exocrine (ADEX) subtypes[80]. These subtypes overlapped with the Collisson' data, except the immunogenic subtype. As Collisson and colleagues have only used microdissected tumor epithelia for their analysis, this may explain the absence of immune infiltrate if present as those are part of the stroma[74].

In 2016, Noll and colleagues reported that subtyping of PDAC according to Collisson is feasible using IHC staining of paraffin embedded tumor sections for cytokeratin-81 (KRT81) and hepatocyte nuclear factor 1A (HNF1A), which are both genes of the PDAssinger set[81]. The QM subtype was defined as $KRT^{+}/HNF1A^{-}$, the exocrine-like subtype as $KRT^{-}/HNF1A^{+}$ and the classical subtype as double negative for both markers ($KRT^{-}/HNF1A^{-}$). Noll also reported double positivity in 14 out of 231 immuno-stained PDACs, for which no subtype has been defined. Muckenhuber and colleagues improved the PDAC stratification by defining a cut-off value for KRT81 IHC staining. PDAC with less than 30% positivity for KRT81 was considered to be negative for the respective marker[82]. Subtyping was feasible in 86% to 99% of samples in three independently analyzed cohorts. As the prognostic value of PDAC subtyping has been shown by others[72,81], Muckenhuber also analyzed the predictive properties[82]. PDAC harboring the exocrine-like subtype ($KRT^{+}/HNF1A^{-}$) showed a significantly better response to FOLFIRINOX compared to patients treated with gemcitabine-based regimens of the same subtype. However, the improved response did not impact OS[82]. In the study of Collisson, a reduced response to gemcitabine treatment was seen in two- dimensional (2D) PDAC cell culture assays for samples which have been classified as QM, when compared to classical subtype cell lines[72]. Hence, the feasibility of subtype specific therapies are currently investigated in various prospective trials[14].

6.3 Patient –derived organoids as a three-dimensional cell culture system

Organoids constitute a three-dimensional self-organizing structure originated from stem cells. Compared to conventional 2D cell culture models, organoids harbor most differentiated cell types from the respective tissue they have been established from[83]. Stem cell types which can initiate organoids

are embryonic stem cells, induced pluripotent stem cells and adult stem cells (ASCs), which have been identified in nearly all mammalian organs. A single ASC can give rise to a new organoid culture, however in the context of precision medicine research it is more common to use ASC containing tissue units derived from biopsies or surgical resections to establish human patient derived organoids (PDOs). To maintain the stem cell and stem cell like properties in organoid cultures mimicking the organ specific stem cell niche via complex growth factor and inhibitor supplements is required. Furthermore, a laminin-rich extracellular matrix (ECM) is crucial to maintain the capability of self-organization of organoids[84]. The most used ECM for organoid cultivation is Matrigel, a gelatinous protein mixture secreted by Engelbreth-Holm-Swarm mouse sarcoma cells[85].

The first report of successful established PDO cultures derived from adult stem cells was published in 2009 by Sato and colleagues from the Hans Clevers group[86]. In his study, Sato generated PDOs from leucine-rich repeat containing G protein-coupled receptor 5 (Lgr5)-expressing single cells which have been shown previously to represent one population of adult stem cells in the intestine. Subsequently, the Hans Clevers lab developed protocols allowing the generation and long-term cultivation of stomach organoids derived from murine Lgr5 or Troy expressing adult stem cells[87,88]. Today, organoids can be generated from a vast variety of human tissues (Figure 3). The biggest hurdle in PDO generation is the identification of essential signaling pathways that need to be stimulated or inhibited by medium supplements for mimicking the organs specific adult stem cell niche.

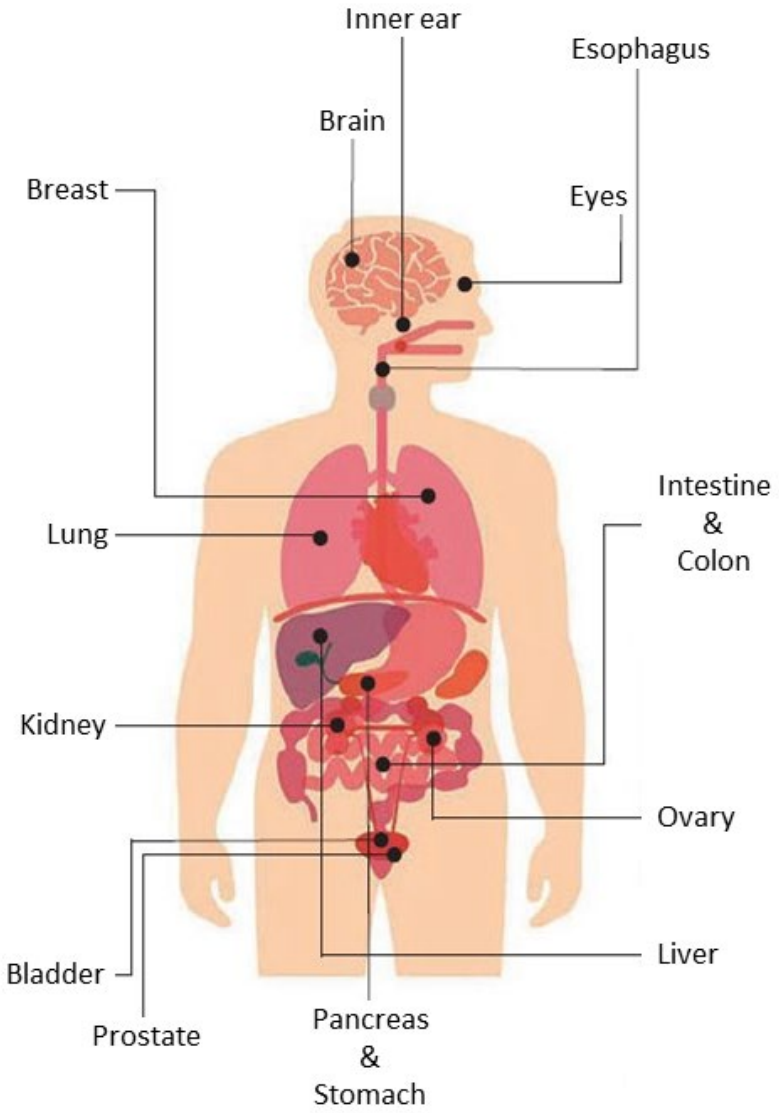

Figure 3 - Landscape of human tissue organoid models. Human epithelial tissues which can be used for PDO culture initiation. Modified from Artegiani *et al*[89].

6.3.1 Pancreatic ductal adenocarcinoma organoids

The first generation of murine pancreatic organoids was reported by Huch *et al.* in 2013[90]. Within two years, Boj and colleagues described the initiation of human pancreatic tissue and PDAC derived organoids[91]. In her study, Boj identified common known PDAC driver mutations in patient tissue derived PDAC organoids and defined the complex medium composition for long-term propagation of both, normal pancreatic and PDAC organoids. According to Boj and colleagues, PDAC organoids require the supplements of A83-01 and noggin as TGF-β signaling pathway inhibitors to prevent cell differentiation, as this would limit expansion of the cell culture, which is essential for long term cultivation. Addition of conditioned WNT3A and Rspondin medium on the other hand mediates and

maintains stem cell properties. The stimulation of the EGFR and FGFR signaling pathways using EGF and FGF10, as well as the inhibition of NOS with the help of nicotinamide also improves organoid growth. N-acetylcysteine as a medium supplement acts as a ROS scavenger and B27 increases organoid formation efficacy[92]. Within the scope of this study, N2 was added additionally to the PDAC PDO medium as Broutier and colleagues shown that it is highly efficient for the initiation of PDO cultures[93]. A protocol for long-term cultivation of normal pancreatic tissue derived organoids has been established by Georgakopoulos and colleagues and is feasible by the addition of prostaglandin E2 (PGE2) and the of TGFβ inhibitor Forskolin[94].

In spite of well characterized niche factors required for PDAC PDO growth, rates of successful outgrowth vary between the research groups that managed to establish biobank depositories. Boj and colleagues described take rates of 75% and 83%, however with low sample sizes of four and six respectively[91]. In 2018, Tiriac and colleagues from the Tuveson lab reported successful PDAC PDO outgrowth rates from surgical resection specimens of 78% (61/78) and 72% (43/60) for biopsy samples obtained using EUS FNA[95]. Similar PDAC PDO initiation rate were reported by Driehuis and colleagues (62% outgrowth rate, 52 out of 83 samples)[96]. Other groups went on further to achieved PDAC PDO generation using xenografts by successful transplanting human PDAC tissue specimens into mice[97].

6.3.2 Applications of patient derived organoids

PDOs present a promising *in vitro* model system for many research fields, such as disease modeling (Figure 4). In 2013, a PDO based assay has been established to predict cystic fibrosis patients´ response to CFTR modulators[98]. Within the same disease model system CRISPR/Cas9 technology has been used to repair CFTR mutations via homologous direct repair, resulting in a healthy phenotype[99]. Human intestinal PDOs also have been used to investigate the biology of SARS-CoV-2 and have proven to be a suitable model system for further research of this infectious disease[100]. Other infectious pathogens studied using the advanced cell culture models of organoids were for example *Helicobacter pylori*, *Escherichia coli*, *Vibrio cholera*, *Clostridium difficile* and *Shigella*[84,101,102]. First promising results in the field of regenerative medicine were achieved by Yui and colleagues, which succeeded to use *ex vivo* expanded murine colon organoids to repair tissue damage of the murine colon[103]. Research on the biology of cancer is one of the most prominent approaches PDOs were used for within the recent years, with focus on disease modeling, cancer evolution and the identification of novel targets for precision medicine (drug discovery)[95,104,105]. Tumor PDOs are also extensively used for patient treatment response prediction. For colorectal and breast cancers, a high correlation between individual patients´ response and PDO drug sensitivity has been shown[106,107]. However, for other cancers such as liver

cancer and PDAC prospective clinical trials are urgently needed to assess the predictive value of patient treatment outcome.

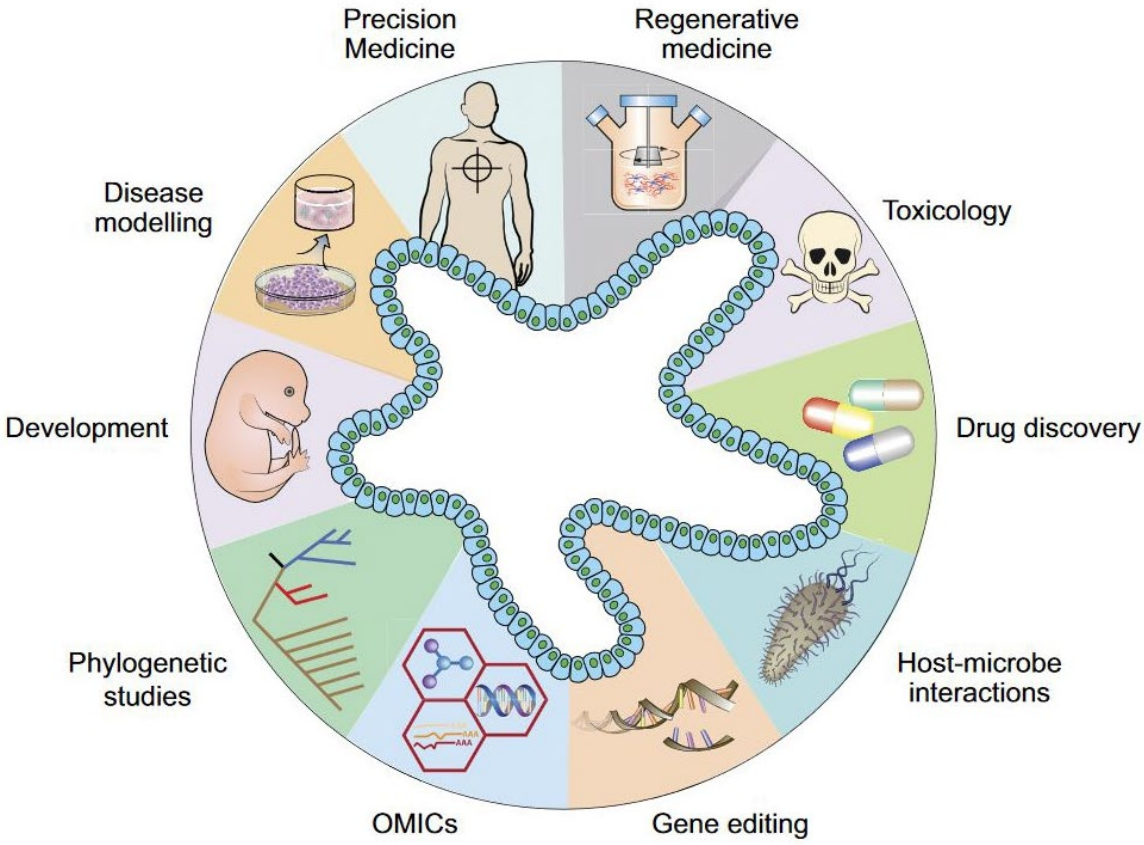

Figure 4 – Applications of PDOs in science. Illustrated in the diagram are the most common applications of PDOs such as regenerative medicine, toxicology, drug discovery, the biology of infectious diseases, gene editing via CRISPR/Cas technology, analysis of multi-omics data, phylogenetic studies, developmental biology, modeling of diseases and precision medicine. Source of image: Corro and colleagues [84].

6.4 The NeoResponse trial

6.4.1 Aim of study and design

The LA PDAC patients´ response to neoCTX is routinely assessed using CT imaging. However, it has been shown, that standard imaging is not suitable for treatment outcome validation as Ferrone and colleagues have shown[50]. In their study, response to FOLFIRINOX treatment in LA PDAC and BR PDAC patients was seen in 30% of cases using CT imaging technique. Yet, surgical resection was achieved in 90% of the individuals.

We therefore sought to identify new biomarkers that allow the response prediction of LA PDAC patients to systemic neoadjuvant chemotherapy. The design of the NeoResponse trial is based on using organoids derived from tumor specimens obtained by ENA FUS as a promising tool to address the unmet need of adequate response to therapy .

Patients with LA PDAC that fulfil the inclusion criteria of this clinical proof of concept trial will undergo an EUS guided FNA for histological confirmation of the malignant disease. This measure is mandatory for the initiation of the neoCTX and is carried out independently of the clinical trial. At this point, an additional biopsy is taken to obtain tissue for the establishment of PDAC organoids. In case of a successful outgrowth of patient PDOs, pharmacotyping of the clinically relevant combination therapies of FOLFIRINOX and Gem/Pac will be conducted, independent of which neoCTx protocol is administered to the patient. The response of the PDAC PDO will then compared to the patient' individual response to the treatment. Additional parameters such as PFS and OS will be included into the statistical analyzes.

Initially this non-randomized, non-blinded study with a pure explorative character was designed as mono centric trial. However, starting in April 2021 patients were recruited in the "Städtisches Krankenhaus Dresden Friedrichstadt" to increase the number of study patients.

6.4.2 Inclusion and exclusion criteria

The initial inclusion criteria for study enrollment is a high grade suspicion of a PDAC assessed using CT imaging. Patients were then considered for the trial if following conditions were met:

- Histopathological a locally advanced PDAC is confirmed which is unresectable or borderline resectable
- The staging happens to be cT3-4 cNx M0
- The non-presence of distant metastasis via CT imaging of the thorax and abdomen
- A systemic neoadjuvant therapy is planned
- There is no contraindication (e.g. pregnancy) for such a systemic neoadjuvant therapy
- The patient is older than 18 years
- The ECOG is ≤ 2
- The patient is able and willing to give written consent

Patients with PDAC recurrence after preceding complete/incomplete surgical resection of the tumor were not considered for this study. An additional exclusion criteria is any previously conducted systemic and/or targeted tumor therapy.

It was estimated that data from 40 evaluable patients is needed to finish this descriptive exploratory trial. Considering a take rate of 50% for PDO initiation and an additional dropout of 20% of patients after staging (e.g. due to detection of distant metastasis), 100 patients need to be recruited, which will take approximately 24 months. The overall duration of the study was planned for 36 months.

Aim of the study

Pancreatic cancer is the 14th most common malignant disease causing 466.000 deaths in 2020 worldwide. The prognosis remains poor as most of the patients present with advanced disease at the time of diagnosis, which is reasoned with the silent progression of disease at early stages. Surgical resection is the only potential curative measure. However, only 20% of patients can undergo surgery after diagnosis as in most cases the tumor already contacted or infiltrated adjacent major vessels, which makes an operation technically impossible. Neoadjuvant chemotherapy is the favored treatment as it might turn unresectable tumors into resectable ones. Yet, multi-drug neoCTx therapy is associated with severe side effects and dose reduction or treatment discontinuation is required with unknown impact on chemotherapy outcome. There is a clinical unmet need to identify novel biomarkers for response prediction and patient individual therapy optimization.

The questions to address in this thesis are:

I. Does RDI reduction of neoCTx treatment impact on the outcome of therapy?

II. Can we recapitulate the histopathological and molecular characteristics of PDAC tumours by using a living biobank of PDAC organoids from surgical resection specimens and EUS FNA biopsies? Is it possible to classify PDAC into different subtypes based on their histological and molecular characteristics?

III. Does pharmacotyping of PDAC organoids reveal the individual drug sensitivities and resistances from both, CTx naïve and neoCTx pretreated patient derived PDOs?

IV. Do human PDAC PDOs resemble a tool to predict the neoCTx response of individual patients treatment?

Taken together, this thesis will determine how PDAC patient derived tumor organoids might help improving the treatment of disease by assessing if optimal therapy options vary between individual PDAC patients.

Materials and Methods

8.1 Materials

8.1.1 Devices

Table 2 - Technical devices

Device	Name	Manufacturer
Analytical balance	CP124S	Sartorius AG, Göttingen, Germany
Centrifuge	MicroStar 17R	VWR, Darmstadt, Germany
	MiniStar	VWR, Darmstadt, Germany
	Centrifuge 5430	Eppendorf AG, Hamburg, Germany
	Biofuge PrimoR	Heraeus, Hanau, Germany
	Centrifuge 5810R	Eppendorf AG, Hamburg, Germany
	Rotanta 460R	Hettich, Tuttlich, Germany
Electrophoresis power supply	PowerPac 200	BIO RAD
Aspiration system	Vacuum suction system AZ 04	DITABIS AG, Pforzheim, Germany
Gel documentation system	Vilber Fusion Fx	Vilber, Collégien, France
Incubator	INCU-Line IL 53	VWR, Darmstadt, Germany
	Heracell 150i	Thermo Fisher Scientific, Waltham, US
	MCO-19 AIC(UV)	Sanyo, Osaka, Japan
Fluorescence microscope	LSM880 Laser Scanning Microscop	Carl-Zeiss AG, Oberkochen, Germany
Laminar flow hood	Herasafe KS	Thermo Fisher Scientific, Waltham, US
Liquid nitrogen tank	Biosafe MDβ	Thermo Fisher Scientific, Waltham, US
Magnetic mixer	IKA RTC basic	IKA-Werke GmbH, Staufen, Germany
Microscope	EVOS FL Auto	Life Technologies, Carlsbad, US
	Axiovert 40C	Carl-Zeiss AG, Oberkochen, Germany
Multimode microplate reader	Varioskan LUX	Thermo Fisher Scientific, Waltham, US
Microwave	MW802	Exquisit, Kaarst, Germany
PCR cycler	Mastercycler epgradient	Eppendorf AG, Hamburg, Germany

pH meter	FiveEasy plus	METTLER Toldeo, Columbus, US
Pipette controller	Easypet 3	Eppendorf AG, Hamburg, Germany
Precision balance	TE3102S	Sartorius AG, Göttingen, Germany
Quantitative Real Time PCR cycler	GeneAmp 5700 Step One Plus	Applied Biosystems, Waltham, US
Electrophoresis power supply	Powersource 250V	VWR, Darmstadt, Germany
Spectrophotometer	NanoVue Plus	GE Healthcare, Chicago, US
Thermomixer	Thermomixer Comfort	Eppendorf AG, Hamburg, Germany
Vortex mixer	ZX3 advanced vortex mixer	VELP Scientifica, Usmate Velate, Italy
	Classic vortex mixer	Fisher Scientific, Waltham, US
Water bath	VWB	VWR, Darmstadt, Germany
Multipette	Multipette E3	Eppendorf AG, Hamburg, Germany
Gel electrophoresis system (agarose gels)	EasyCast B2	Thermo Fisher Scientific, Waltham, US
Rocking table	CAT ST5	neoLab, Heidelberg, Germany
Thermomixer	Thermomixer C	Eppendorf AG, Hamburg, Germany
Automated nuclear acid extraction system	QIAcube	Qiagen, Hilden, Germany
Tissue embedding system	Leica EG1150H	Leica, Wetzlar, Germany
Microtome	Leica RM2265	Leica, Wetzlar, Germany

8.1.2 Additional material

Table 3 - Additional material

Material	Name	Manufacturer
48 well plates	48 well cell culture plate	Corning, New York, US
384 well plates	Cell culture micro plate, PS, F-bottom	Greiner Bio-One, Kremsmünster, Austria
Glass pipettes	glass Pasteur pipettes	Thermo Fisher Scientific, Waltham, US
Falcons 15/50 ml	Greiner 15/50 ml tubes	Greiner Bio-One, Kremsmünster, Austria

Microscope slide	Microscope slide	Engelbrecht Medizin und Labortechnik GmbH, Edermünde, Germany
Cover glasses	cover glasses 24x50 mm	Paul Marienfeld GmbH & Co. KG, Lauda-Königshofen, Germany
Scalpel	Carbon steel scalpel #10	Aesculap AG, Tuttingen, Germany
Freezing container	Mr. Frosty freezing container	Thermo Fisher Scientific, Waltham, US
Embedding cassettes	Biopsy embedding cassettes	Engelbrecht Medizin und Labortechnik GmbH, Edermünde, Germany

8.1.3 Commercial kits

Table 4 - Commercial kits and reagents

Application	**Name**	**Manufacturer**
RNA isolation	RNeasy Mini Kit	Qiagen, Hilden, Germany
genomic DNA isolation	QIAamp DNA Mini Kit	Qiagen, Hilden, Germany
cDNA synthesis	qScript cDNA Synthesis Kit	Quantabio, Gaithersburg, US
Cell viability reagent	PrestoBlue Cell Viability Reagent	Thermo Fisher Scientific, Waltham, US
Immunohistochemistry detection kit	Signal Stain Boost Detection Kit (Mouse&Rabbit)	Cell Signaling Technology, Danvers, US
qRT-PCR Mix	GoTaq pPCR Master Mix	Promega, Madison, US

8.1.4 Enzymes

Table 5 - Enzymes

Enzyme	**Manufacturer**
Collagenase II	Sigma-Aldrich, St. Louis, US
Dispase II	Roche, Basel, Swizz
Phusion High-Fidelity DNA Polymerase (2 U/µl)	Thermo Fisher Scientific, Waltham, US

8.1.5 Fine chemicals

Table 6 - Fine chemicals

Fine chemical	**Manufacturer**
Butanol (C_4H_9OH)	Clinic pharmacy, UKD
Ehtanol (C_2H_5OH)	VWR, Radnor, US
Formaldehyde (4%)	SAV Liquid Production GmbH, Flintsbach am Inn, Germany
Alcoholic 1% eosin solution	Clinic pharmacy, UKD
Surgipath Paraplast (Paraffin)	Leica, Wetzlar, Germany
Xylene	VWR, Radnor, US
Hematoxylin	Clin Tech, Guildford, UK
Hydrochloride acid (37%)	VWR, Radnor, US
Entellan	Merck, Darmstadt, Germany
Methanol (CH_3OH)	VWR, Radnor, US
Isopropanol (C_3H_8OH)	VWR, Radnor, US
Hydrogen peroxide, 30% (H_2O_2)	Merck, Darmstadt, Germany
Sodium citrate tribasic dihydrate	Sigma Aldrich, St. Louis, US
Sodium chloride (NaCl)	Carl Roth, Karlsruhe, Germany
Tris	Sigma Aldrich, St. Louis, US
TrisHCl (1 M)	Sigma Aldrich, St. Louis, US
Magnesium chloride ($MgCl_2$)	Carl Roth, Karlsruhe, Germany
Sodium hydroxide (NaOH)	Carl Roth, Karlsruhe, Germany
Mowiol	Carl Roth, Karlsruhe, Germany
dNTPs	Carl Roth, Karlsruhe, Germany
Dimethyl sulfoxide (DMSO)	WAK-Chemie GmbH, Bad Homburg, Germany
Ethylenediaminetetraacetic acid (EDTA)	Thermo Fisher Scientific, Waltham, US
Acetic acid	VWR, Radnor, US
Nonident P-40	US-Biological, Salem, US
Sodium deoxycholate	AppliChem, Darmstadt, Germany
Ultrapure distillated water (dH_2O)	Thermo Fisher Scientific, Waltham, US

8.1.6 Biochemicals

Table 7 - Biochemicals

Biochemical	Manufacturer
HEPES	Thermo Fisher Scientific, Waltham, US
Dulbecco's Modified Eagle Medium (DMEM): Nutrient mixture F12	Gibco, Thermo Fisher Scientific, Waltham, US
GlutaMAX	GE Healthcare, Chicago, US
Primocin	Invitrogen, Thermo Fisher Scientific, Waltham, US
Penicillin/streptomycin	Gibco, Thermo Fisher Scientific, Waltham, US
Dulbecco's 1x phosphate-buffered saline (1x DPBS)	Gibco, Thermo Fisher Scientific, Waltham, US and Sigma Aldrich, St. Louis, US
Matrigel (#356231)	Corning, New York, US
WNT3A	Conditioned medium, produced at AG Stange
Noggin	Conditioned medium, produced at AG Stange
Rspondin	Conditioned medium, produced at AG Stange
B27	Invitrogen, Thermo Fisher Scientific, Waltham, US and Sigma Aldrich, St. Louis, US
N2	Invitrogen, Thermo Fisher Scientific, Waltham, US and Sigma Aldrich, St. Louis, US
Gastrin	Sigma-Aldrich, St. Louis, US
recombinant murine epithelial growth factor (mEGF)	Invitrogen, Thermo Fisher Scientific, Waltham, US and Sigma Aldrich, St. Louis, US
recombinant human FGF10 (hFGF10)	PeproTech, Rocky Hill, US
Nicotinamide	Sigma-Aldrich, St. Louis, US
N-acetyl-L-cysteine	Sigma-Aldrich, St. Louis, US
A-83-01	Tocris Bioscience, Bristol, UK
Y-27862	Sigma-Aldrich, St. Louis, US
ACK lysing buffer	Gibco, Thermo Fisher Scientific, Waltham, US and Sigma Aldrich, St. Louis, US
Cell Recovery Solution	Corning, New York, US
Goat serum	Sigma-Aldrich, St. Louis, US
Bovine serum albumin (BSA)	Carl Roth, Karlsruhe, Germany
Tween20	SERVA, Heidelberg, Germany
Paraformaldehyde	Carl Roth, Karlsruhe, Germany
TritonX-100	Sigma-Aldrich, St. Louis, US
Irinotecan	EVER Pharma GmbH, Gröbenzell, Germany
Oxaliplatin (ELOXATIN)	Sanofi-Aventis Deutschland GmbH, Frankfurt a.M., Germany
5-FU (5-FU medac)	Medac, Gesellschaft für klinische Spezialpräparate mbH, Wedel, Germany

Gemcitabine	HEXAL AG, Holzkirchen, Germany
Paclitaxel (NeoTaxan)	HEXAL AG, Holzkirchen, Germany
Agarose	SERVA, Heidelberg, Germany
6x purple loading dye	New England Biolabs, Ipswich, US
GeneRuler 1kb plus DNA ladder	Thermo Fisher Scientific, Waltham, US
GelRed Nucleic Acid Stain (20,000x)	Biotium, Hayward, CA

8.1.7 Primary antibodies

Table 8 - Primary antibodies

Antibody	Purpose	Dilution	Blocking	**Manufacturer**
mouse-anti-CK19 mAB (BA16; ab20210)	IHC	IHC 1:100	5% goat block	Abcam, Cambridge, UK
mouse-anti-TP53 mAB (1C12; #2524)	IHC	IHC 1:200	5% goat block	Cell Signaling Technology, Danvers, US
mouse-anti-KRT81 mAB (36-Z; sc-100929)	IHC, IF	IHC 1:150 IF 1:50	5% goat block	Sana Cruz Biotechnology, Dallas, US
rabbit-anti-CFTR mAB (ab131553)	IHC, IF	IHC 1:300 IF 1:50	5% goat block	Cell Signaling Technology, Danvers, US

8.1.8 Secondary antibodies and fluorescent dyes

Table 9 - Secondary antibodies

Antibody/Dye	Purpose	Dilution	**Manufacturer**
DAPI	IF	1:2000	Sigma-Aldrich, St. Louis, US
Phalloidin Alexa Fluor 568	IF	1:100	Thermo Fisher Scientific, Waltham, US
Goat-anti-mouse Alexa Fluor 488	IF	1:200	Thermo Fisher Scientific, Waltham, US
Goat-anti-rabbit Alexa Fluor 488	IF	1:200	Thermo Fisher Scientific, Waltham, US

8.1.9 Nucleic acids

8.1.9.1 Polymerase chain reaction (PCR) primers

Table 10 - PCR primers

Primer name	Sequence (5’ – 3’)	Product size [bp]
h*KRAS*_Exon2_fwd	AGCGTCGATGGAGGAGTTTG	395
h*KRAS*_Exon2_rev	TGTATCAAAGAATGGTCCTGCAC	
h*KRAS*_Exon3_fwd	CCAGACTGTGTTTCTCCCTTC	286
h*KRAS*_Exon3_rev	TGCATGGCATTAGCAAAGAC	

8.1.9.2 Quantitative Real Time PCR (qRT-PCR) primers

Table 11 - qRT-PCR primers

Primer name	Sequence (5’ – 3’)	Product size [bp]
qPCR_h*GAPDH*_fwd	GCA CCA CCA ACT GCT TAG	166
qPCR_h*GAPDH*_rev	ATG ATG TTC TGG AGA GCC CC	
qPCR_h*ACTB1*_fwd	AAA TCT GGC ACC ACA CCT TC	185
qPCR_ h*ACTB1* _rev	AGA GGC GTA CAG GGA TAG CA	
qPCR_h*CFTR*_fwd	CAGCGCCTGGAATTGTCAG	102
qPCR_h*CFTR*_rev	TGAAGCCAGCTCTCTATCCC	
qPCR_h*HNF1a*_fwd	ACG ACG ATG GGG AAG ACT TC	139
qPCR_h*HNF1a*_rev	GAC TTG ACC ATC TTC GCC AC	
qPCR_h*KRT81*_fwd	CTACCTCCGCAAGTCAGACC	114
qPCR_h*KRT81*_rev	TCTGAGATGTGCGACTGGAG	

8.1.9.3 Software

Table 12 - Software

Software	Version	Developer
GraphPad Prism	Version 8.4	GraphPad Software, San Diego, US
Benchling	-	Benchling, San Francisco, US

8.2 Methods

8.2.1 PDAC Patient cohort

Medical data from patients diagnosed with resectable PDAC between 2016 and 2021 at the University Hospital Dresden have been used for retrospective analyses for the following parameters: patients' age, gender, tumor differentiation (grading), T-, R-, N- and CRM-status. In order to investigate the impact of dose- or cycle number reduction on patients´ response to neoCTx treatment (i.e. FOLFIRINOX or the Gem/nab-Pac), patients with LA PDAC that have been hospitalized at Dresden University Hospital between 2014 and 2021 were analyzed. Inclusion criteria were the availability of the following chemotherapeutic parameters: therapy agent, number of cycles administered, reduction of dose or termination of therapy if necessary, and the assessment of the tumor regression grade (TRG) by a broad certified pathologist. The TRG evaluation was done according to Le Scodan[52] using parameters such as the proportion of severely degenerative cancer cells (SDCCs) and necrotic areas in the resected tumor (Table 12). Only patients that received at least three 28 day-cycles of the Gem/nab-Pac or four 14 day-cycles of the FOLFIRINOX without reduction of doses were considered as "full course" treated. Any reduction in dosing or termination of measure was defined as "adapted" therapy. Patients treated with any other chemotherapy except FOLFIRINOX or Gem/Pac were excluded from the analysis. This was also applicable for patients that switched to the respective other treatment protocol later than cycle 1.

Table 12 - Tumor regression grade classification according to Le Scodan 2008

Tumor regression grade	Response to neoCTx	Proportion of SDCCs	Necrosis
TRG1	Minor	< 50%	absent
TRG2	Intermediate	50 – 80%	small spotty areas
TRG3	Major	> 80%	larger areas

Chi-Square testing was performed for analyzing the impact of neoCTx dose adaption on tumor regression grade. Furthermore, the influence of a full dose or adapted dose neoCTx on the R- and N-status, as well as the impact of the TRG on the R- and N-status was conducted via Chi-Square testing in Graph Pad Prism 8.4 (GraphPad, CA, USA).

8.2.2 Tissue sampling

Patient tissue and blood sampling, as well as PDO generation and cultivation has been approved by the local ethics committee (#EK451122014). Written consent was obtained from all patients before tumor specimens were received and processed. All tissue samples that have been processed for PDO generation were surveyed by board-certified pathologists to confirm PDAC disease according to the World Health Organization criteria.

8.2.3 Cell culture techniques

All cell culture methods have been conducted under sterile conditions. PDOs always were cultivated at 37°C and 5% (v/v) CO_2.

8.2.3.1 PDO generation from surgical resection specimens

Tumor specimens were minced into small pieces (< 1 mm^3) and further processed by incubating in digestion media for 2-4 h in a heat block at 37°C and 700 rpm. The digestive reaction was stopped by centrifuging at 400 x g for 5 min at 4°C and aspiration of the supernatant containing Collagenase II and Dispase II. The pellet was resuspended in 2 ml of F+++ medium and the sample incubated for 2 min to allow larger fragments to settle in the reaction tube. Cell clusters passing through a 200 µl pipette tip were transferred into a new reaction tube, followed by several washing steps with 1x DPBS. The remaining sample was resuspended in Matrigel in dependence of the pellet size and plated as 20 µl drops on a 48-well plate. After incubating 10 min at 37°C in an incubator the polymerized Matrigel drops were covered with 240 µl of PDAC medium supplemented with the rock inhibitor Y-27632.

F+++ medium (500 ml)	10 mM HEPES
	1x GlutaMAX
	1x Primocin
	1x penicillin/streptomycin
Digestion medium	F+++ supplemented with
	0.625 mg/ml Collagenase II
	2.5 mg/ml Dispase II

PDAC medium (50 ml)	12.2 ml F+++ medium
	25.0 ml conditioned WNT3a medium
	5.0 ml conditioned noggin
	5.0 ml conditioned Rspondin
	1.0 ml B27 (50x)
	0.5 ml N2 (100x)
	0.5 ml nicotinamide (1 M)
	0.5 ml gastrin (1 µM)
	0.1 ml Primocin (500x)
	0.1 ml N-acetyl-L-cysteine (1 mM)
	0.05 ml mEGF (50 µg/ml)
	0.05 ml hFGF10 (100 µg/ml)
	0.01 ml A83-01 (10 mM)
PDAC medium + Y27632 (10 ml)	9.990 ml PDAC medium
	10 µl Y27632 (10 mM)
Pancreas medium (10 ml)	9.980 ml PDAC medium
	10 µl PGE2 (10 mM)
	10 µl Forskolin (10 mM)

8.2.3.2 PDO generation from fine needle aspiration samples

Endoscopic ultrasound (EUS) guided fine needle aspiration (FNA) samples were received from the Department of Medicine 1 at the University Hospital Carl Gustav Carus Dresden and the Department of Endoscopy and Gastroenterology at the Städtisches Klinikum Dresden Friedrichstadt. Due to the limited amount of sample, the processing of tissue was amended accordingly: The retrieved FNA material was directly transferred into a collection tube containing digestion medium without mechanical shredding. The incubation time in a heat block at 37°C and 700 rpm was reduced to 30-45 min. Following a centrifugation step of 5 min at 300 x g and 4°C, sample contamination with blood coagulate was removed by re-suspending the pellet in 500 µl ACK lysing buffer and a 3 min incubation at room temperature. Two washing steps with 1x DPBS were performed before the pellet was re-suspended in Matrigel, plated as 20 µl drops in 48-well plates and covered with 240 µl PDAC medium supplemented with Y-27632 after polymerization of the Matrigel.

8.2.3.3 Passaging and cultivation of PDOs

Human PDAC PDOs were passaged once a week with a split ratio of 1:2 up to 1:6 depending on the proliferation dynamics of the individual organoid line. For this purpose, Matrigel drops from up to four wells were pooled in a 15 ml reaction tube with the help of a 1000 µl pipette. The PDOs were mechanically dissociated using a fire polished glass Pasteur pipette and washed two times with 1x DPBS. The pellet was re-suspended in Matrigel and plated as drops on 48-well plates as described in section 3.2.3.1 & 3.2.3.2. PDAC medium without Y-27632 supplement has been used for all cultures beyond the first passage. Medium was replaced every 3-4 days, when no passaging of PDO lines was necessary.

8.2.3.4 Freezing and unfreezing PDOs

For long term preservation of human PDOs, cells from up to 4 wells have been harvested and mechanically dissociated as described in section 3.2.3.3. After washing with 1x DPBS the PDO pellet was re-suspended in 500 µl recovery cell culture freezing medium, transferred into a freezing container and stored at -80 °C for 24 h before storage in liquid nitrogen.

1 ml preheated F+++ medium was added to a vial of cryopreserved organoids for rapid unfreezing. The sample was transferred into a 15 ml collection tube containing 6 ml of F+++ and centrifuged for 5 min at 300 x g and 4°C. The cell pellet was further handled as described in 3.2.3.1. Human PDOs were cultivated in PDAC medium supplemented with Y-27632 after unfreezing for one passage.

8.2.4 Staining of human PDAC PDOs

8.2.4.1 Fixation and paraffin embedding of PDOs

Human PDOs from at least 10 dense growing wells (48-well plate) were harvested to obtain sufficient material for paraffin embedding. The sample was directly centrifuged for 5 min at 300 x g and 4°C without mechanical dissociation. Matrigel contaminations were removed by adding 1 ml of cell recovery solution and incubation for 30 min on ice. After washing with 1x DPBS, fixation of the PDOs was performed using 4% formaldehyde and incubated for 1 min at room temperature. Removal of formaldehyde was carried out by washing 2 times with 1x DPBS. Next, the sample was dehydrated by subsequent incubation for 3 min in 25%, 50% and 70% ethanol (v/v). Optionally, PDOs were stained with eosin to facilitate embedding and sectioning of the samples. Therefore, PDOs were incubated for 5 min at room temperature in 1% eosin diluted in 96% ethanol followed by repeated washing with 96% ethanol. The sample was incubated in butanol three times for 3 min before resuspension in 500 µl

liquid paraffin and incubation at 56°C for 30 min. The embedded PDOs were transferred into an embedding cassette and 2.5 µM thick section were cut using a microtome.

8.2.4.2 Hematoxylin and eosin staining of PDOs

Staining of cell nuclei (hematoxylin) and cytoplasm (eosin) was done on paraffin embedded PDO sections by de-paraffinizing in xylene and isopropanol for 5 min. Subsequently, the samples were rehydrated by incubating in 96% ethanol and 70% ethanol for 3 min respectively. Next, hematoxylin staining was done for 2 min followed by briefly dipping the slides into acetic dH_2O. The development of the staining was achieved by rinsing 10 min with warm tap water. Next, the samples were incubated in eosin for 3 min and dehydrated by incubating in 70% and 96% ethanol for 2 min successively. Afterwards, the samples were incubated in isopropanol and xylene for 5 min each and mounted in entellan. Bright field images were taken using the EVOS FL Auto microscope for analysis of the stainings.

8.2.4.3 Immunohistochemistry staining of PDOs

For immunohistochemistry (IHC) stainings, paraffin embedded PDO sections were de-paraffinized by incubating these in xylene for 10 minutes. Sample rehydration was achieved by subsequently incubating in 95%, 85% and 70% ethanol for 3 min, followed by a 10 min washing step with 1x TBST buffer. The quenching of endogenous peroxidases was conducted by incubating in methanol supplemented with 0.8% H_2O_2 for 20 min at room temperature. After washing 3 times in 1x TBST for 3 min, antigen retrieval was performed by boiling the samples in 0.01 M sodium citrate buffer (pH 6.0) in a microwave three times for 3 min at 540 W and allowed to cool for 3 min in between. This was followed by three additional heating/boiling steps at 230 V for 3 min each with 3 min cooling phases in between. The samples were washed in 1x TBST again before blocking with 5% goat block solution for 1 h at room temperature. The primary antibody (diluted as indicated in Table 8) was applied and incubated overnight at 4°C in a humidified chamber. Unbound antibodies were removed by washing 10 min with 1x TBST. Horseradish peroxidase (HRP) conjugated SignalStain boost IHC detection reagent was applied to the sample and incubated for 30 min at room temperature in a humidified chamber. HRP substrate chromogen concentrate was added, and the staining monitored on a microscope. The enzymatic reaction was stopped by washing with 1x TBST. A counterstaining with H&E as described in section 3.2.4.2 was performed for improved visualization and samples imaged using the EVOS FL Auto microscope.

10x TBS buffer (500 ml)	43.83 g NaCl 12.11 g Tris base add H_2O to 500 ml
1x TBS-T buffer (1000 ml)	100 ml 10x TBS buffer 0.5 ml Tween20 add H_2O to 1000 ml
0.1 M sodium citrate buffer (500 ml)	14.7 g sodium citrate tribasic dihydrate add dH_2O to 500 ml
0.01 M sodium citrate buffer (1000 ml)	100 ml 0.1 M sodium citrate buffer 10 ml Tween20 adjust pH to 6.0 with conc. HCl add dH_2O to 1000 ml
5 % goat block (50 ml)	330 µl TrisHCl (1.5 M) 0.5 g $MgCl_2$ 250 µl Tween20 0.5 g BSA 2.5 ml goat serum add dH_2O to 50 ml

8.2.4.4 Immunofluorescence staining of PDOs

Organoids from 6-8 dense grown wells from a 48-well plate were harvested and pooled in a 15 ml collection tube. The remaining Matrigel was removed using cell recovery solution as suggested by the manufacturer. After repeated washing with 1x DPBS, the pellet was re-suspended in 7 ml 2% paraformaldehyde solution for fixation and stored at 4°C overnight. The supernatant was removed after centrifuging 5 min at 300 x g and 4°C, the pellet resuspended in 1 ml 0.3% TritonX-100 permeabilization solution and incubated at room temperature for 20 min. The samples were then centrifuged for 5 min at 300 x g and 4°C, the supernatant aspirated, and the pellet resuspended in 500 µl IF blocking solution before incubating 1 h at room temperature. The primary antibodies used were diluted (according to table 8) in IF blocking solution and the PDOs resuspended. After 2 h

incubation at room temperature, unbound antibodies were removed by repeated washing with IF washing buffer. Next, the pellet was re-suspended in 500 µl IF blocking solution containing the secondary antibody, DAPI and phalloidin, diluted in IF blocking solution. Repeated washing was done with IF washing buffer after 2 h incubation at room temperature and the pellet re-suspended in 50 µl Mowiol before applying onto microscope slides. Images were taken on a confocal laser-scan-microscope (Zeiss LSM 550 and Zeiss LSM 880 Airyscan).

2% paraformaldehyde solution (100 ml)	2 g paraformaldehyde Add 1x DPBS to 100 ml Adjust pH to 7.4
Permeabilization solution (10 ml)	0.3 ml TritonX-100 9.7 ml 1x DPBS
IF blocking solution (50 ml)	0.5 g BSA 50 µl TritonX-100 49.95 ml 1x DPBS
IF washing buffer (50 ml)	50 µl Tween20 50 µl TritonX-100 49.9 ml 1x DPBS

8.2.5 Pharmacotyping of PDAC PDOs

8.2.5.1 Single drug assays

PDAC PDOs drug sensitivity was evaluated for irinotecan, oxaliplatin and 5-FU, which are part of the FOLFIRINOX therapy as well as gemcitabine and paclitaxel, which are components of the Gem/Pac protocol.

Dense growing PDO cultures were collected and pooled in a 15 ml collection tube. PDOs from one well (48-well plate) were used to prepare 20-40 samples on a 384-well plate, depending on the individual PDO line growth rate. A fire polished glass pipette was used to mechanically dissociate the PDOs prior to centrifugation and washing with 1x DPBS. The cell pellet was re-suspended in 75% Matrigel diluted

with PDAC culture medium and seeded as 15 µl samples into a 384-well plate. After Matrigel polymerization 40 µl PDAC culture medium was applied to each sample before allowing the cell clusters to form organoids for 24 h. Next, the medium was replaced with allocated serial diluted chemotherapeutic compounds. Each dilution was performed in duplicates including the blank, which was composed of 75% Matrigel and PDAC culture medium. Six wells were used as negative control where PDOs were cultured in PDAC medium without drugs. The medium was refreshed after 72 h and viability was measured at day 6 by quantifying the metabolic activity in each sample using the PrestoBlue viability reagent. PrestoBlue viability assessment was performed as suggested by the manufacturer and analyzed using a Varioskan LUX plate reader with the following settings: samples were shaken for 5 seconds, and fluorescence measured from the bottom with an excitation and emission wavelength of 560 nm and 590 nm respectively. After empirically assessing suitable titration ranges, the 5 chemotherapeutic drugs used were diluted as follows:

Drug	**Dilution 1**	**Dilution 2**	**Dilution 3**	**Dilution 4**	**Dilution 5**	**Dilution 6**	**Dilution 7**
Irinotecan [µM]	300	60	18.75	7.5	2.5	1	0.1
Oxaliplatin [µM]	500	100	39	15.63	6.25	2.5	0.5
5-FU [µM]	1000	100	25	5	1	0.1	0.01
Gemcitabine [nM]	390	97.6	39	15.63	6.25	2.5	1
Paclitaxel [nM]	200	40	15	5	2	0.8	0.2

All drug dilutions were freshly prepared in in PDAC medium prior to use. Single drug assays were repeated at least 3 times for each PDO line tested within a range of 5 passages.

8.2.5.2 Drug combination assays

After assessing the single drug sensitivity for the first 10 PDAC lines, the mixture ratios for the FOLFIRINOX and Gem/Pac drug combination were defined as the compounds individual mean IC_{50} values. The FOLFIRINOX single agents irinotecan, oxaliplatin and 5-FU were mixed in a 1 : 3.5 : 3.5 ratio respectively, while gemcitabine and paclitaxel were mixed 1 : 0.64. Eight different dilutions were tested

for both multi-drug regimens. The drug doses "n" for FOLFIRINOX or Gem/Pac was defined as follows: 10 µM irinotecan + 35 µM oxaliplatin + 35 µM 5-FU or 14 nM gemcitabine + 9 nM paclitaxel, respectively. PDO seeding, assay design, duration of drug treatment and readout was analogous to the single drug assays as described in section 3.2.5.1 but with the following dilution steps:

CTx	Dilution 1	Dilution 2	Dilution 3	Dilution 4	Dilution 5	Dilution 6	Dilution 7	Dilution 8
FOLFRINOX	6.25n	2.5n	**n**	n/3	n/9	n/27	n/81	n/243
Gem/Pac	10n	4n	2n	**n**	n/2	n/4	n/8	n/20

Three individual experiments were conducted for each PDO line within 5 passages to avoid clonal expansion bias.

8.2.5.3 Modified drug combination assays

The analysis of how single drugs contribute to cytotoxicity *in vitro* in the FOLFIRINOX multi-drug protocol was performed by leaving out irinotecan, oxaliplatin, or 5-FU from the CTx mixture. PDAC PDO preparation and seeding, assay design, drug dilution numbers and steps, duration of drug treatment and the readout were analogous to the drug combination assays as described in section 3.2.5.2. The individual drug impact on cytotoxicity in the Gem/Pac group were investigated by merging single drug and drug combination data retrospectively.

8.2.5.4 Drug assay data analysis and interpretation

PDO drug assays were analyzed by normalizing the mean value of each dilution step to the mean of the negative control after blank subtraction. The obtained relative viability data were used to plot dose-response curves in GraphPad Prism 8.4 followed by the calculation of the area under the curve (AUC) value. Further comparison of PDO lines individual drug sensitivities was achieved via z-score normalization using the formula $z= (x-\mu)/\sigma$, where x is the mean AUC from three individual conducted pharmacotyping assays, µ is the mean AUC from all PDO lines tested for a specific drug and σ is the standard deviation from all PDO lines analyzed.

The relative area under the curve was calculated by dividing individual AUC values by the maximum AUC for each drug dilution range respectively. The comparison of the PDO cohort of CTx naïve and neoCTx cell lines was done via Mann-Whitney testing performed in GraphPad Prism 8.4.

The analysis of leave-on-out drug assays for FOLFIRINOX was done using the ANOVA test based on PDO lines AUC data. The modified Gem/Pac assays was done analogue for the overlapping dilution range from all three conditions (Gem/Pac vs. Gem vs. Pac) (* $p < 0.05$, ** $p < 0.01$, *** $p < 0.001$). Pearson correlation analysis was done in GraphPad Prism 8.4 for assessing the connection between FOLFIRINOX and Gem/Pac sensitivities. Investigating the correlation between the lowest single drug z-score and the respective drug combination z-score was also done using Pearson correlation.

8.2.6 DNA & RNA techniques

8.2.6.1 DNA isolation from PDAC organoids

To ensure sufficient starting material organoids from 5-10 wells from a 48-well plate were collected in a 15 ml collection tube. Cell recovery solution was applied, and samples incubated on ice for at least 30 min for non-enzymatic digest of the Matrigel. After repeated washing with 1x DPBS, the pellet was further processed according to the manufacturer instruction from the QIAamp DNA mini kit to obtain genomic DNA, which was eluted in dH_2O instead of elution buffer. The DNA concentration was assessed using the NanoVue Plus spectrophotometer.

8.2.6.2 Polymerase chain reaction and gel electrophoresis

Sequencing of the Kirsten rat sarcoma viral oncogene (*KRAS*) was done to confirm the malignant origin of newly established PDO lines, since *KRAS* is mutated in around 90-95% of PDAC[108]. Most of the gain-of-function mutations are located in *KRAS* exon 2 and exon 3, which is why both exons have been amplified in a PCR reaction, followed by a gel electrophoresis quality control and sample shipment for sequencing to the Eurofins Genomics. The PCR amplification for both, exon 2 and 3, was done with the following PCR mix and cycler protocol:

PCR mix	
genomic DNA	100 ng
Primer forward (10 µM)	1 µl
Primer reverse (10 µM)	1 µl
5x Phusion Taq buffer	4 µl
Phusion Taq (2U/µl)	0.2 µl
DMSO	0.6 µl
dH_2O	add to 20 µl

Cycler program		
98°C	2 min	
98°C	10 sec	35 cycles
64°C	20 sec	
72°C	25 sec	
72°C	5 min	
15°C	hold	

The PCR samples were analyzed via gel electrophoresis to assess successful DNA amplification prior sequencing. Agarose (0.8 – 1.2 % w/v) was dissolved in 1x TAE buffer by heating in a microwave. Gel Red (1:10000) was added for later visualization of nucleic acids in the Vilber Fusion Fx gel documentation system and loading buffer applied to the samples to a final concentration of 1x before loading on the gel. Gene ruler 1kb plus ladder has been used for fragment size determination and sample separation performed by default for 1 h at 100-120 V.

50x TAE buffer (1000 ml)	242.0 g Tris 57.1 ml acetic acid 100 ml 0.5 M EDTA pH 8.0 dH_2O up to 1000 ml
1 x TAE buffer (1000 ml)	20 ml 50x TAE buffer dH_2O up to 1000 ml

8.2.6.3 RNA isolation from PDAC PDOs and cDNA synthesis

Organoid collection and processing prior RNA isolation was conducted as described in section 3.2.6.1. The RNeasy Mini Kit was used following the manufacturer's protocol for further cell pellet processing. RNAse free water was used to elute total RNA and concentration measured with the NanoVue Plus Photospectrometer.

Synthesis of complementary DNA (cDNA) from PDO derived RNA was performed using the qScript cDNA synthesis Kit and the following reaction protocol as suggested by the manufacturer:

Sample Mix	
RNA	500 ng
5x qScript reaction mix	4 µl
qScript RT (20x)	1 µl
dH2O	add to 20 µl

Cycler program	
22°C	5 min
42°C	30 min
85°C	5 min
4°C	hold

8.2.6.4 Quantitative Real-Time PCR

Quantitative real-time PCR (qPCR) was used for expression analysis of the *KRT81*, *CFTR* and *HNF1A* gene in human PDAC PDO lines. The genes *GAPDH* and *ACTB1b* were utilized as house-keeping controls. Primers for all genes were chosen to span at least one exon, have similar amplicon lengths of 80 – 150 bp and at least one GC-clamp on the 3' end. Each sample was pipetted and run in a GeneAmp 5700 Step One Plus cycler as follows:

qPCR mix	
cDNA	2 µl
Primer forward (10 µM)	2.5 µl
Primer reverse (10 µM)	2.5 µl
2x GoTaq qPCR Master Mix	12.5 µl
CXR reference dye	0.25 µl
dH_2O	5.25 µl

Cycler program		
50°C	2 min	
95°C	10 min	
95°C	30 sec	40 cycles
60°C	1 min	
60°C	1 min	

Primer efficiency was first determined to be at least 90% before expression analysis was conducted. The data were processed according to Hellemans and colleagues[109], which allowed using more than one house-keeping gene for more precise expression interpretation within the analyzed population. First, the arithmetical means from all PDO lines and genes analyzed were calculated for converting quantitative cycle values into relative quantities (RQs). Next, the sample-specific normalization factor (NF) was obtained by calculating the geometrical mean of the two house-keeping genes *GAPDH* and *ACTB1b* RQs. Dividing RQ by NF gives the relative expression within the population. Accordingly, the PDO lines specific gene expression is not normalized to a particular control, but the mean of all samples included into the analysis.

Results

9.1 Chapter 1 – The efficacy of neoCTx in LA PDAC patients is negatively impacted by drug dose adaptations

Most PDAC patients present with unresectable LA PDAC when diagnosed[33]. Neoadjuvant chemotherapy is the treatment of choice to potentially achieve resectability by tumor burden reduction. The standard therapy regimens FOLFIRINOX and Gem/nab-Pac showed promising response rates in the past but are associated with high rates of grade 3 & 4 side effects[33,38,40]. Dose reduction of standard of care or a switch of therapy are options to ensure the continuation of treatment. Yet, severe adverse effects can also result in a complete discontinuation of therapy, which might negatively impact the patients´ prognosis and outcome.

In order to investigate the effect of neoCTx dose adaption or termination of treatment on patients' response to therapy, data from LA PDAC patients were retrospectively analyzed. 59 patients have been identified that fulfill the inclusion criteria (see Chapter 3.2.1.) and that were hospitalized at the University Hospital Dresden between 2014 and 2021. Additionally, data from 66 patients diagnosed with initially resectable PDAC were recorded for comparison of several prognostic markers such as lymph node and resection margin status of neoCTx and CTx naïve patients (Table 13, Supplementary table 1 + 2).

The gender was almost equally distributed (34 male vs 32 female) and the median age in the group of patients that presented with initially resectable PDAC (CTx naïve patients) was 69 years (Table 14). Three resected tumors were smaller than 2 cm (T1; 4.5%) while the majority of PDAC was 2 cm (T2; 57.6%) in diameter or larger (T3, 37.9%). Poorly and moderately differentiated tumors were nearly equally distributed. The lymph node and resection margin status (N-Status and R- Status, respectively) have been shown to be independent predictor of OS in PDAC. Resection with tumor free margins (R0) or microscopic tumor infiltrates (R1) was achieved in 72.7% and 19.7% respectively. Regarding the N-status, the majority of LA PDAC cases of the CTx naive cohort were all lymph node positive and between one and four (46.9%; N1) or more (36.4%; N2) tumor infiltrated ascendant lymph nodes were found.

Within the neoCTx pretreated patients (neoCTx patients) the median age was 65 years and 45.8% of the cohort were male. The analysis of tumor size was not included due to the lack of sufficient pre-neoCTx data. As the patients have received systemic treatment, the tumor differentiation grade (G-status) was not assessed. Two-thirds (69.5%) of the patients received FOLFIRINOX and one-third (30.5%) Gem/nab-Pac. Of note, the median age of patients receiving FOLFIRINOX and Gem/nab-Pac

was 62 and 73 years, respectively. More than half (52.5%) of all pretreated patients showed minor response (TRG1) to the therapy, while in 32.2% and 15.3% an intermediate (TRG2) and major response (TRG3) was determined.

Table 13 – PDAC patient cohort

PDAC cohort		
Variable	**Value**	**[%]**
Patients	66	100.0
Median age	69	-
Male sex	34	51.5
T-status:		
T1	3	4.5
T2	38	57.6
T3	25	37.9
Grading:		
G2	31	47.0
G3	34	53.0
R-status:		
R0	48	72.7
R1	13	19.7
n.d.	5	5.6
N-status:		
N0	11	16.7
N1	31	46.9
N2	24	36.4

LA PDAC cohort		
Variable	**Value**	**[%]**
Patients	59	100.0
Median age	64	-
Male sex	27	45.8
neoCTx regimen:		
FOLFIRINOX	41	69.5
Gem/nab-Pac	18	30.5
Median age:		
FOLFIRINOX	62	-
Gem/nab-Pac	73	-
Tumor reg. grade:		
TRG 1	31	52.5
TRG 2	19	32.2
TRG 3	9	15.3
R-status:		
R0	43	72.9
R1	10	16.9
n.d.	6	10.2
N-status:		
N0	23	39.0
N1	25	42.4
N2	11	18.6

Similar to CTx naïve patients, R0 resection was achieved in most of the cases (72.9%). In two out of five resected tumors no infiltrated lymph nodes were seen (39.0%) and N2 was seen in less than one-fifth of patients (18.6%) compared to the primary resectable patients.

Nearly one-third of patients neoadjuvantly treated with either FOLFIRINOX or Gem/nab-Pac did not complete their treatment (29.3% and 27.8%, respectively) (Figure 5A). In most cases, the therapy was continued with reduced dose (n= 15; 88%), while in two cases neoCTx with FOLFIRINOX was

discontinued after cycle three due the onset of severe side effects. Strikingly, in one of these patients the pathological assessment revealed a R0 status, lymph node status N0 and major tumor regression grade. Nevertheless, TRG3 and TRG2 occurred more often in the cohort of FOLFIRINOX treated patients receiving the complete course of treatment compared to patients with dose reductions (p= 0.144, Chi^2-test) **(**Figure 5B). The same negative trend of dose adaption was seen for Gem/nab-Pac treated patients as only minor (4/5 TRG1) and intermediate (1/5 TRG2) pathological response was observed when regimen dose was adapted (p= 0.41, Chi^2-test).

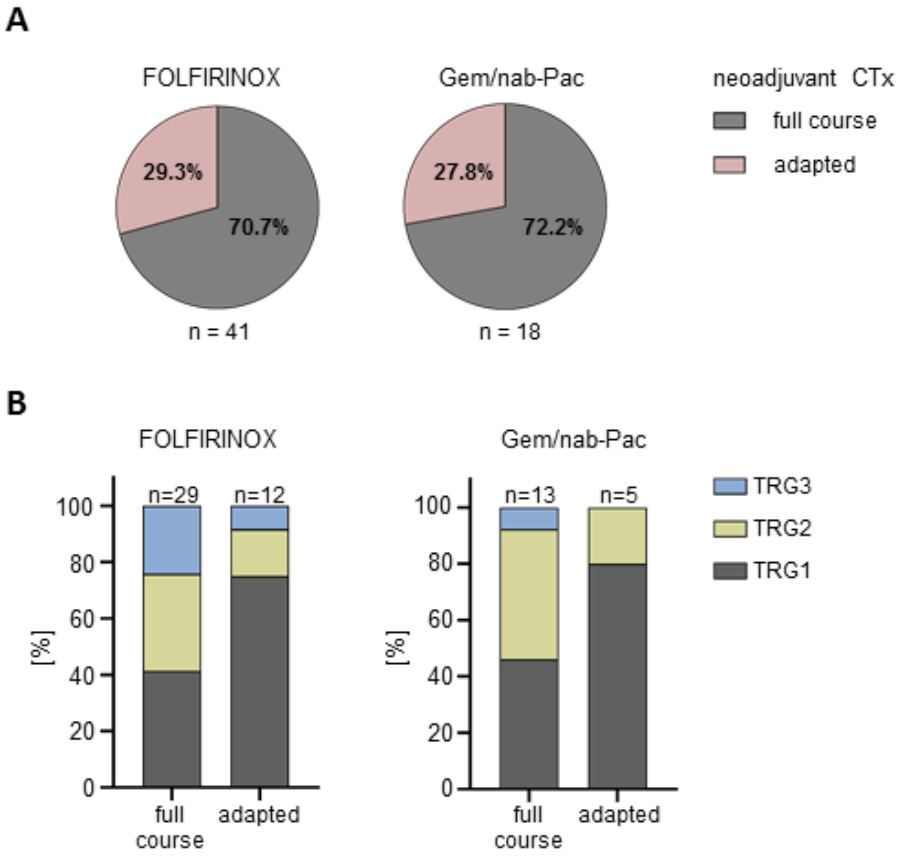

Figure 5 - NeoCTx dose adaptation impacts tumor regression grade in LA-PDAC patients. A) Distribution of LA PDAC patients receiving full course or dose adapted neoadjuvant chemotherapy (neoCTx) with either FOLFIRINOX or gemcitabine + nab-paclitaxel (Gem/nab-Pac). **B)** Frequency of minor- (TRG1), intermediate- (TRG2) and major pathological response rate (TRG3) in LA PDAC patients administered completed course regimen or dose adapted neoCTx with FOLFIRINOX or Gem/nab-Pac. Modified from Hennig *et al.*[110]

The R- and N-status are independent parameters impacting OS of PDAC patients and we sought to analyze the influence of neoCTx dose adaption on R and N status in more detail. In our cohort, an adaption in chemotherapy dose significantly increased the chance for microscopic tumor infiltrates present in the resection margins (10.8% vs. 37.5%, p= 0.023, Chi^2 test) (Figure 6A). No significant

difference was seen for the R0 resection frequency between CTx naïve and neoCTx patients (R0 resection: CTx naïve 78.7%, TRG1 75%, TRG2, 81.25%, TRG3 100%; p= 0.432, Chi^2 test). Yet, in all patients that showed major response to neoCTx (n= 9) R0 resection was achieved in 100% of cases. The adaption of dosing did not alter the N-status assessed from surgical resected tumors (p= 0.602, Chi^2 test) (Figure 6B), in contrast to TRG (p= 0.003, Chi^2 test). A minor response to the treatment already reduced the chance for N2 compared to CTx naïve patients (N2: TRG1 23.8% vs 36.4%). The effect was more prominent with increased TRG (N2: TRG2 14.8%, TRG3 0%). Concomitantly, N0 was more frequent the better the response to the neoCTx was (N0: CTx naïve 16.7%, TRG1 33.3%, TRG2 74%, TRG3 54.5%).

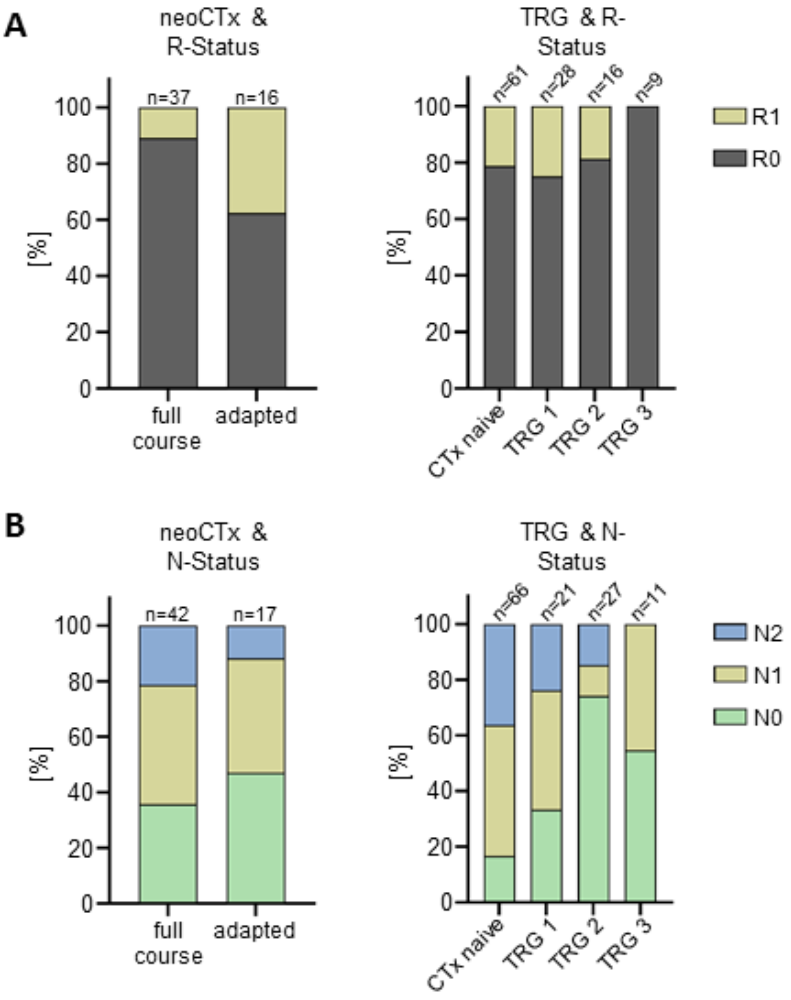

Figure 6 – The Neoadjuvant chemotherapy dose adaptation impacts the R- and N-status in LA-PDAC patients. A) Influence of neoCTx dose adaption on the frequency of microscopic tumor infiltrated (R1) resection margins and tumor free resection margins (R0) and distribution of R-status in CTx naïve patients and in dependence of TRG. B) Influence of neoCTx dose adaption on the number of lymph nodes infiltrated with tumor cells (N0 = 0, N1 < 4, N2 >= 4) and N-status in dependence of TRG and CTx naïve patients. Modified from Hennig *et al.*[110].

Taken together, an adaption of the neoCTx protocol due to the onset of severe side effects of grade 3 & 4 was necessary in one third of all LA PDAC patients, independent of which treatment has been administered. In addition, any reduction of drug dose significantly impacted the TRG, R and N status.

9.2 Chapter 2 – Generation and characterization of a PDAC PDO biobank

Patient-derived organoids resemble a novel three-dimensional *in vitro* tool with many potential applications. For instance, they could be used to identify resistances and sensitives to any anti-cancer drug, which might result in PDAC patient individualized systemic treatment protocols. Nonetheless, the generation of PDOs from primary tumor specimen remains challenging due to the difficulty of accessing tissue and the complexity of maintaining organoid cultures, specifically the handling and the media composition required for long term cultivation. Based on the published data from Broutier[93], Boj[91] and their colleagues an initial protocol for the generation of PDAC PDOs from chemotherapy naïve (CTx naïve) patients was assembled, were tissue samples were minced into small pieces of 1 mm^3 size and digested overnight in digestion medium, followed by repeated washing to circumvent a potential source of contamination, and seeding as Matrigel drops in tissue culture plates (Figure 7A + B). Images were taken instantly after seeding and subsequently before passaging the PDO lines on a weekly basis. We observed that PDOs emerged mainly from large tissue clusters, while no outgrowth within 7 days at passage zero was seen in tissue samples that have been digested to single cells (not shown). The sample processing resulted in a take rate of 20-30% when the initial protocol was followed (Figure 7C). As a result, we modified the method for PDO generation from surgical resection specimens by continuously reducing the concentrations of both digestion enzymes Collagenase II and Dispase II as well as the incubation time with these enzymes, which resulted in the finalized protocol as described in section 3.2.3.1. This led to an increased number of PDOs initiated within passage zero (Figure 7B) and concurrently, led to an increased take rate which peaked at 80% (Figure 7C). Whilst establishing our living biobank depository of CTx naïve PDAC PDOs, various organoid morphologies have been observed, i.e. thin- or thick-walled spheres and grape-like structured clusters (Figure 7D). We noticed that morphologies shown for DD385, DD753 and DD1078 were exclusively for PDAC, while the thin-walled morphology was common for both, wild type pancreatic PDO as well as PDAC PDOs.

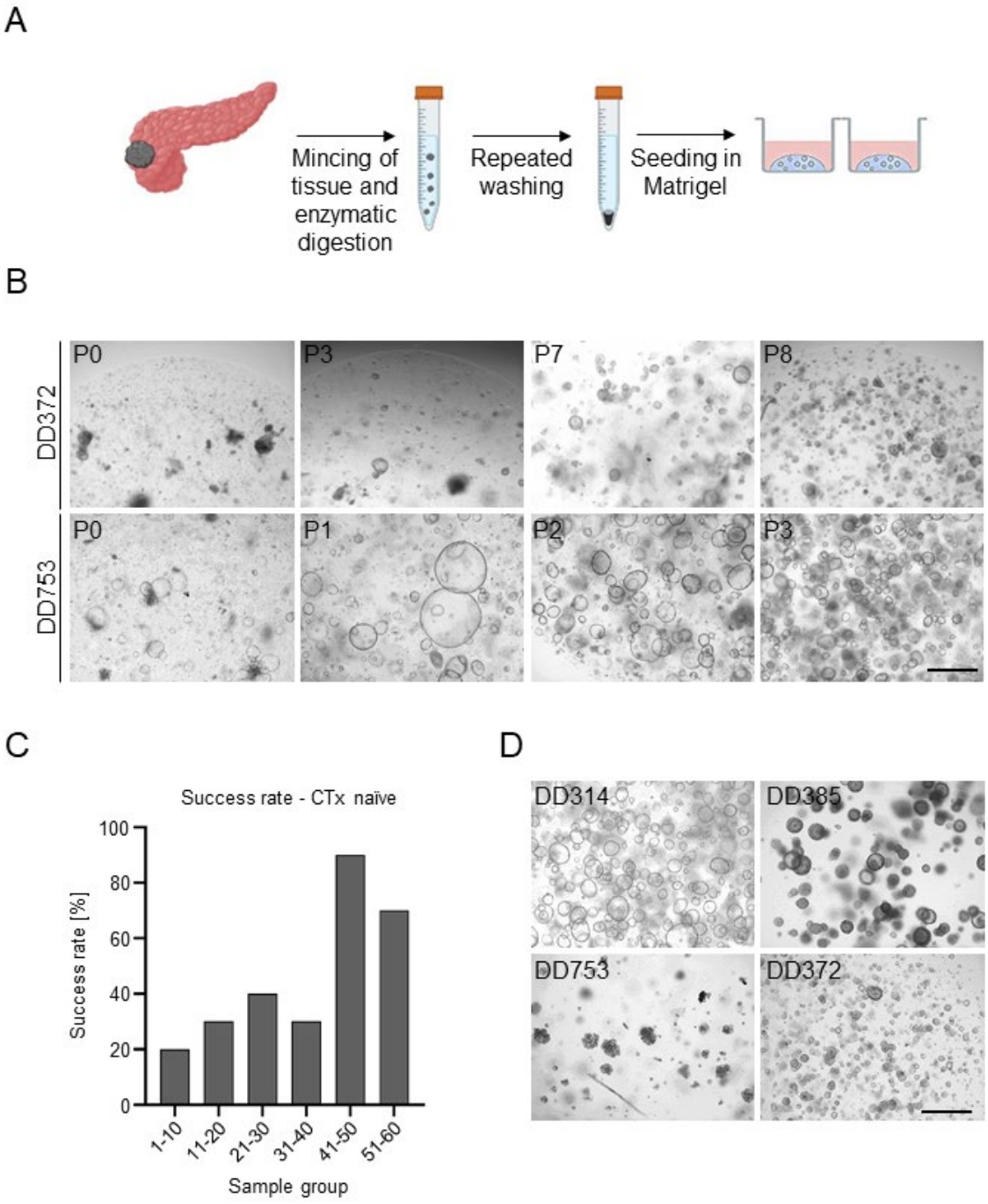

Figure 7 - Establishing PDAC PDOs from primary tissue. A) Schematic workflow of tissue processing for PDO generation. **B)** Bright field images from two PDAC PDO lines from passage zero to the time point stable growth was observed. **C)** Success rates for organoid line generation from CTX naïve patient derived tumor tissue samples divided into groups of 10. **D)** Bright field images of PDAC PDOs illustrating the different morphologies observed. Scale bars indicate 1000 µM.

In total, 66 tissue samples from 66 CTx naïve patients with diagnosed PDAC disease undergoing surgery at the University Hospital Carl Gustav Carus Dresden between December 2016 and March 2021 were processed for the generation of our PDO biobank at the time this thesis was written. 30 PDO lines were generated resulting in a growth rate of 45.5%. In order to investigate which disease associated parameters might influence the likelihood for the generation of a stably growing PDO line, samples were grouped according to the size of the original tumor (T1: < 20 mm, T2: 20 – 40 mm, T3 > 40 mm diameter) and its differentiation grade (G2: moderate differentiated, G3: poorly differentiated). Most patients presented with T2 or T3 (57.6% and 37.9%, respectively), while only 3 patients (4.5%) had a PDAC smaller than 2 cm in diameter. Hence, tumor size did not impact the take rate (p= 0.677, Chi^2 test) and only a marginally trend was observed of improved PDO outgrowth for T1 tumors (Figure 8). The differentiation grades G2 and G3 were equally distributed (47% and 53%) and did not influence PDO growth (p= 0.964, Chi^2 test).

In summary, the parameters T- and G-status did not influence the outcome of PDO generation. Yet, PDO generation from pancreas precursor lesions, i.e. intraductal papillary-mucinous neoplasms (IPMN) or intraepithelial neoplasias (PanIN), was not successful. This was also observed for acinar cell carcinoma, neuroendocrine tumors (NETs), cystadenoma and pancreatic cystic tumors, which represent rare variants of pancreatic cancers except NETs. PDO generation from adenosquamous pancreatic cancers was successful in one out of four samples.

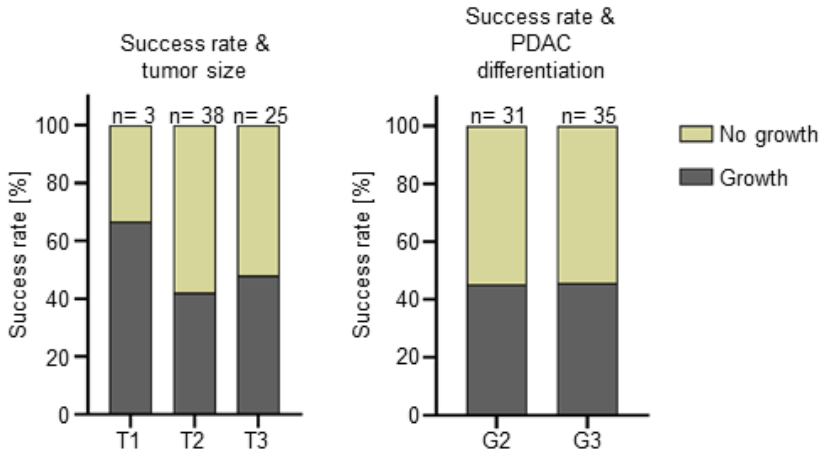

Figure 8 – Successful PDAC PDO initiation is not affected by tumor size or differentiation grade. The diagrams illustrate the take rate of PDAC PDO lines grouped according to the patients' tumor size (T1-T3) or differentiation grade (G2 or G3) within the cohort of 66 CTX naïve patients.

The outgrowth of putatively normal pancreatic PDOs has been observed in almost all processed samples. However, non-malignant pancreas PDOs cannot grow in PDAC medium after passage 6-10. Despite this the nonmalignant PDO contamination can outgrow PDAC PDOs and therefore challenges the expansion of the remaining tumor PDOs as depicted in Figure 9. DD372 showed solid growth of large thin-walled spheroid PDOs from passage 1 to passage 6. Within passage 7 all putatively normal pancreatic PDOs disappeared simultaneously, which was associated with an outgrowth of PDOs harboring a dense and lumen filled morphology which is typically for tumor PDOs.

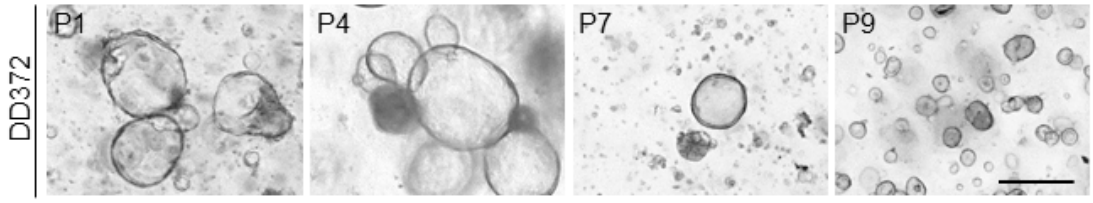

Figure 9 – Low passage PDAC PDO lines can be contaminated with pancreatic PDOs. Bright field images from the PDO line DD372 harboring mostly wild type pancreatic PDOs until passage 7. At higher passages tumor PDOs with typical morphology resemble the dominant population within the PDO line. Scale bar indicates 400 µM.

As mentioned above, the long-term cultivation of non-malignant pancreatic PDOs in PDAC medium is not possible. Georgakopoulos and colleagues published an improved protocol that allowed cultivation of pancreatic PDOs for up to 180 days by the addition of the TGFβ inhibitor forskolin and prostaglandin E2 (PGE2) to the PDAC cultivation medium[111]. The adaption of the respective protocol resulted in highly efficient outgrowth of large thin-walled spherical PDOs established from total pancreatectomy tissue samples (Figure 10). These resected specimens harbored non-infiltrated areas assessed by a board-certified pathologist. The take rate was 57% (4 out of 7) and cultivation was maintained for 10 passages. The growth kinetic was much faster than observed for PDAC PDOs allowing the expansion of high PDO numbers within 1-2 weeks after sample processing.

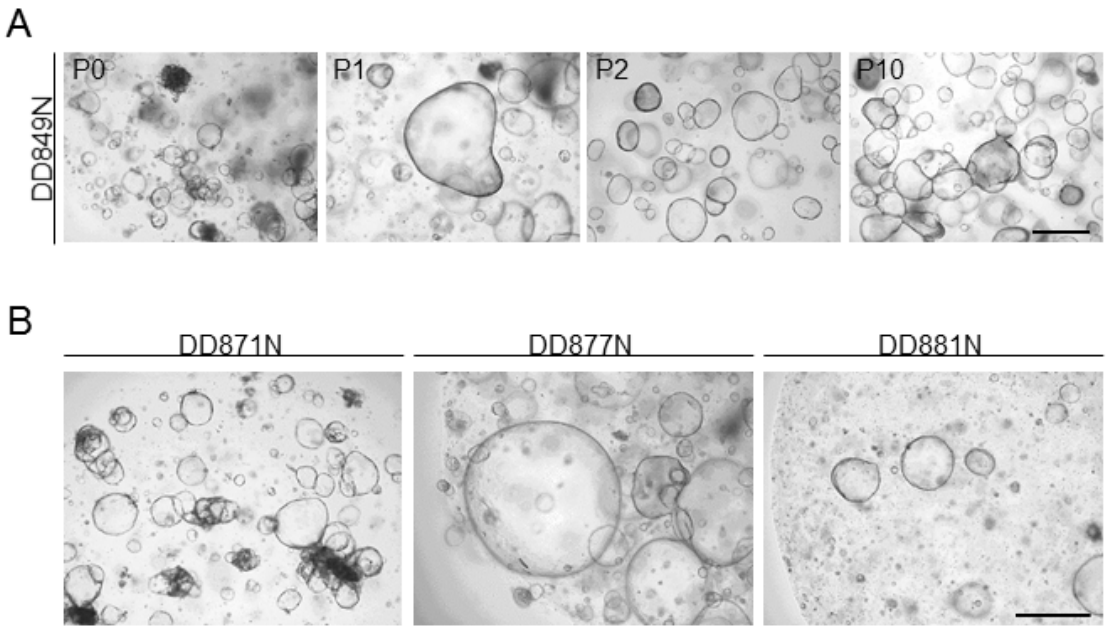

Figure 10 - Generating normal pancreatic PDOs from human tissue samples. A) Bright field images from the human pancreatic PDO line DD849N from passage zero to passage three. **B)** Bright field images from three additional pancreatic PDO lines showing similar morphologies. Scale bar indicates 1000 µM.

NeoCTx PDOs could be used to uncover resistances to chemotherapeutic drugs that have been administered to the respective patient prior surgery and might guide clinicians in decision making for choosing the optimal adjuvant therapy protocol. As generating PDAC and pancreatic PDOs from CTX naïve patients have been successfully established, we sought to investigate whether surgical resection specimens from neoCTx patients display differences in their take rate, morphology or growth dynamics.

Tumor tissue samples from 43 neoCTx patients have been collected between September 2017 and June 2021 of which 22 neoCTx PDOs were established. The average take rate was 51.1% and no increase over time was observed despite the improvement of tissue processing protocols (Figure 11A). Surprisingly, classifying neoCTx samples according to the patients' tumor regression grade based on Le Scodan and colleagues[52] revealed a worse/lower success rate for PDO generation with increasing TRG (TRG1: 62.5%, TRG2: 46.2%, TRG3: 0%; p= 0.062, Chi^2 test) (Figure 11B).

Concomitantly, PDO lines were expanded faster when the corresponding patient showed minor response to the neoCTx compared to patients with intermediate response (Figure 11C). No PDO line was established from patient derived tissue that had a TRG3 assessed by the pathologist. Here, all four samples classified as TRG3 resulted in only thin-walled spherical PDOs and cultivation after passage 6 to 10 was not possible.

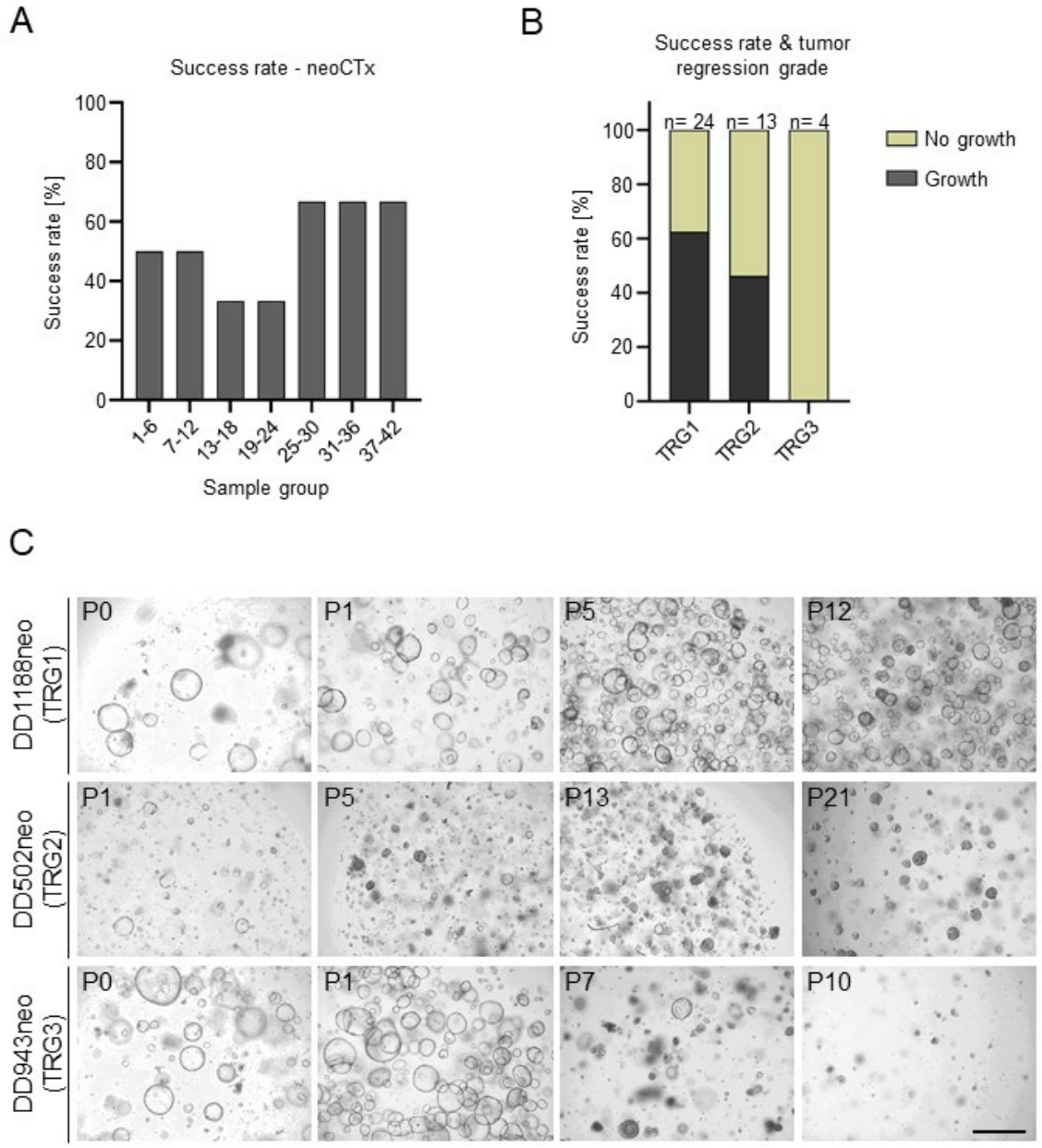

Figure 11 - Impact of PDO generation success rate dependents on TRG after neoCTx. A) Success rates for PDO line generation from neoCTx patient derived tumor tissue samples divided into groups of 6. **B)** Frequency of successful neoCTx PDO generation according to the patients´ TRG regardless of which therapy protocol or dose has been administered. **C)** Bright field images taken from the neoCTx PDO lines DD1088neo, DD502neo and DD943neo derived from patients with a TRG1, TRG2 or TRG3 respectively. Scale bar indicates 1000 µM.

As the majority of PDAC patients present with unresectable disease at time point of diagnosis, it is also important to establish PDOs from endoscopic ultrasound guided fine-needle aspiration (EUS-FNA) samples. This is an ethically approach, as EUS-FNA is routinely performed in patients with LA PDAC for histological verification, which is required to initiate systemic neoCTx using multi-drug protocols. From April 2018 to July 2021 38 biopsies from 32 patients have been processed for PDO generation. The

PDO generation from biopsy samples is challenging as the start material is of very small sample size and mostly contaminated with blood cells, such as erythrocytes. Nevertheless, the PDO outgrowth was achieved in samples regardless of the amounts of blood cells within each biopsy (Figure 12A).

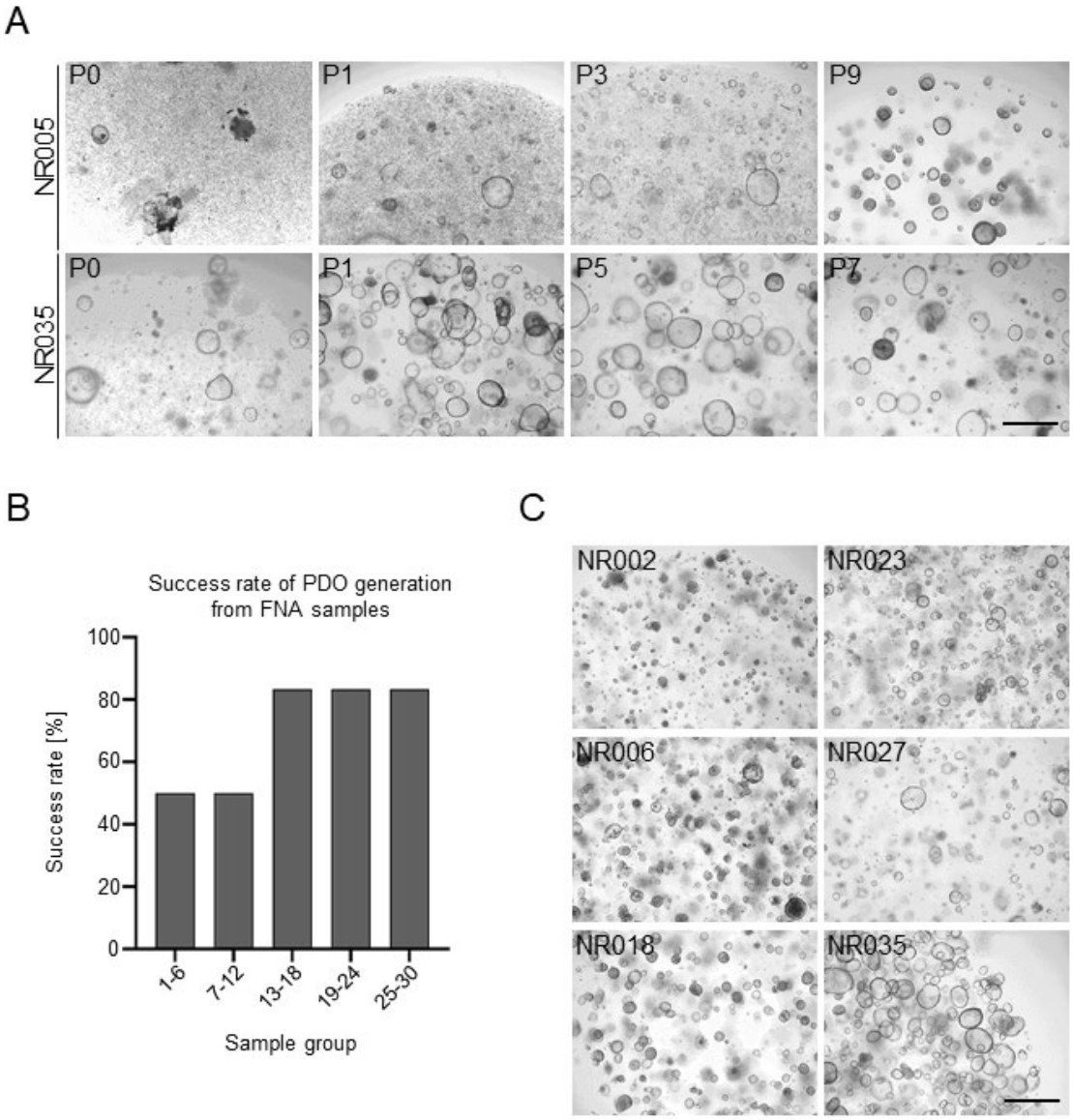

Figure 12 – PDAC PDO can be generated from material of small sample size derived by EUS-FNA. A) Bright field images from different passages from the biopsy sample derived PDAC PDAC lines NR005 and NR035. NR005 showed a high degree of contamination with blood cells at early passages, whilst tissue from NR035 was treated with ACK-buffer prior to cultivation. **B)** Success rates for PDO line generation from EUS-FNA samples divided into groups of 6. **C)** Bright field images from six successful established PDAC PDO lines illustrating the diversity of morphologies. Scale bars indicate 1000 µM.

Initially the success rate was 50% for the first 12 histologically confirmed PDAC samples received using the same protocol as for processing tissue from surgical resection specimens (Figure 12B). Optimization of the protocol including a reduced digestion time of only 30 minutes and the omission of mechanically mincing the FNA sample, led to an increased take rate of 80%. The take rate remained stable for the additional 18 samples collected. Overall, the success rate for PDO generation from FNA samples was 66.7% (20 out of 30). The main reasons for outgrowth failure are overdigesting of the samples, contaminations (in 2 out of 30 samples) with fungi or poor quality of obtained tissue due to the lack of sufficient epithelial cells to establish PDOs from. Different morphologies have also been observed for FNA derived organoid lines similar to the those of PDOs generated from surgical resection specimens (Figure 12C). The majority of FNA-derived PDOs displayed thick-walled spheres with a lumen, a mass- or a grape-like morphology. In six cases, a second EUS-FNA was needed due to insufficient material for assessment by the pathologists. Interestingly, it was observed in some cases that the generation of a PDO outperformed the pathological assessment for malignancy. In one case, the first biopsy taken allowed the generation of a stable growing PDO line (NR050). This line exhibited a PDAC associated morphology since the beginning of culturing. For another case, tumor organoids formed before the analysis or the FNA sample by board certified pathologists was done (NR035).

Suspicious lesions, which is found during surgical exploration, e.g. in liver or the peritoneum, is routinely send for pathological evaluation, as surgical PDAC resection is not recommended in case of distant metastasis according to the ASCO- and ESMO guidelines. Yet, this procedure presented with an opportunity to obtain material of a suspected metastasis to generate PDO lines. Six PDO lines from PDAC liver metastasis have been established successfully and their origin was confirmed by pathologists (Figure 13). Other surgical specimen derived from the peritoneum or blood plasma accumulated in the abdomen (ascites) allowed the generation of stably growing PDOs (i.e. two PDOs from ascites samples and three PDOs from peritoneal metastasis). In addition, one adjacent lymph node metastasis PDO line was established, however, it did not resemble distant metastasis. In most cases, low amounts of starting material were obtained resulting in a relatively low take rate. The PDO generation for non-primary tumor material led to the generation of liver metastasis PDOs (6/16) , ascites (2/4) and for peritoneal carcinoma (3/12). No PDO line derived from lung metastasis was established out of the two samples that were received.

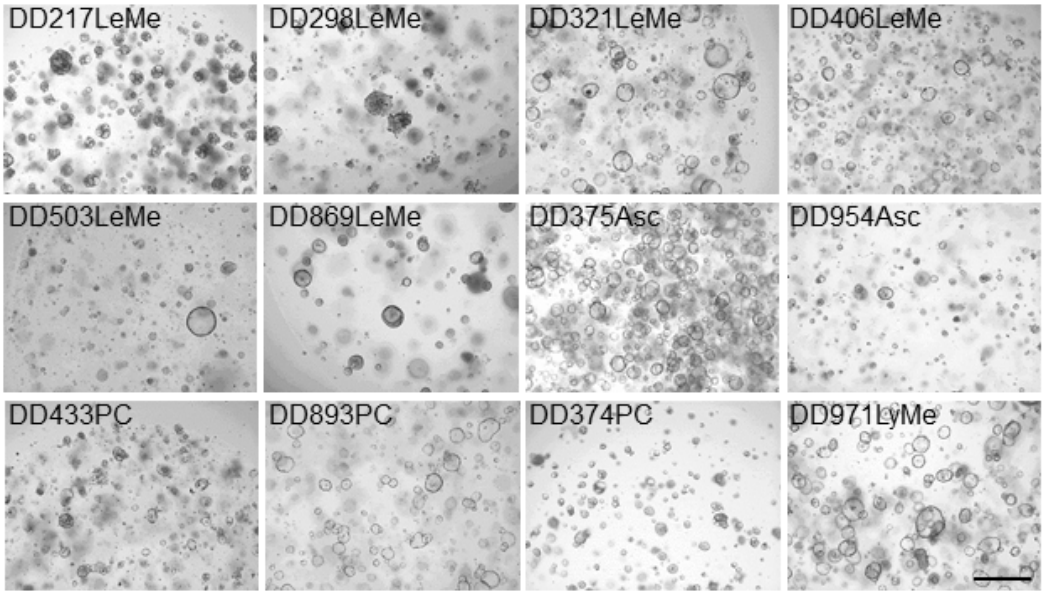

Figure 13 – PDO generation from metastatic PDAC lesions. Representative bright field images were taken to illustrate the morphologies of various PDAC metastasis PDO lines. LeMe = liver metastasis, Asc = ascites, PC = peritoneal carcinoma, LyMe = lymph node metastasis. Scale bars indicate 1000 µM.

PDACs exhibit desmoplasia characterized by high stroma content, which can resemble 90% of the whole tumor mass. Therefore, early passages of new PDO lines showed growth of adherent mesenchymal cells on the bottom of 48-well plates. Careful detachment of the Matrigel drop during passaging of the new PDO line at passage zero allowed the mechanical separation of epithelial and mesenchymal cell populations. Subsequently, the remaining adherent stroma cells can be expanded by adding PDAC medium to the 48-well plate, while PDOs were cultivated further on separated plates (Figure 14). This resulted in the generation of cancer associated fibroblasts (CAFs) cultures harboring a matching stable growing PDO line for 6 samples.

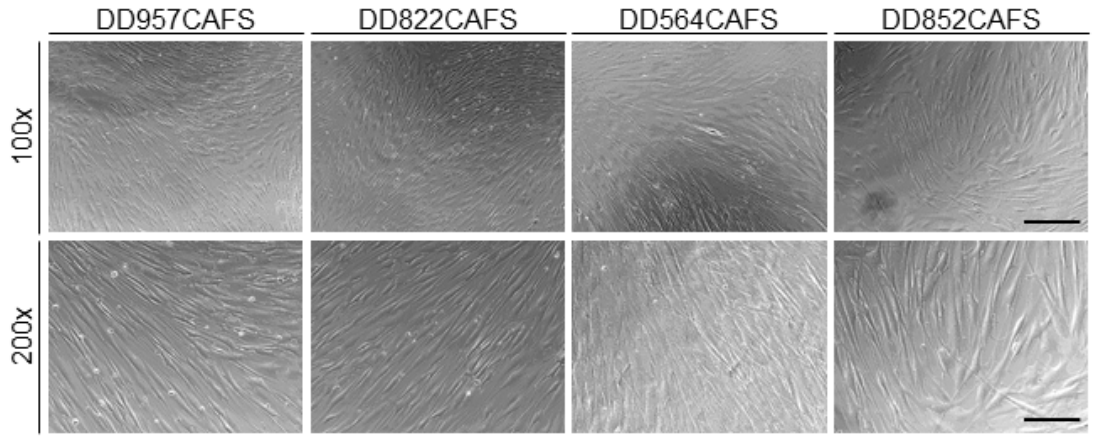

Figure 14 – Cancer associated fibroblast can be establish simultaneously to PDO lines. Representative bright field images from four CAF lines generated in parallel to patient tissue derived PDOs. Scale bars indicate 400 µM (100x) and 200 µM (200x).

In total, around 200 tissue samples have been processed resulting in 90 PDO lines growing beyond passage ten between December 2016 and June 2021. Of these PDO lines, 72 PDOs have been generated from primary tumor tissue samples, specifically 52 lines were established from surgical resection specimens from CTx naïve (n= 30) and neoCTx patients (n= 22), and 20 from CTx naïve FNA biopsies. PDOs from PDAC metastasis were generated in 12 cases and normal pancreatic PDOs from 4 specimens (Table 15).

Table 14 – Overview of the PDAC PDO biobank generated between December 2016 and June 2021

Tissue of origin	Number of PDO lines established	Overall take rate [%]	Take rate last 10 samples processed [%]
Primary PDAC			
CTx naïve (surgery)	30	45.5	70
neoCTx (surgery)	22	51.1	70
FNA biopsy	20	66.7	70
PDAC metastasis			
Liver	6	37.5	30
Peritoneum	3	25	20
Ascites	2	50	n.a.
Lymph node	1	100	n.a.
Others			
Pancreatic tissue	4	57	n.a.

Next, it was sought to evaluate whether PDO generation can be achieved in a clinically relevant timeframe. Retrospectively, the duration from sample processing till the generation of the first cryopreserved PDO sample was assessed. As protocols for the PDO generation improved over time, the last 15 PDO samples that have been successfully established were included into the retrospective analysis. Regardless of the type of starting material, no difference was observed regarding the time required for banking the first vial of cryopreserved PDOs (Figure 15A). The median for CTx naïve surgical resection specimens was 25 days, for neoCTx samples 23 days and for FNA biopsy samples 20 days (p= 0.658, one-way ANOVA).

The *KRAS* gene is mutated in ~95% of PDAC and was characterized by pyro sequencing to confirm the malignant origin of new generated organoid lines. KRAS G12D, G12V or G12R mutations were found in 43 out of 45 cases, which describes a gain-of-function mutation due to an exchange of the 12th amino acid (Figure 15B). Rare KRAS activating mutations were found in two PDAC PDO lines (Q61H and V14A).

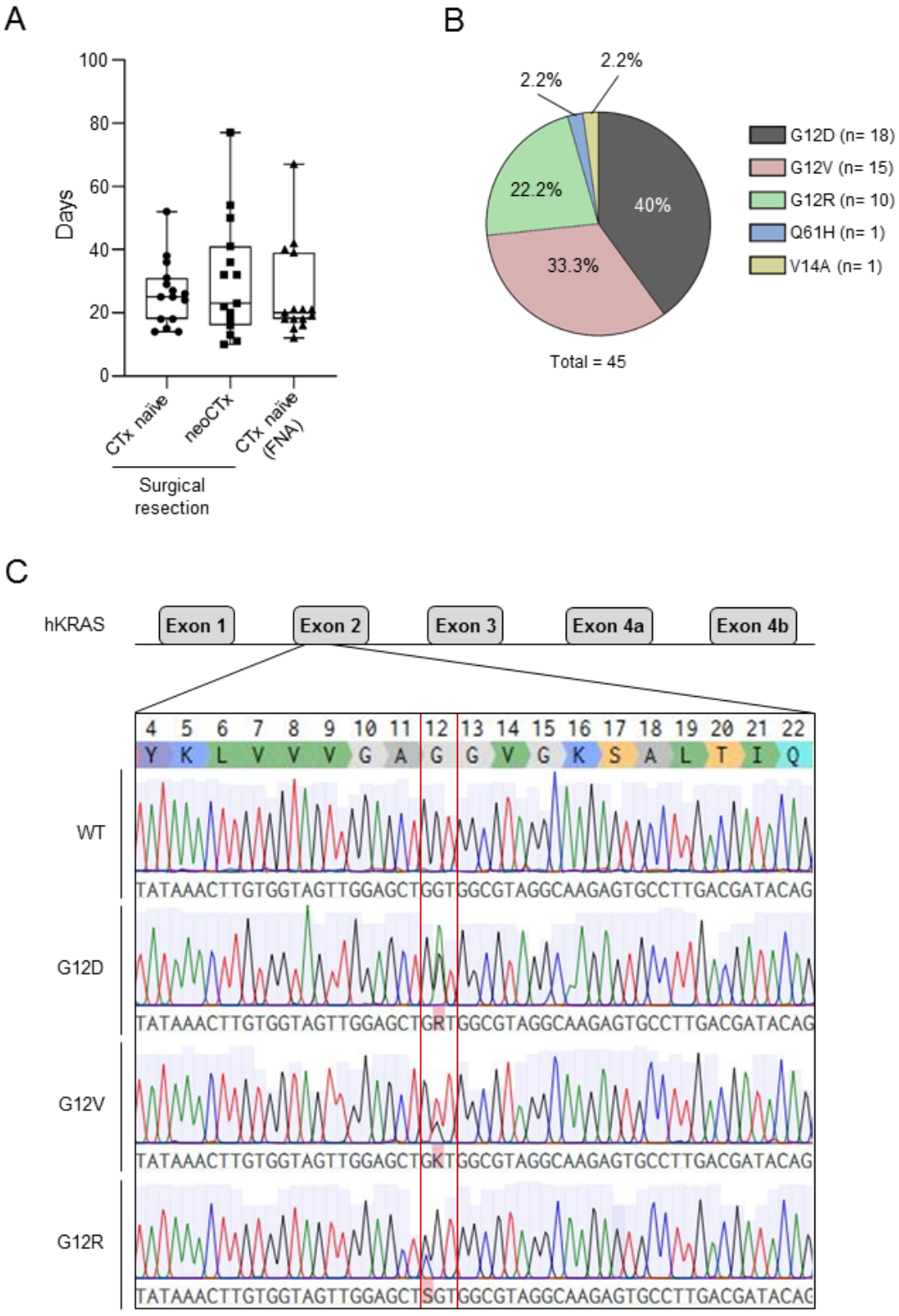

Figure 15 – Confirmation of PDAC PDOs generation within three weeks. A) Box plots depicting the time required from tumor sample processing until first vial of cryopreserved organoids from the last 15 successful generated PDO lines from surgical resection specimens (CTx naïve or neoCTx) or EUS FNA biopsies. Box plots depict the min-max value and mean. Modified from Hennig *et al.*[110]. **B)** *KRAS* mutations distribution found in 45 PDAC PDO lines sequenced are illustrated in a pie-chart. **C)** Representative results from the pyro sequencing as chromatograms verifying wild type (WT) KRAS, KRAS G12D, G12V or G12R mutations.

Pyro sequencing allows the identification of single nucleotide mutations when present in the sample in more than 10 % of alleles. Since *KRAS* often is mutated on one allele, a double peak is visible in the chromatogram on the respectively position (Figure 15C). In five cases (DD355neo, NR002, DD593neo, DD753, DD909) no wild type *KRAS* was detected, indicating the loss of the non-mutated allele. Of note, these five lines show rapid growth and require 1:6 to 1:10 splitting once a week. In some cases, no mutated *KRAS* was detected, especially when DNA was extracted from early passages. However, the respective PDO lines were considered to be originated from tumor cells if robust growth beyond passage 10 and/or displaying PDAC-like morphology was observed.

Further characterization of PDAC PDOs was done by immunohistochemically analysis of cytokeratin 19 (CK19) and tumor protein 53 (TP53) on serial sections of paraffin embedded primary tumors and their respectively matching paraffin embedded organoid lines DD314 and DD385 (Figure 16). CK19 is a marker expressed in epithelial cells of PDAC and not in the stroma, which often resembles up to 90% of the PDAC mass. Both PDO lines exhibit a strong CK19 expression proving their epithelial origin and phenotype *in vitro*. The PDAC line DD314 harbors a TP53 p.Pro223Alafs*3 frame shift mutation due to a GGCT insertion in exon 6 detected in 95.99% of all sequencing reads. This frame shift mutations leads to a premature stop codon and thereby a truncated non-functional protein. In line with that, no signal was detected in the IHC staining of the PDO and the corresponding primary tumor tissue. The opposite was observed for the primary tissue sections from which the PDO line DD385 was established, were a strong nuclear staining for TP53 was detected. The matching PDO line DD385 also showed a prominent nuclear TP53 staining.

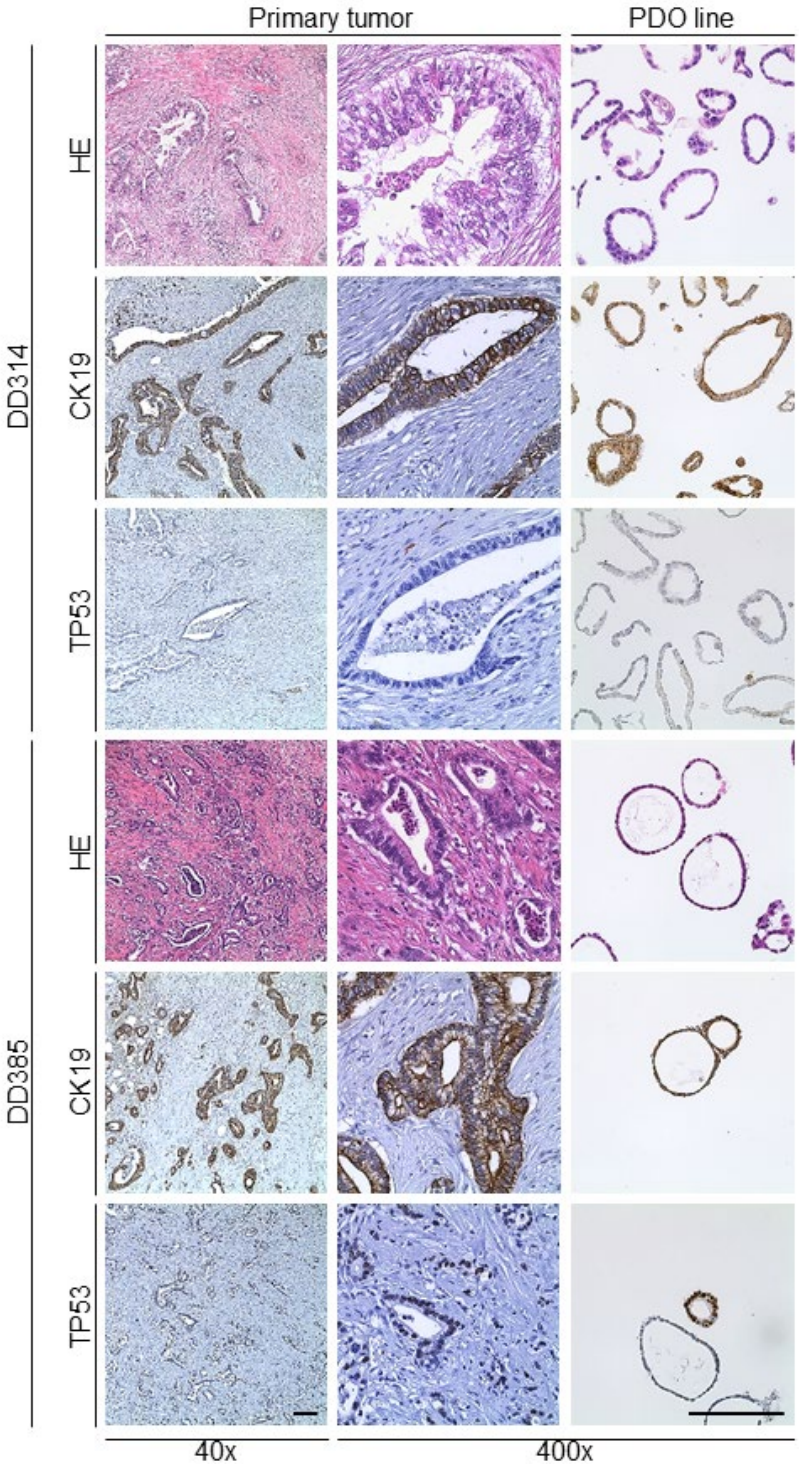

Figure 16 – PDAC PDOs share molecular properties with their matched tumor tissue. H&E and IHC staining for CK19 and TP53 on two primary tumor tissues and their corresponding PDAC PDO lines were performed showing high similarity between *in vivo* and *in vitro* systems. Scale bars indicate 400 µM. Modified from Hennig *et al.*[110].

It has been shown that PDAC can be classified into different molecular subtypes. Collisson and colleagues identified the classical-, exocrine-like- and quasi-mesenchymal subtypes, which have prognostic value[72]. According to Noll and colleagues[81], these three PDAC subtypes can be assigned by determining the protein level of HNF1A and KRT81 via IHC staining. However, a specific antibody for HNF1A was not available for several years. It was therefore assessed whether CFTR might be a potential alternative biomarker for HNF1A as it is part of the PDA assigner gene set, which classifies the exocrine-like subtype[72]. To address this question, RT-qPCR was performed to analyze the expression of both genes, *HNF1A* and *CFTR* in a set of 10 PDAC PDO lines (Figure 17A).

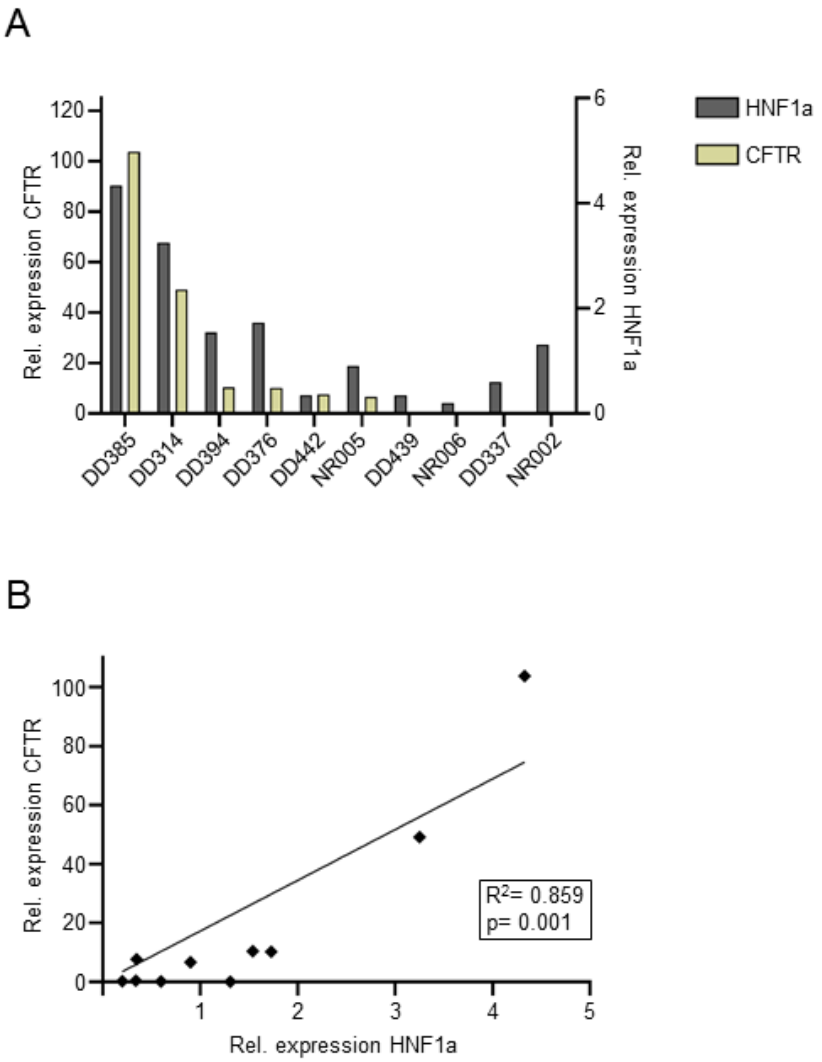

Figure 17 - The expression of *HNF1A* and *CFTR* correlate in human PDAC PDOs. A) Expression levels of *HNF1A* and *CFTR* assessed by RT-qPCR analysis in 10 PDAC PDO lines, which have been established from surgical resection specimens except NR002, NR005 and NR006. The relative expression refers to the respective mean expression within the pool of analyzed samples after normalizing to the house-keeping genes *GABDH* and *ACTB1*. **B)** Pearson correlation analysis revealed a linear correlation between the expression levels of *HNF1A* and *CFTR* in human PDAC PDOs (R^2= 0.859, Pearson correlation analysis, two-tailed, α = 0.05). Modified from Hennig *et al.*[112].

The PDAC organoid lines DD385, DD314, DD394, DD376, DD442 and NR005 were considered to co-express *HNF1A* and *CFTR.* DD439, DD337 and NR002 showed *HNF1A* but no *CFTR* expression, while NR006 was negative for both markers. Furthermore, a significant linear correlation was detected between the relative expression levels of both genes (R^2= 0.859, p= 0.001, Pearson correlation, two-tailed) (Figure 17B). In addition, RT-qPCR was performed for 13 newly established PDAC lines (DD355neo, DD372, DD412neo, DD429, DD564neo, DD577neo, DD578neo, DD593neo, DD682 (NR023), DD754 (NR027), DD776neo, DD921 (NR034) and NR018). High mRNA levels of *HNF1A* and *CFTR* were detected in DD372, DD921 (NR034), DD577neo, DD754 (NR027), NR018, DD429, DD564neo and DD593neo. A relatively high *HNF1A* but low *CFTR* expression was observed for DD412neo, DD776neo and NR002. DD682 (NR023), DD578neo and DD355neo showed an expression of both genes below the empirically determined threshold and were considered negative. Using Pearson correlation analysis of the 13 PDO lines showed a significant linear correlation (R^2= 0.587, p= 0.002, Pearson correlation, two-tailed).

Taken together, 14 out of the 23 PDAC PDO lines analyzed showed a high expression for *HNF1A* and *CFTR* whilst 6 out of 23 PDO lines examined showed no expression of both genes. Three PDO lines were only positive for *HNF1A* while *CFTR* expression was below the defined threshold (Figure 18).

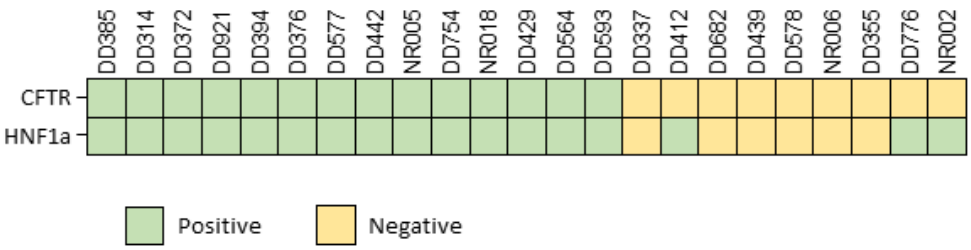

Figure 18 – PDAC PDOs exhibit differential mRNA levels for *HNF1A* and *CFTR*. The heatmap illustrates the expression levels of *HNF1A* and *CFTR* as positive (shown in green) or negative (shown in yellow) in 23 PDAC PDO lines.

To assess if mRNA expression correlates with protein expression, immunofluorescence (IF) staining for CFTR and KRT81 were performed on 10 PDAC PDO lines. The PDO line DD314 showed a high *CFTR* level, which was also detected using IF staining (Figure 19, Supplementary Figure 1). However, no signal for KRT81 was detected, which implies that DD314 is classified as the exocrine-like PDAC subtype. In contrast, DD337 was negative for CFTR protein expression, whilst strong staining for KRT81 was observed. This correlates with the *CFTR* mRNA data and assigns DD337 to the quasi-mesenchymal subtype. Besides DD314, the PDO lines DD376, DD385, DD394 and DD442 were exclusively positive for CFTR using IF staining. On the other hand, a strong KRT81 but no CFTR signal was detected in DD439

and NR006. NR005 exhibited neither KRT81 nor CFTR signal and NR002 was positive for both markers on protein level. In both cases, protein and mRNA levels for CFTR did not correlate.

In conclusion, 8 out of 10 stained PDO lines have been classified to the most frequent PDAC subtypes: exocrine-like ($CFTR^{+}/KRT81^{-}$) or quasi-mesenchymal ($CFTR^{-}/KRT81^{+}$). Only one of the tested PDAC lines classified as classical subtype ($CFTR^{-}$ /$KRT81^{-}$). The subtyping of one PDO line was not possible due to the strong expression of both markers ($CFTR^{+}/KRT81^{+}$). Furthermore, IF stainings for CFTR and mRNA expression data were consistent in 8 out of 10 PDO lines analyzed.

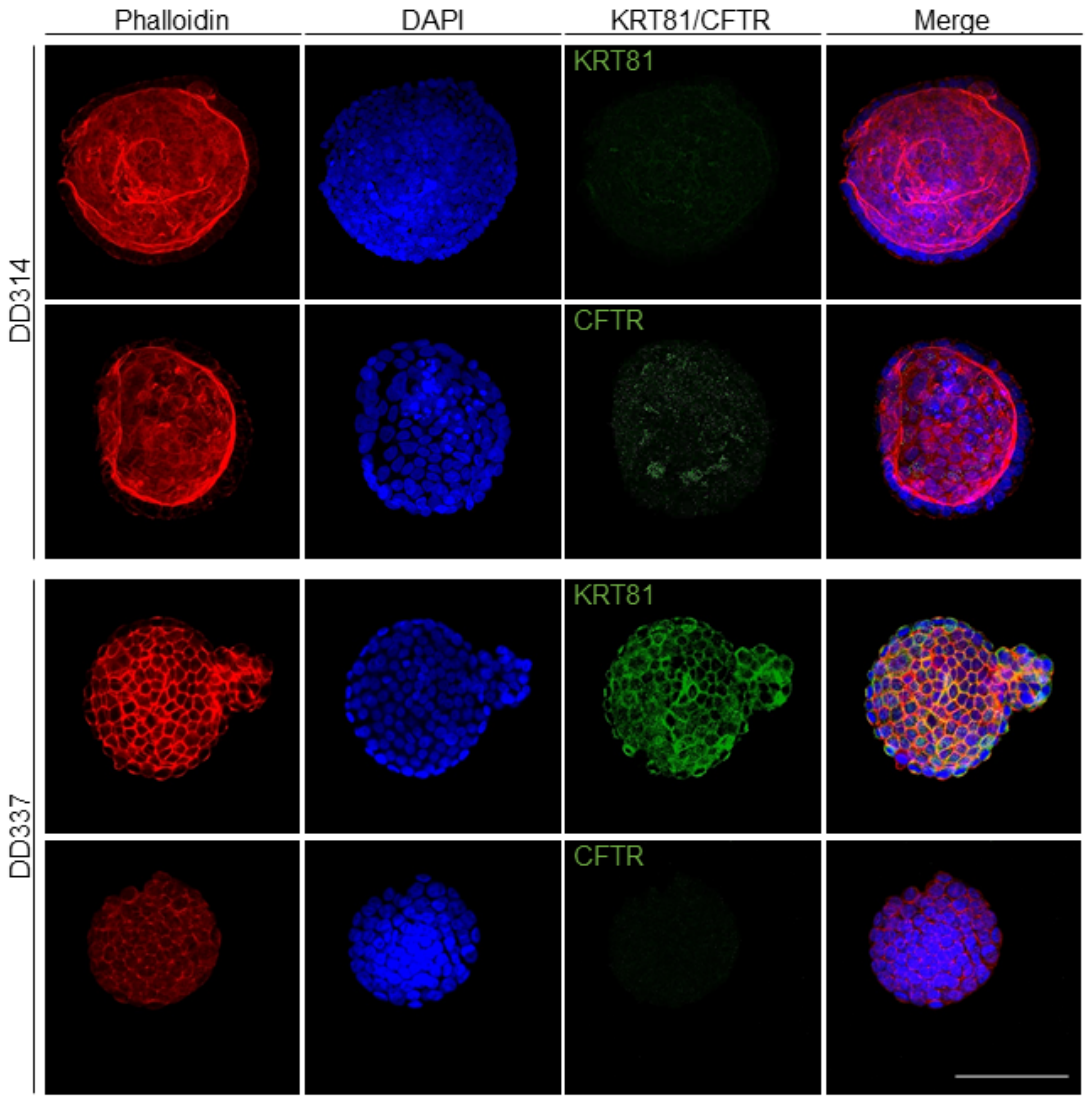

Figure 19 – CFTR and KRT81 are mutual exclusive for most PDAC PDOs. Representative confocal immuno-fluorescence microscopy images of the PDAC PDO lines DD314 and DD337 stained for CFTR and KRT81. DAPI stained cell nuclei and Phalloidin stained F-Actin. Scale bar indicates 200 µM. Modified from Hennig *et al.*[110].

To examine if PDOs recapitulate the same PDAC subtype as the primary tumor from which they were derived from, IHC stainings for CFTR and KRT81 were performed on 7 paraffin embedded PDAC tumor sections that matched the following PDOs: DD314, DD337, DD376, DD385, DD394, DD439 and DD442 (Figure 20, Supplementary Figure 2). The primary tumor corresponding to DD314 showed a strong CFTR staining and minimal KRT81 expression, which is in line with the subtyping of DD314. The PDO line DD337 revealed the quasi-mesenchymal subtype, which was also seen by strong KRT81 and no CFTR expression of the primary tumor tissue.

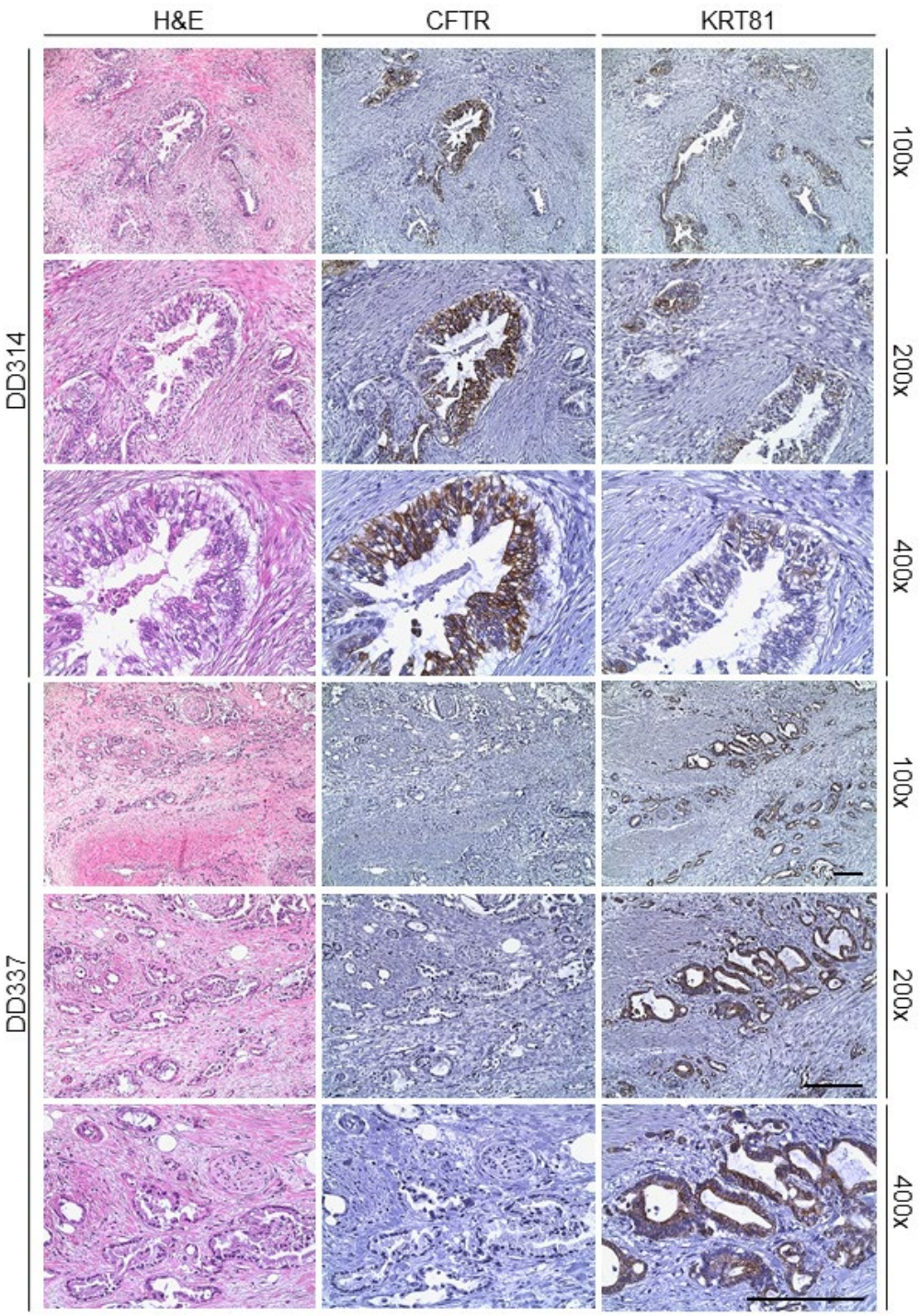

Figure 20 – CFTR and KRT81 are mutually exclusively in primary PDAC tissue. IHC staining of CFTR and KRT81 on paraffin embedded primary tumor tissue sections allows molecular subtyping of PDACs. Scale bars indicate 200 µM. Modified from Hennig *et al.*[110].

The staining of primary tumor sections matching to DD376, DD385, DD394 and DD442 exhibited the same staining pattern ($CFTR^+$/ $KRT81^-$) as seen for DD314. The tumor tissue matching to DD439, however, stained positive for CFTR and KRT81 which contrasts with the PDO line that only showed strong KRT81 expression.

In summary, CFTR and KRT81 expression patterns is preserved in the matched established organoid lines in six out of seven primary tumors examined (Figure 21).

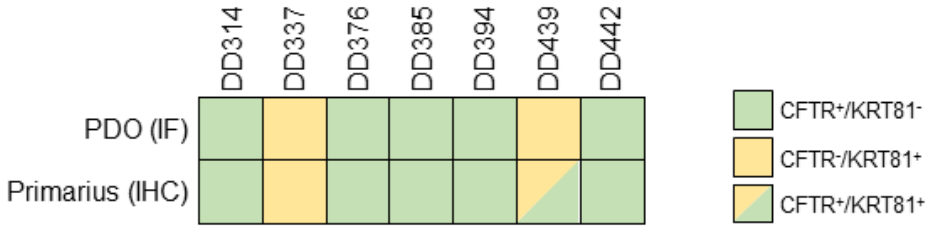

Figure 21 – PDOs preserve the PDAC subtype of their respective tissue of origin. The heatmap illustrates the assessed PDAC subtypes of exocrine like (green, $CFTR^{+}/KRT81^{-}$) and quasi-mesenchymal (yellow, $CFTR^{-}/KRT81^{+}$) in 7 PDO lines and their corresponding primary tumor. Subtyping was carried out by IF staining on PDOs and IHC on paraffin-embedded primary tumor tissue sections.

9.3 Chapter 3 – Detection of drug resistances and sensitivities in PDAC PDOs can guide optimized CTx treatments

PDAC PDOs share molecular properties with their tissue of origin in most cases and can be established rapidly with high take rates even from minimal starting material such as EUS-FNA samples. At first it was sought to assess response of PDO lines to common clinically relevant chemotherapeutic substances. This so called pharmacotyping is of relevance to address the question whether PDAC PDOs represent a new tool for predicting patients' response to (neo-) adjuvant CTx treatment. Requirements for such drug screening platform are (i) low number of PDOs for the assay, (ii) a minimal amount of Matrigel and cultivation medium, (iii) high reproducibility and an experimental setting that could be automated in the future.

Initially, a 96-well plate-based system has been used to determine the optimal dilution range for five chemotherapeutic drugs used: irinotecan, oxaliplatin, 5-FU, gemcitabine, and paclitaxel, all of which are compounds of the standard of care multi-drug regimens FOLFIRINOX (irinotecan, oxaliplatin and 5-FU) and gemcitabine/nab-paclitaxel (gemcitabine and paclitaxel). However, 50 µl Matrigel and 100 µl medium per sample and dilution as well as a high number of PDOs are required to conduct drug assays with this setting. As a result, the assay was switched to a 384-well plate format, which significantly reduced both, the amount of Matrigel and medium needed by 70% and 60% respectively. Furthermore, between up to three dense growing wells (48-well plate) are sufficient for testing all five chemotherapeutic drugs in one experiment. Next, diluting Matrigel with cultivation medium was tested and revealed that 75% Matrigel does not affect the reproducibility of the experiments. Lower Matrigel content resulted in an outgrowth as 2D cell culture which impacted the response to the drugs tested. Overall, the amount of Matrigel needed, which is very cost-intensive, was reduced from 50 µl to 11.25 µl per sample.

To evaluate the robustness of the drug response across different PDO passages, pharmacotyping of PDO line DD442 by exposing to irinotecan, oxaliplatin and 5-FU (Figure 22A) as well as gemcitabine and paclitaxel (Figure 23A) was performed in three individual experiments over a period of 6 passages. For all the used drugs, the empirically adjusted dilution ranges were suitable to display the minimum and maximum cytotoxic drug mediated effects. In addition, the measured viabilities corresponded to the bright field microscopy images taken for all samples (Figure 22B & 23B).

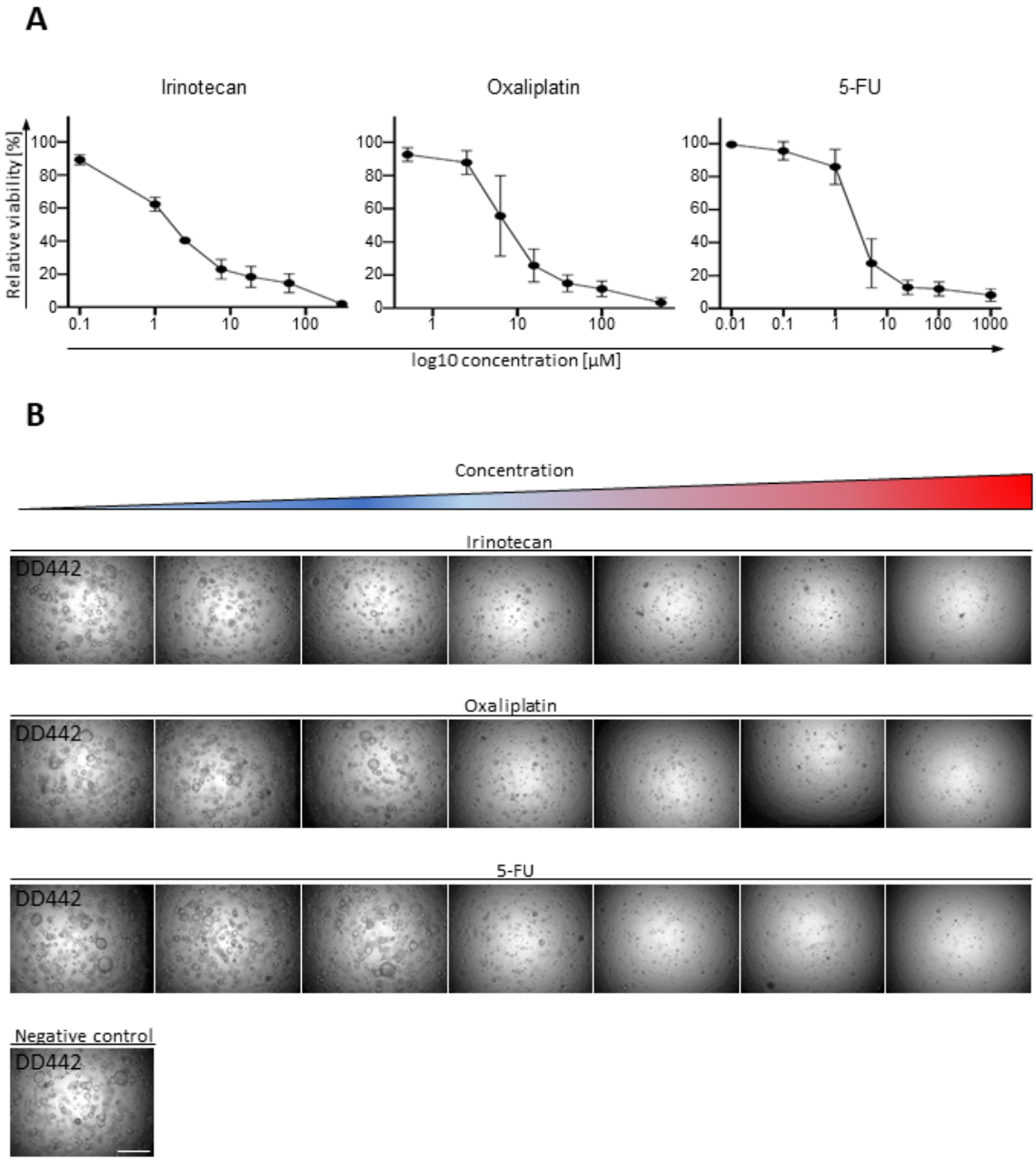

Figure 22 – PDAC PDO irinotecan, oxaliplatin and 5-FU pharmacotyping in 384-well plate format resembles a suitable robust setting. A) Dose response curve for DD442 PDAC PDOs treated with different concentrations of irinotecan, oxaliplatin and 5-FU. Illustrated is the mean of three biological replicates with standard deviation error bars. **B)** Bright field images were taken from each dilution step after 144h of drug treatment with irinotecan, oxaliplatin and 5-FU. Scale bar indicates 1000 µM.

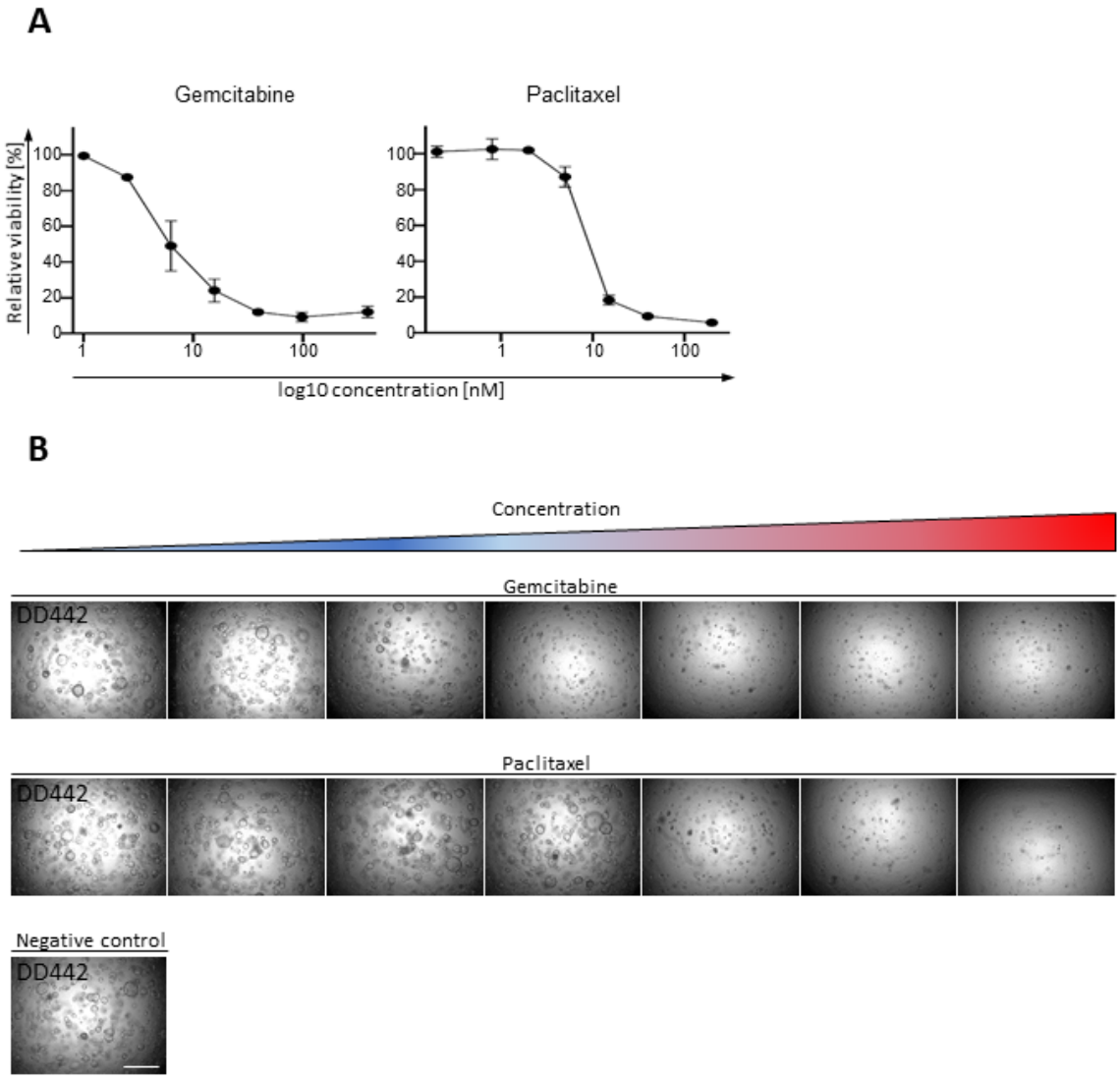

Figure 23 – **Establishing a 384-well plate system for gemcitabine and paclitaxel pharmacotyping of PDAC PDOs. A)** Dose response curve for DD442 PDAC PDOs treated with different concentrations of gemcitabine and paclitaxel. Illustrated is the mean of three biological replicates with standard deviation error bars. **B)** Bright field images were taken from each dilution step after 144h of drug treatment with the respective chemotherapeutic compound. Scale bar indicates 1000 µM.

After the platform for PDO pharmacotyping has been established, 10 PDAC organoid lines from CTx naïve patients have been characterized in terms of their individual response to irinotecan, oxaliplatin, 5-FU, gemcitabine, and paclitaxel (Figure 24A). A diverse response has been observed between all PDO lines tested. Subsequently each sample's AUC was calculated followed by normalizing via z-score determination (Figure 24B). No co-occurrence of resistances was seen. DD314 and DD376 showed poor response to three substances (z-score > 0.75), while DD337, DD385 and DD439 were resistant to two drugs. Three PDO lines (DD372, DD429 and DD728) were resistant to one out of five drugs tested. DD442 and DD909 were not resistant to any drug tested, but sensitive to two and four substances respectively (z-score < -0.75).

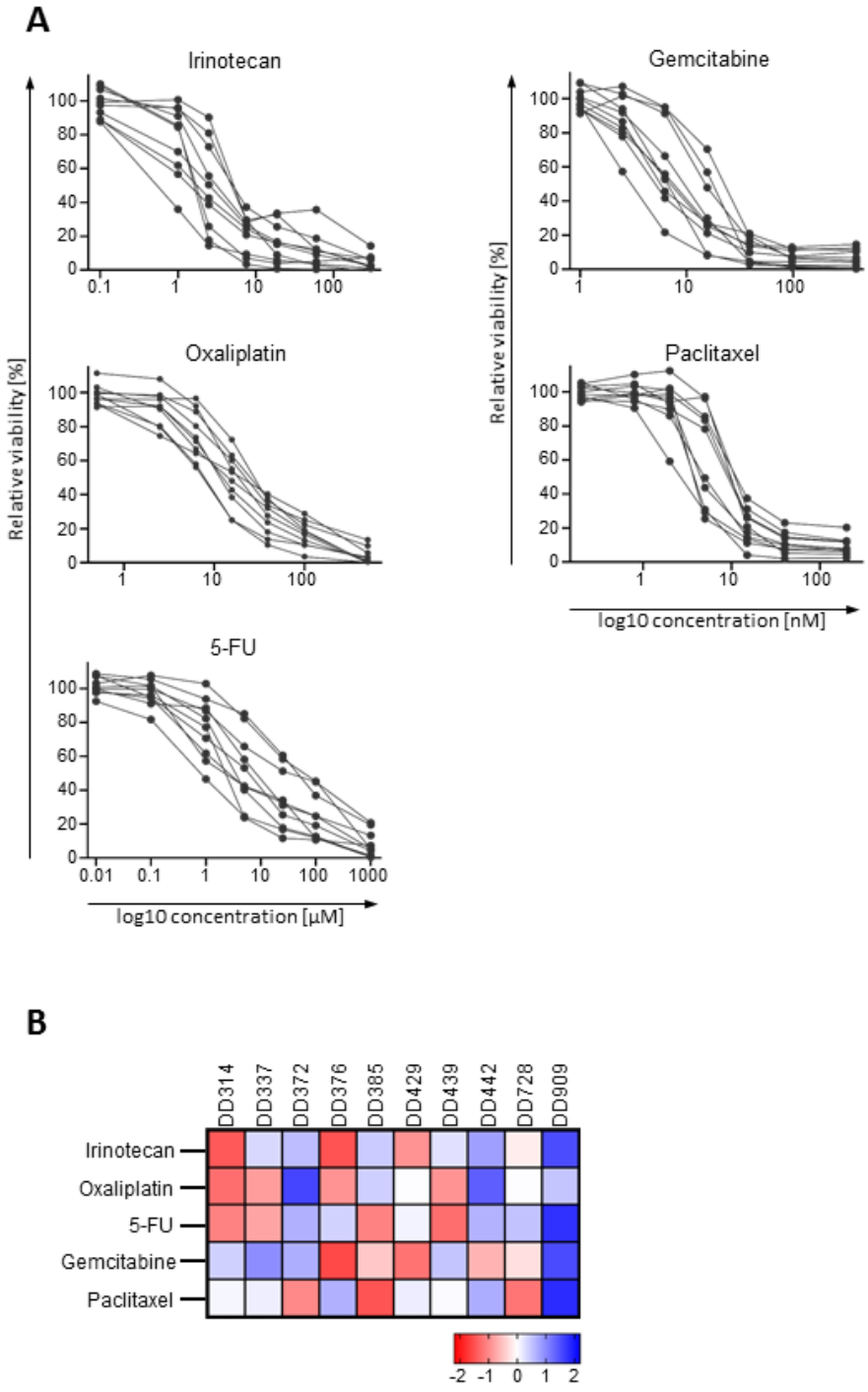

Figure 24 – Pharmacotyping of 10 CTX naïve PDAC PDO lines reveals individual drug response profiles. A) Drug dose-response curves for 10 PDAC PDO lines treated with single agent irinotecan, oxaliplatin, 5-FU, gemcitabine, or paclitaxel. Three individual experiments were performed for each PDO line and drug and mean viabilities for each dilution step illustrated. **B)** Heat map of z-score normalized drug responses. Sensitivity and resistance to drug treatment is indicated by blue and red colored boxes, respectively.

FOLFIRINOX and Gem/nab-Pac are the standard of care for neoCTx of LA PDAC. Multi-drug protocols are also commonly used in the adjuvant setting (of note, after surgical resection of the primary tumor). For this reason, PDAC PDO lines from CTx naïve patients that previously have been analyzed for their response to single agents were treated with the drug combination FOLFIRINOX and Gem/Pac. All 10 PDO lines showed an individual pattern with respect to the response to both protocols (Figure 25A). The viability measured for each sample corresponded to the number and size of organoids observed on microscopically images taken (Figure 25B). The normalization via z-scoring of AUCs was performed for both treatments for classification of PDO lines into sensitive (z-score ≤ -0.75), intermediate (0.75 > z-score > -0.75) and resistant lines (z-score ≥ 0.75) (Figure 25C). A poor response for FOLFIRINOX was observed for the PDO lines DD337 and DD385. PDO lines that have been classified as good responders for the same treatment were DD372 and DD909. Besides DD385, the organoid line DD728 showed resistance to the Gem/Pac regimen, while DD337 and DD376 were sensitive to the respective therapy. To the contrary, DD385 was resistant to both multi-drug treatments. The PDO line DD337 showed resistance and sensitivity to one of each treatment (Figure 25C + D).

Pearson correlation analysis was performed revealing no connection between sensitivities and resistances to FOLFIRINOX and Gem/Pac in PDAC PDOs (R^2= 0.19, p= 0.21) (Figure 25D).

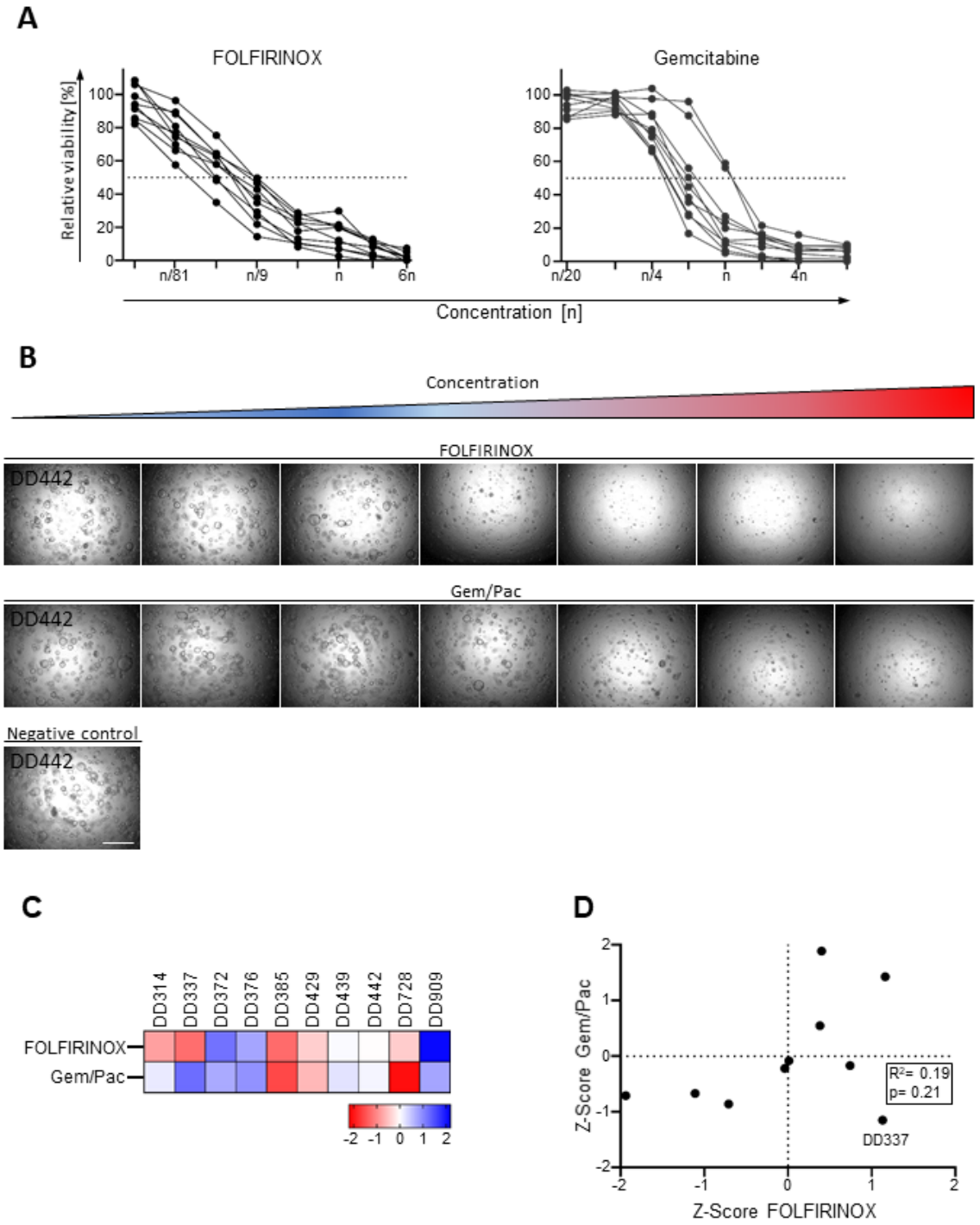

Figure 25 - PDAC PDOs show cell line individual drug responses to FOLFIRINOX and Gem/Pac multi-drug therapy. A) Drug dose-response curves (mean of three individual experiments) for 10 PDAC PDO lines derived from CTx naïve patients treated with FOLFIRINOX or Gem/Pac combination therapy. **B)** Bright field images taken from each dilution step after 144h of drug treatment with the respective regimen. Scale bar indicates 1000 µM. **C)** Heat map of z-score normalized AUCs from FOLFIRINOX or Gem/Pac treated PDAC PDOs. Sensitivity and resistance to drug treatment is indicated by blue and red colored boxes, respectively. **D)** FOLFIRINOX and Gem/Pac treatment z-scores from 10 CTx naïve PDO lines were analyzed using Pearson correlation analysis. Modified from Hennig *et al.*[110].

It has not been investigated how neoCTx impacts the drug sensitivity of residual disease in the patient after PDAC surgery. However, this could be of importance when choosing the adjuvant therapy protocol for neoCTx patients. Therefore, six PDAC PDOs established from surgical resection specimens from patients that were treated with FOLFIRINOX in the neoadjuvant setting, were characterized with respect to their response to irinotecan, oxaliplatin and 5-FU (Figure 26A). For all six neoCTx PDAC PDO lines an individual response pattern was observed. Comparison of AUC_{rel} between CTx naïve and neoCTx PDAC PDOs revealed no significant differences in drug response to irinotecan, oxaliplatin or 5-FU (irinotecan p= 0.27; oxaliplatin p= 0.09; 5-FU p= 0.9, Mann-Whitney test) (Figure 26B). Yet, a trend towards poor response to oxaliplatin was identified for PDAC PDOs, which have been established from FOLFIRINOX pretreated patients.

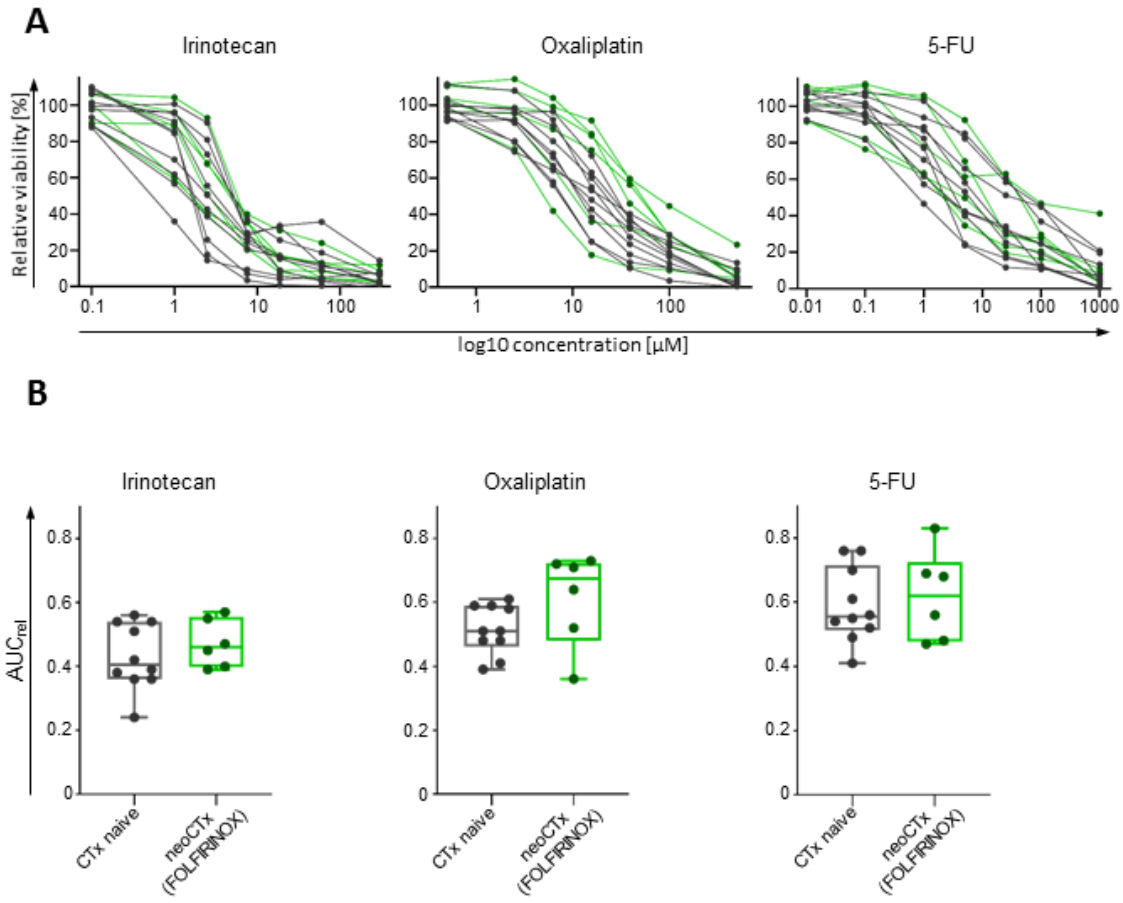

Figure 26 – Comparison of CTx naïve and neoCTx response to single agent irinotecan, oxaliplatin or 5-FU. A) Dose response curves from 10 CTx naïve (black lines) and six neoCTx (green lines) PDO lines treated with irinotecan, oxaliplatin or 5-FU. The viability in % at different drug concentrations is illustrated. **B)** Box plot diagram showing the relative AUC (AUC_{rel}) calculated from the dose-response curves from A) separated according to the cohort of CTx naïve and neoCTx PDO lines.

In addition to the substances included in the FOLFIRINOX protocol, the response to gemcitabine and paclitaxel, which are components of the Gem/nab-Pac regimen, were compared between PDOs derived from CTx naïve and neoCTx patients. Four PDO lines were successfully established from patients that were only treated with Gem/Pac and subsequently were pharmacotyped (Figure 27A). The most sensitive PDO lines to Gem/Pac were found in the group of CTx naïve lines. AUC_{rel} analysis showed a nearly significant difference between both groups in their response to paclitaxel (p= 0.08, Mann-Whitney test) and no impact on gemcitabine sensitivities (p= 0.43, Mann-Whitney test) (Figure 27B).

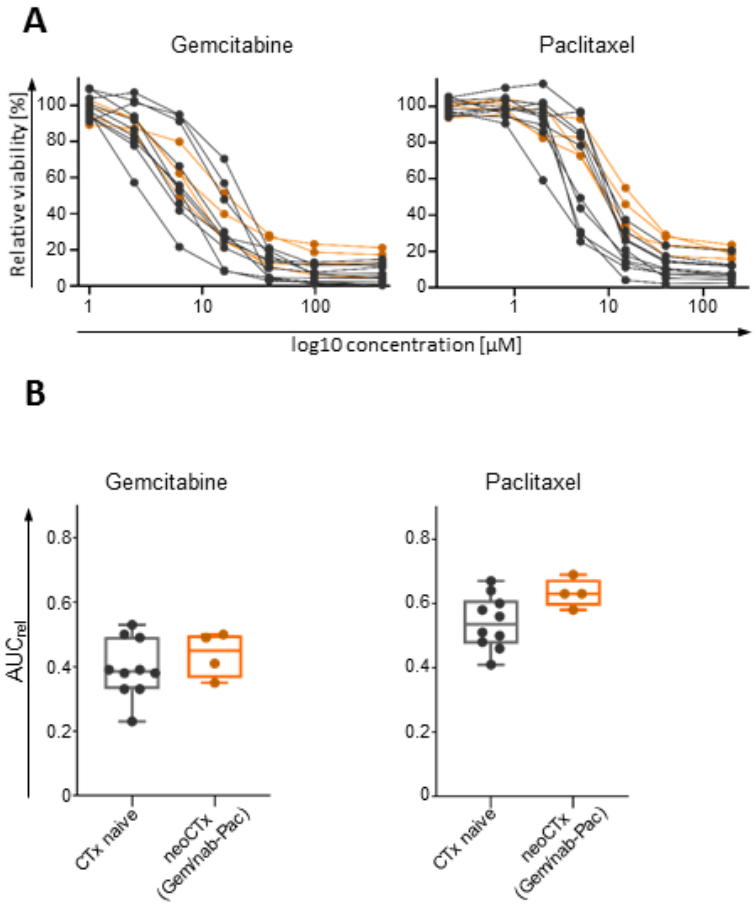

Figure 27 - Comparison of CTx naïve and neoCTx response to single agent gemcitabine or paclitaxel. A) Dose response curves from 10 CTx naïve (black lines) and four neoCTx (orange lines) PDO lines treated with gemcitabine or paclitaxel. The viability in % at different drug concentrations is illustrated. **B)** Box plot diagram showing the relative AUC (AUC_{rel}) calculated from the dose-response curves from A) separated according to the cohorts of CTx naïve and neoCTx PDO lines.

Subsequently, the impact of neoCTx treatment on drug response was investigated in the multi-drug setting by treating neoCTx PDAC PDOs with either FOLFIRNOX or Gem/Pac. In total, eight FOLFIRINOX and five Gem/Pac pretreated PDO lines have been included into the analysis. PDO line individual responses to both regimens were observed and more distinct compared to single drug assay data (Figure 28A). Merging of FOLFIRINOX drug assay data from 10 CTx naïve and eight neoCTx PDO lines showed that the two worst responding organoid lines were established from pretreated patients that received the respective CTx regimen (Figure 28B). Furthermore, the two most sensitive PDO lines to FOLFIRINOX were generated from CTX naïve patients. In line with that, the PDO line with the highest resistance to Gem/Pac treatment was established from a Gem/nab-Pac pretreated patient. Yet, no significant differences for both regimens were seen (FOLFIRINOX p= 0.282; Gem/Pac p= 0.051; Mann-Whitney test), but a clear tendency to reduced sensitivity to Gem/Pac in neoCTx patients was observed (Figure 28B).

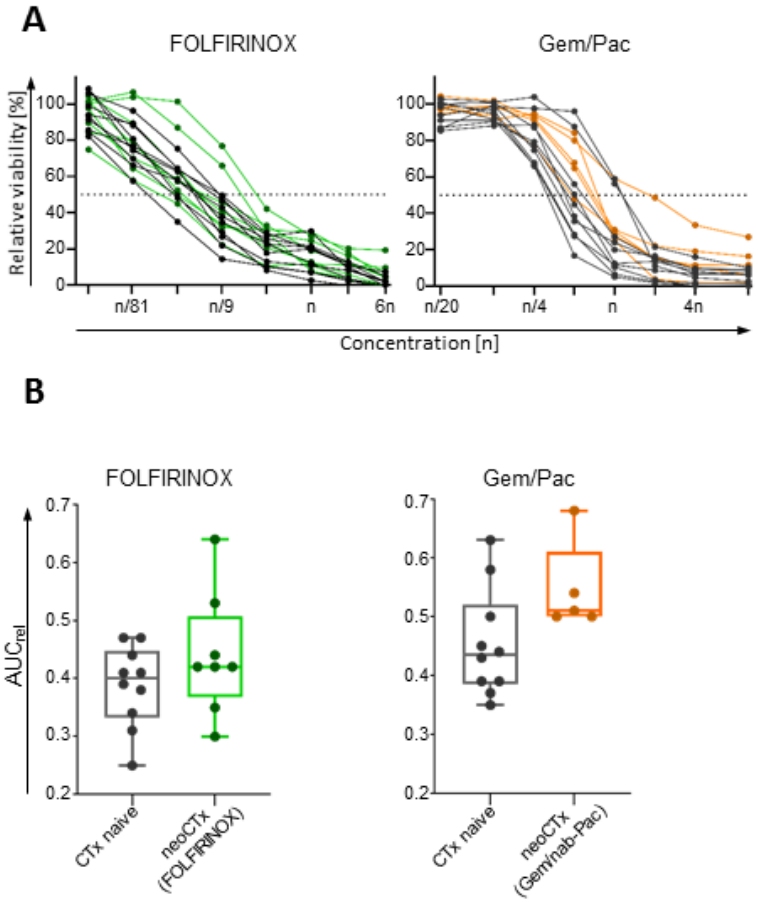

Figure 28 - NeoCTx with FOLFIRINOX or Gem/Pac shapes PDAC PDOs sensitivity to multi-drug regimens. A) Dose-response curves from CTx naïve and neoCTx PDO lines treated with different concentrations of either FOLFIRINOX or Gem/Pac. For each multi-drug concentrations, the mean relative viability in % from three independent experiments is illustrated. Data from CTx naïve PDO lines are depicted in dark grey. Drug assay data from FOLFIRNOX or Gem/nab-Pac pretreated patients are green and orange, respectively. **B)** Box plots illustrating AUC_{rel} values of CTx naïve or neoCTx PDO lines treated with either FOLFIRINOX or Gem/Pac multi-drug regimen according to patients' pretreatment. Modified from Hennig *et al.*[110].

To examine if any common pattern between single- and multi-drug responses data are present, z-score normalization was performed included drug assay results from both groups, CTx naïve and neoCTx PDO lines (Figure 29A). Sensitivity for a chemotherapeutical drug or drug combination was considered when z-scores were -0.75 or below, while resistance was determined when z-scores were 0.75 or higher. Because of that, the five PDO lines DD909, DD593, DD372 and DD376 showed FOLFIRINOX sensitivity. Except for DD376, none of these PDO lines showed resistance to any single drugs included in the respective multi-drug regimen. In contrast, the PDO lines DD577, DD412, DD355 and DD394, all resistant to FOLFIRINOX, showed poor response to at least two compounds part of the respective combination treatment. Using the same thresholds, six Gem/Pac sensitive PDO lines were identified (DD337, DD376, DD909, DD372, DD577 and DD439). Except for DD577 and DD439, all PDO lines were sensitive for one substance, gemcitabine, or paclitaxel. Interestingly, DD577 showed intermediate sensitivity for both single drugs and still responded well to the combination of both. DD394, DD728, DD1076, DD1152, DD355 and DD385 showed Gem/Pac resistance and were also resistant to at least one of the two single drugs if determined. Pearson correlation analysis revealed a strong connection between the z-score to either FOLFIRINOX or Gem/Pac treatment and the z-score of the most efficient single drug which is part of the respective combination regimen (FOLFIRINOX R^2= 0.58, p= 0.0001; Gem/Pac R^2= 0.47, p= 0.0009; Pearson correlation) (Figure 29B). This observation implies that not all chemotherapeutical substances within a given combination therapy drive cytotoxicity equally.

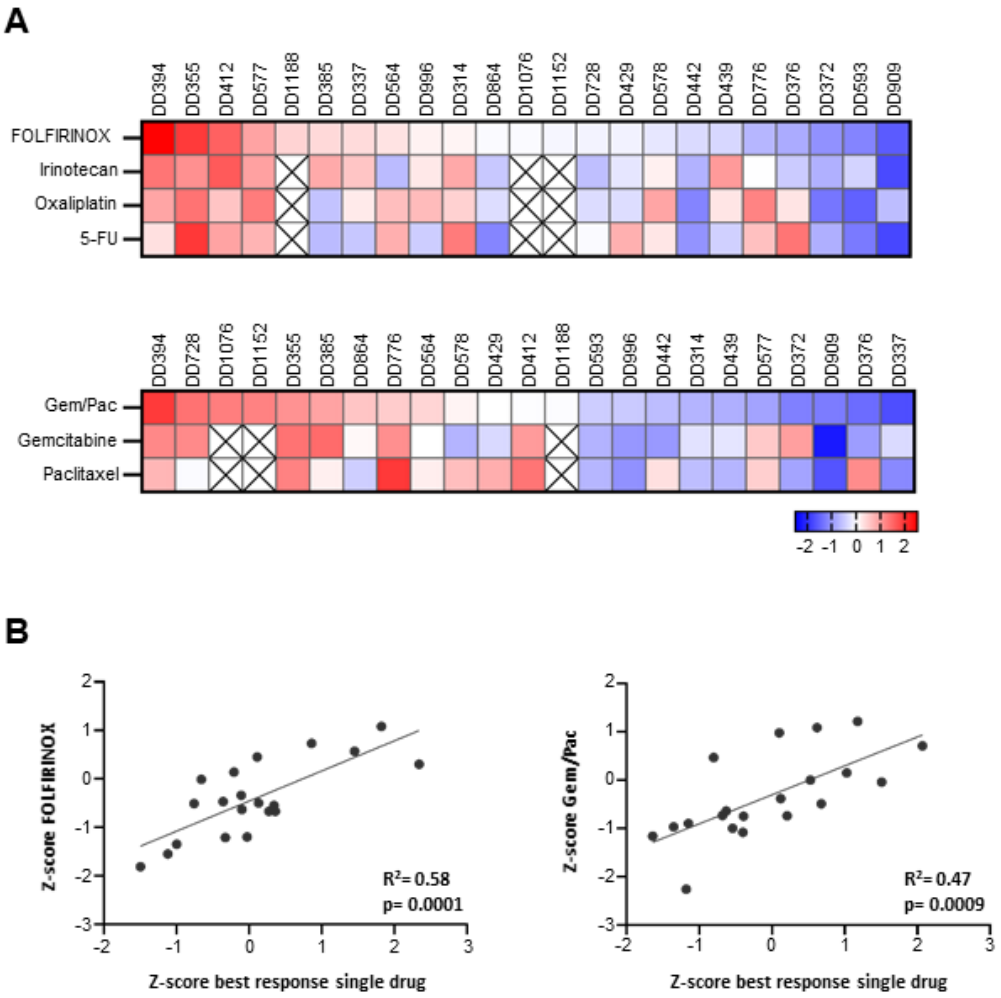

Figure 29 – PDAC PDOs response to FOLFIRINOX or Gem/Pac depends on the most efficient single drug of the corresponding regimen. A) Heat map showing z-scores calculated from AUC values of all 23 PDAC PDO lines treated with FOLFIRINOX, Gem/Pac or the respective single agent irinotecan, oxaliplatin, 5-FU, gemcitabine, and paclitaxel. Blue = good response, White = intermediate response, Red = poor response, empty boxes = not determined. **B)** Pearson correlation analysis of z-scores from 20 FOLFIRINOX (left) and 20 Gem/Pac (right) treated PDO lines and their corresponding lowest single-drug z-score. Modified from Hennig *et al.*[110].

The PDO lines DD385, DD439 and DD564 revealed sensitivity and resistance for a least one FOLFIRINOX compound (Figure 29A), which represents them as ideal candidates for the analyses of individual substance efficacy in drug combination treatments. Subsequently, these PDO lines were treated with different concentrations of FOLFIRINOX and a modified drug combination containing only two of three drugs (irinotecan + oxaliplatin, irinotecan + 5-FU, oxaliplatin + 5-FU). Additionally, DD412 was included into the analysis, since this PDO line showed poor response to all three substances(Figure 30). For DD385 a significant reduced killing efficacy compared to the triple drug treatment was seen. The removal of 5-FU from the regimen was in line with the high sensitivity determined in single agent experiments (Iri + Oxa vs. FOLFIRINOX; $p< 0.001$; three-way ANOVA). However, removing oxaliplatin from the drug mixture, for which a good response was detected, did not affect the mediated cytotoxicity compared to the triple-therapy (Iri + 5-FU vs. FOLFIRINOX; $p= 0.345$; three-way ANOVA). For irinotecan, no drug response reduction was observed after removal from the complete combination treatment (Oxa + 5FU vs. FOLFIRINOX, $p= 0.653$, three-way ANOVA). Similar results were seen for the PDAC PDO line DD439, previously classified as irinotecan resistant and 5-FU sensitive. A significant reduction of cytotoxicity was only measured, when 5-FU was removed from the FOLFIRINOX regimen (Iri + Oxa or Iri + 5-FU or Oxa + 5-FU vs. FOLFIRINOX: $p= 0.007$, $p= 0.949$ and $p= 0.929$, respectively; three-way ANOVA) indicating that this compound might be the main driver of cytotoxicity. DD564 on the other hand, responded to irinotecan treatment, whilst being resistant to 5-FU. Consequently, cytotoxicity was only negatively impacted when irinotecan was excluded from the treatment (Iri + Oxa or Iri + 5-FU or Oxa + 5-FU vs. FOLFIRINOX: $p= 0.995$, $p= 0.929$ and $p= 0.043$, respectively; three-way ANOVA). For all three PDO lines, DD385, DD439 and DD564, a less severe two-drug treatment was potentially identified which showed similar efficacy to FOLFIRINOX. The analysis of DD412, resistant to irinotecan as well as 5-FU and intermediate responder to oxaliplatin, showed no significant change to any modified FOLFIRINOX (Iri + Oxa or Iri + 5-FU or Oxa + 5-FU vs. FOLFIRINOX: $p= 0.392$, $p= 0.992$ and $p= 0.986$, respectively; three-way ANOVA).

In summary, for PDO lines with a good response to at least one single compound part of FOLFIRINOX, a treatment reduction from three to two substances was possible without impacting the overall drug response. For PDO lines with known intermediate or poor response to all three compounds of the FOLFIRINOX protocol, comparable results have been achieved for leave-one-out combinations.

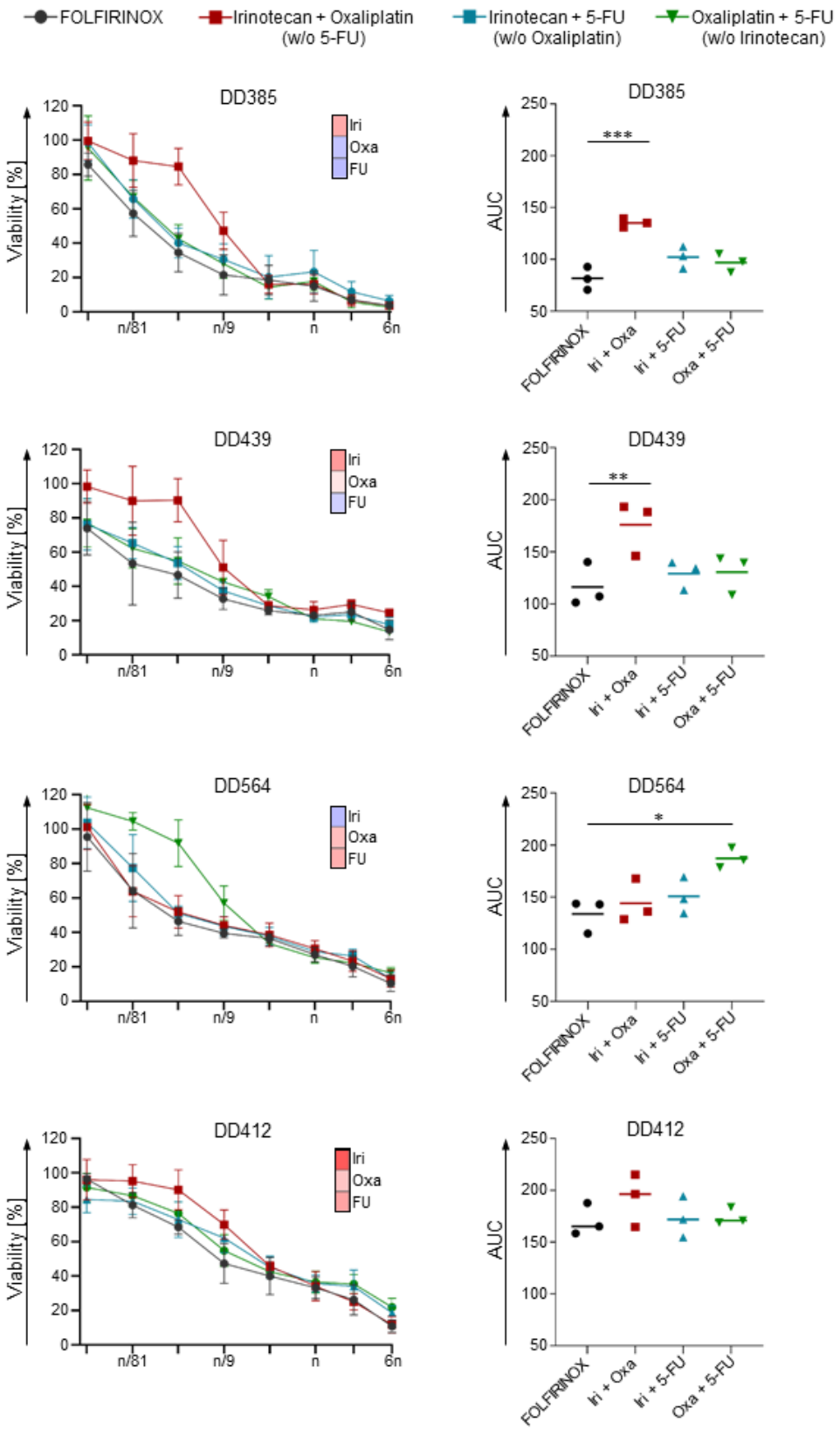

Figure 30 – Adaption of the FOLFIRINOX multi-drug therapies without affecting efficacy can be achieved through PDAC PDO pharmacotyping. Dose response curves of the four PDAC PDO lines DD385, DD439, DD564 and DD412 treated with FOLFIRINOX or the leave-one-out combinations irinotecan + oxaliplatin, irinotecan + 5-FU or oxaliplatin + 5-FU. Colored boxes illustrate the z-scores depicted in Figure 29A and indicate the PDO lines individual response to the single compounds (red = poor response, blue = good response). Statistical analysis was performed using the one-way ANOVA (* $p < 0.05$, ** $p < 0.01$, *** $p < 0.001$). Modified from Hennig *et al.*[110].

Retrospective data analysis has been conducted to assess the impact of modified Gem/Pac on the drug response in the four PDAC PDO lines DD372, DD376, DD429 and DD442, all of which showed resistance to one of the two regimen compounds (Figure 29A). For the PDO line DD372 a reduced response was seen, when paclitaxel was removed, while mono-treatment with the same drug showed nearly identical results as seen for the Gem/Pac dual-drug assay (Gem or Pac vs. Gem/Pac: $p= 0.020$ and $p= 0.824$, respectively; one-way ANOVA) (Figure 31). The opposite was shown for DD376, DD429 and DD442 which are paclitaxel resistant and gemcitabine sensitive. Treatment with single agent gemcitabine was nearly as efficient as the Gem/Pac combination therapy, whilst paclitaxel monotherapy showed a significant reduced mediated cytotoxicity (DD376: Gem or Pac vs. Gem/Pac: $p= 0.171$ and $p< 0.001$; DD429: Gem or Pac vs. Gem/Pac, $p= 0.929$ and $p< 0.001$; DD442: Gem or Pac vs. Gem/Pac, $p= 0.542$ and $p= 0.024$, respectively).

Taken together, for all four PDAC PDO lines treatment with the most efficient single substances resulted in similar response patterns as seen for the combination therapy of Gem/Pac.

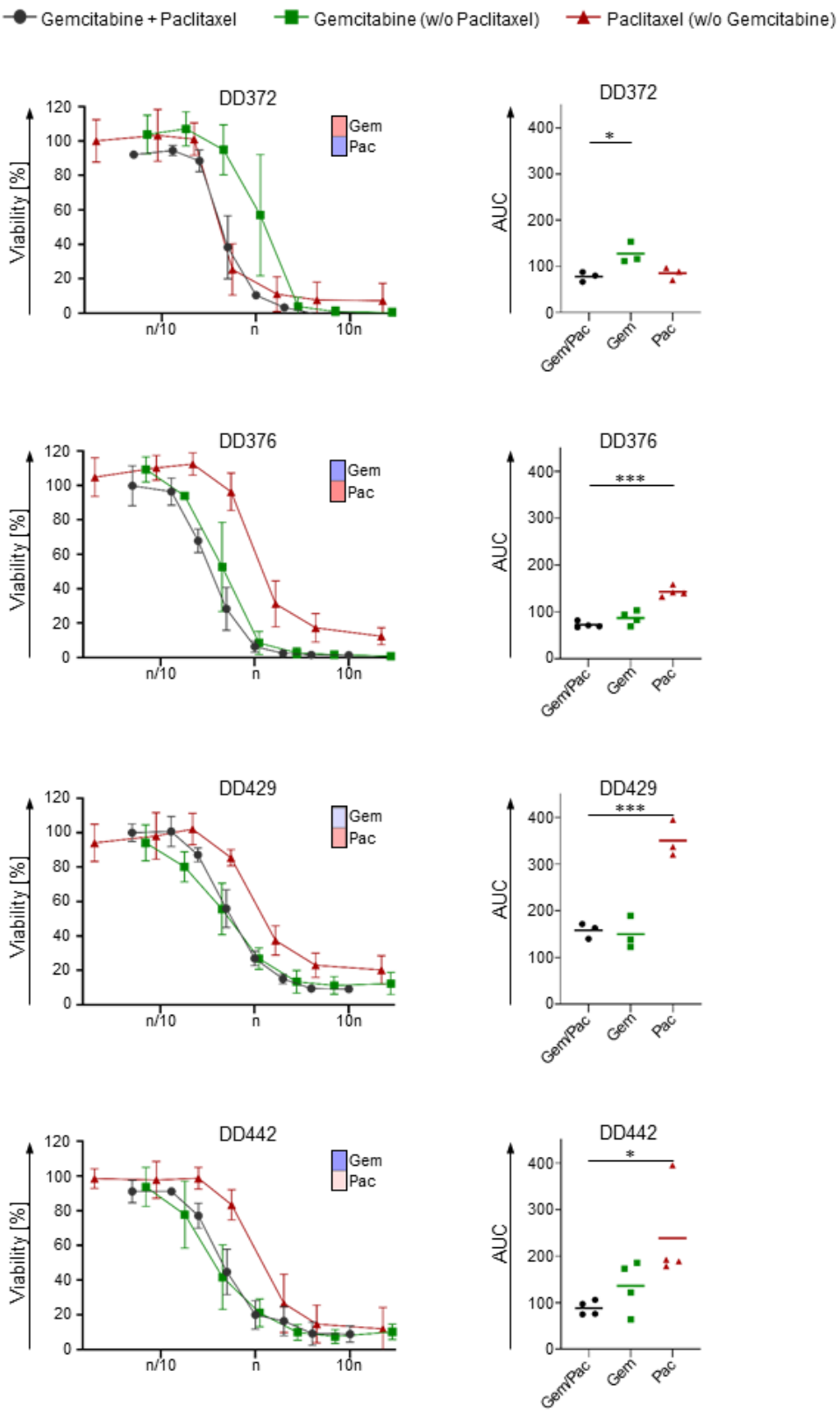

Figure 31 - Adaption of the Gem/Pac multi-drug therapy without affecting efficacy can be achieved through PDAC PDO pharmacotyping. Dose response curves of the four PDAC PDO lines DD372, DD376, DD429 and DD442 treated with Gem/Pac or gemcitabine or paclitaxel as monotherapy. Colored boxes illustrate the z-scores depicted in Figure 29A and indicate the PDO lines individual response to the single compounds (red = poor response, blue = good response). Statistical analysis was performed using the one-way ANOVA (* $p < 0.05$, *** $p < 0.001$). Modified from Hennig *et al.*[110].

9.4 Chapter 4 –NeoResponse: A co-clinical trial to evaluate the PDO model as a tool to predict LA PDAC patients' response to neoadjuvant chemotherapy

PDAC patients' neoCTx outcome is by default assessed using imaging techniques such as computed tomography (CT), comparing the tumor size before and after systemic treatment. Ferrone and colleagues observed response rates of 30% after treatment with the FOLFIROINOX regimen in LA and BR PDAC patients using CT imaging, but achieved R0 resections in more than 90% of patients in the same cohort[50]. This demonstrated that CT imaging alone is not suitable to assess the patients´ response to FOLFIRINOX and that new biomarkers are urgently needed to evaluate the neoCTx treatment outcome in LA PDAC patients.

The NeoResponse trial aims to address this issue by determining the response predictive potential of PDAC PDOs. Since April 2018, patients with unresectable LA PDAC have been recruited for this clinical study at the University Hospital Carl Gustav Carus Dresden. Subsequently, PDAC PDOs were established from EUS-FNA samples and cryopreserved for characterization. If the patient managed to finish the neoCTx with either FOLFIRINOX or Gem/nab-Pac without any RDI reduction and if surgical resection was successful, the respective PDAC PDO line was pharmacotyped in detail and results compared to the patients´ TRG assessed by board certified pathologists.

From April 2018 until September 2021, 55 patients have been recruited for the NeoResponse trial. Within this cohort, 27 individuals are male (49%), 26 (47%) are female and the gender of two patients (4%) is unknown as they have been recruited at the second trial center at the "Städtisches Klinikum Dresden Friedrichstadt". The mean age of the trial patients is 66.8, with the cohort of males being 65.2 years old and the female 68.5 on average. The number of patients being enrolled within 6 months intervals varied from 1 (April 2019 until September 2019) to 15 (October 2018 until March 2019) (Figure 32A). On average, 7.9 patients were recruited every six months and within the last 18 months the recruiting was at a constant level compared to the first one and a half years. Of the 55 patients enrolled for the NeoResponse trial, 32 patients have been excluded from the trial (58.2%). Within the design of the study, a dropout rate of 50% was anticipated. Yet, 15 patients (27.3%) completed the trial with a successful surgical resection after systemic therapy and eight patients (14.6%) are in the process of receiving neoCTx treatment (Figure 32B). The main reasons for patient's dropout were death (18.8%), switch to a palliative care due to distant metastasis or poor ECOG status which did not allow neoCTx (31.3%), and diagnosis of a second disease other than PDAC (21.9%) such as a neuroendocrine tumor, sarcoma, or pancreatitis (Figure 32B).

Within the cohort of patients that completed the trial, 60% were treated with FOLFIRINOX, 26.7% with Gem/nab-Pac and 6.7% each with FOLFIRINOX and later Gem/nab-Pac or Gem/nab-Pac followed by a switch to Gemcitabine monotherapy (Figure 32B).

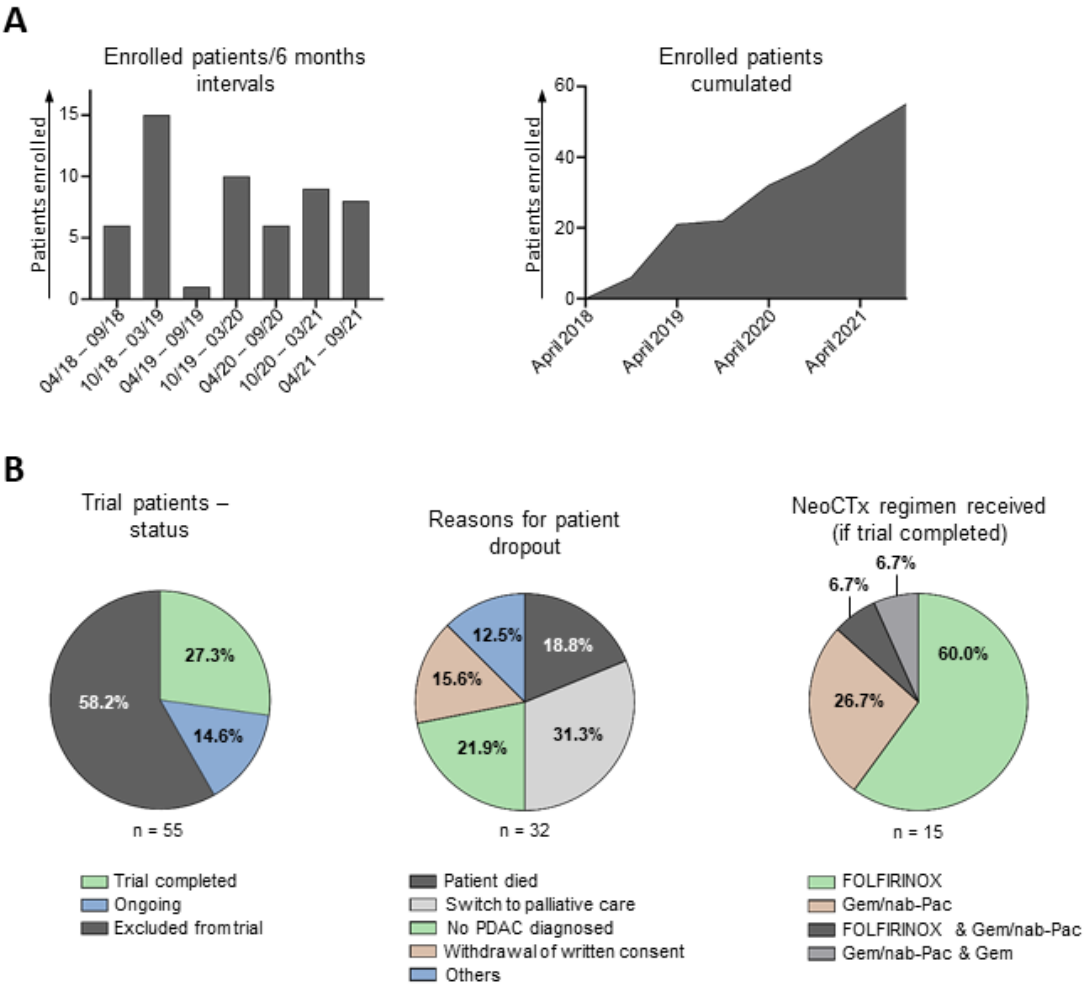

Figure 32 – Overview of the patient cohort enrolled for the NeoResponse trial. A) The number of individuals recruited for the NeoResponse trial recruited from April 2018 until September 2021 in 6 months intervals and the cumulated patient number participating in the clinical trial. **B)** Pie charts illustrating the proportion of study patients that completed the trial, that are still receive neoCTx (ongoing) or that have been excluded from the trial. The reasons for patient drop out is illustrated in a separate pie chart, as well as the neoCTx regimen administered to patients that have completed the trial.

From April 2018 till September 2021, EUS FNA samples from 38 out of 55 patients (69.1%) have been received, whilst no tissue was obtained in 17 cases (30.9%). Previous conducted EUS FNA taken place at another hospital before enrollment into the NeoResponse trial were the main reason for not receiving tumor tissue. Within the complete trial cohort, 31 patients were biopsied once (56.4%) and 7 patients twice (12.7%) (Figure 33A). However, within the cohort of biopsied patients (n = 38) nearly 20% underwent a second EUS FNA. Of the 38 patients a biopsy was taken at the University Hospital Carl Gustav Carus Dresden, 32 samples were histopathological assessed as PDAC. The initiation rate of PDOs from verified PDAC tissue was 65.6% (n= 21), and for two samples (6.3%) PDO outgrowth is still ongoing with missing confirmation of mutated *KRAS* and/or cultivation beyond passage 10. The organoid generation was not successful in 9 cases (28.1%) (Figure 33A). The respective 21 LA PDAC patients of which PDAC PDOs have been established completed the NeoResponse trial in 8 cases (38.1%), and an additional 4 patients (19.0%) are still undergoing neoCTx at this time. Nine patients (42.9%) with successful generated matching PDAC PDOs were excluded from the trial (Figure 33B). Further investigations concerning the unsuccessful generation of PDAC PDOs in 9 cases have shown that a poor biopsy quality was the main reason for PDO initiation failure. This can be explained with the lack of any PDOs growing out in passage zero, which was seen in 6 out of 9 cases (66.7%) (Figure 33B). In two cases, PDOs were growing at passage zero, but due to contamination with bacteria or fungi needed to be discarded. In 1 out of the 9 cases the reasons for failure of PDAC PDO generation is unknown, as good growth dynamics was seen until passage 6 followed by a rapid increase of cell death and the loss of the organoid culture.

Taken together, the main limiting factor of study progress to date is the high dropout rate of enrolled patients, as take rates of PDAC PDOs increased with time and peaked at 80% for the last 18 EUS FNA samples received (Figure 12).

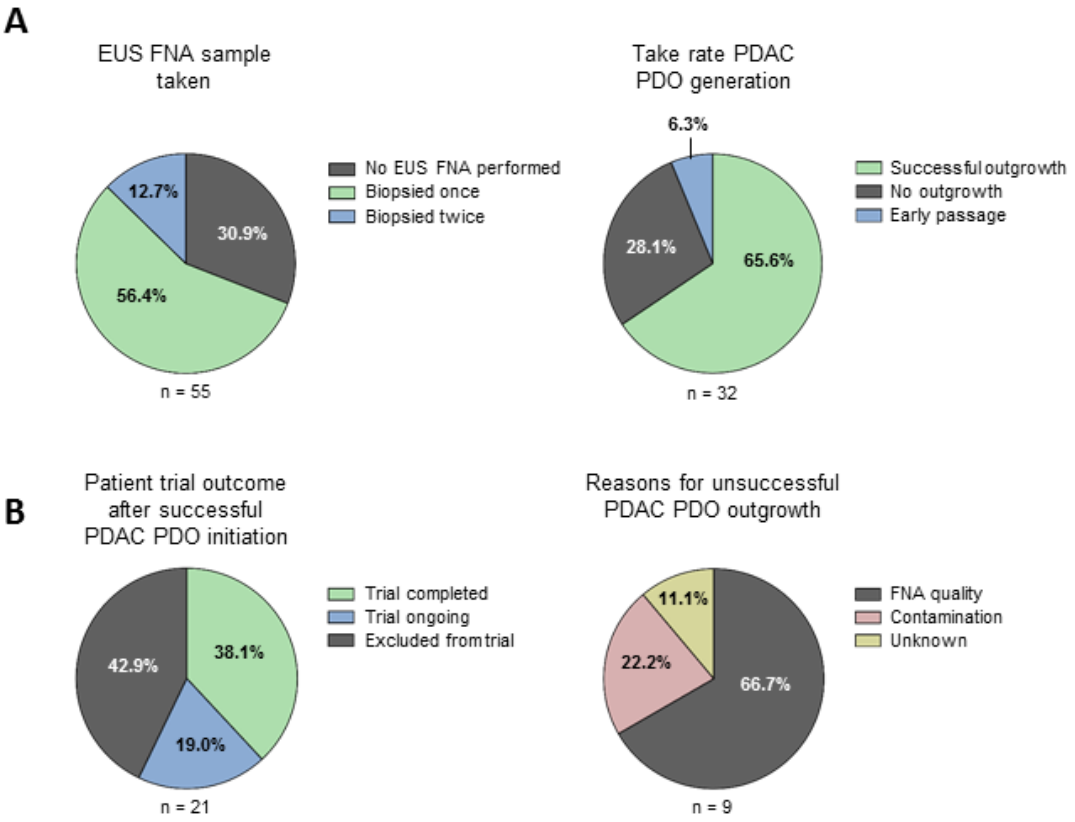

Figure 33 - NeoResponse patient dropout and not PDAC PDO generation take rate limits trial progression. A) Pie charts illustrating the proportion of enrolled NeoResponse patients from which tissue samples have been derived from, as well as the take rate within the cohort of punctured individuals. **B)** Patient trial outcome in case of successful PDAC PDO generation and reasons for organoid generation failure are depicted in pie charts.

NeoResponse patient number 50 was re-punctured due to the lack of sufficient material for histopathologic analysis. From both EUS FNA sessions PDO cultures successfully have been established showing robust growth and a typical PDAC-like dense morphology lacking any cystic shaped organoids (Figure 34).

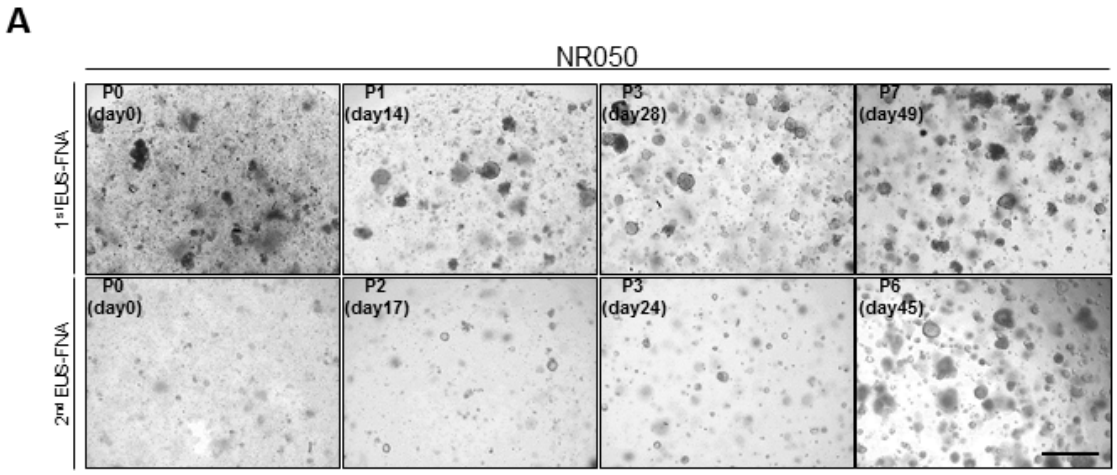

Figure 34 – Multiple PDAC PDOs can be established from the same tumor in case of repeated EUS FNA sessions. Patient NR050 underwent two separated EUS FNAs until histopathological confirmation of PDAC was successful. While in one out of two biopsies taken material for diagnostic was sufficient, starting material was abundant for PDO generation in both cases. Scale bar indicates 400 µM.

Crucial for assessing the neoCTx treatment predictive potential of PDAC PDOs is a sufficient number of patients that complete the trial with the following parameters:

- Sufficient EUS FNA material for initiating a PDO culture
- Histopathological confirmation of an adenocarcinoma of the pancreas
- Successful PDOs establishment
- Patient undergoes neoCTx preferably with standard of care
- Completion of neoCTx without RDI reduction or switch of treatment past cycle 2
- Successful resection of the primary tumor

As previously mentioned, FNA derived tissue samples have been received from 38 out of 55 patients (69%), from which 32 were confirmed as PDAC (58.2% from initial 55 patients) by board certified pathologists. From these 32 histological confirmed PDAC patients, 21 PDO lines have been established (38.2% from 55 patients). For two patients the generation of stable growing organoid is ongoing (Figure 33A). Of all the enrolled NeoResponse patients from which PDO lines have been established, 16 out of 21 cases proceeded to neoCTx treatment initiation (29.1% from 55 patients). Three patients of these did not complete treatment yet. Four patients did not sustain neoCTx resulting in a discontinuation of treatment, which means that 9 out of 55 patients (16.4%) with confirmed PDAC disease and established PDOs finished the systemic treatment. However, only 5 patients received a FOLFIRINOX combination therapy (9.1% out of 55 patients), from which four sustained a full dose protocol (7.3% out of 55 patients) (Figure 35). FOLFIRINOX response prediction via PDAC PDO testing seems to be the more promising regimen, as treatment with Gem/nab-Pac is relatively rare. Only one out of 55 patients with corresponding established organoids finished neoCTx with the Gem/nab-Pac protocol without RDI reduction, followed by successful surgical resection (not shown).

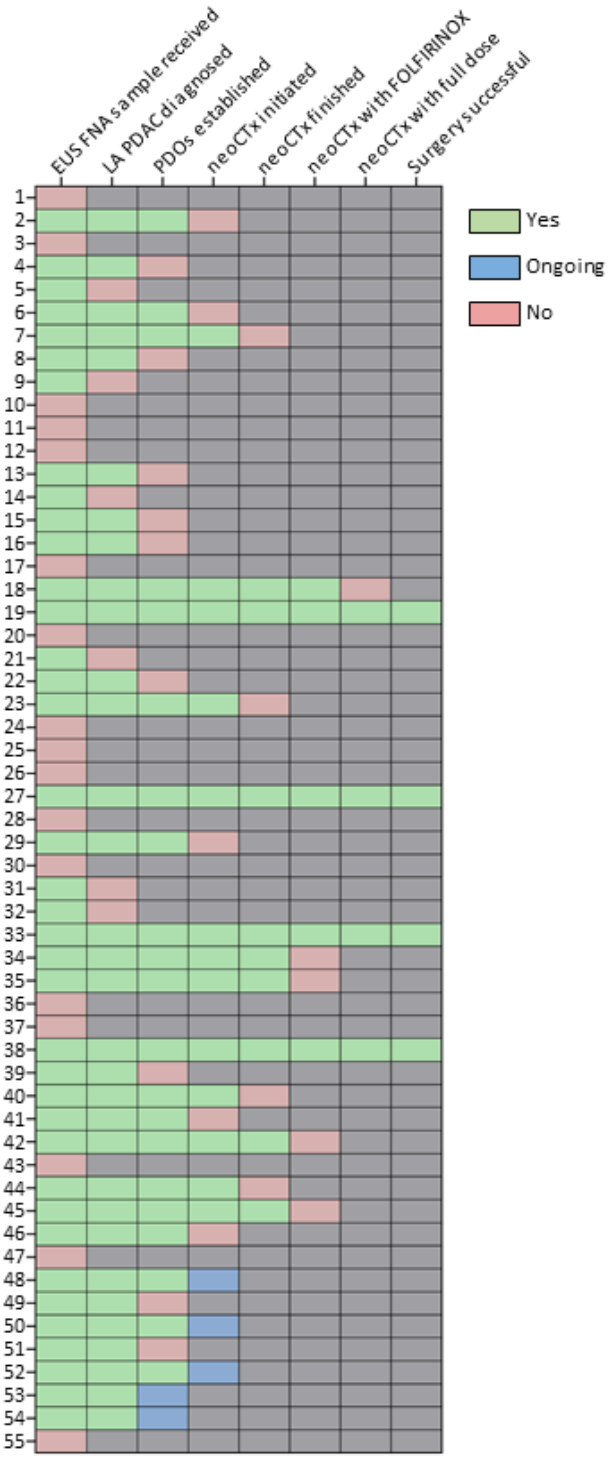

Figure 35 - NeoResponse trial outcome of 55 enrolled patients. Between April 2018 and September 2021, 55 patients have been enrolled for the NeoResponse trial from which four patients completed the trial fulfilling all criteria for investigating the predictive properties of PDAC PDOs for neoCTx treatment outcome. These criteria were (i) an EUS FNA biopsy which has been taken at the University Hospital Carl Gustav Carus Dresden for (ii) PDO culture generation and (iii) pathological confirmation of the PDAC disease, (iv) the initiation of the neoCTx treatment and (v) completion with (vi) FOLFIRINOX without (vii) any RDI reduction as well as the (viii) successful surgical resection of the tumor. Green colored boxes indicate that the respective measure has been successful, blue boxes represent ongoing processes. Red boxes indicate negative results for single measures. In this illustration, patients were not further followed in case of a negative event, although PDAC treatment was continued in case of e.g., unsuccessful PDO generation, or EUS FNA performed in an external hospital (grey boxes).

Although, 15 patients completed the NeoResponse trial by receiving a neoCTx followed by successful surgical resection, only four cases fulfil the aforementioned criteria for experimental assessing the predictive value of PDO from PDAC patients. Subsequently, the PDO lines NR019, NR027 and NR033 were pharmacotyped for drug sensitivity evaluation for FOLFIRINOX. For NR038, pharmacotyping was so far not possible, due to a very slow growth rate and handling difficulties. NR019, NR027 and NR033 showed PDO line individual dose-response patterns after treatment with FOLFIRINOX (Figure 36A). Compared to 11 CTx naïve PDO lines NR019 and NR027 showed poor response to FOLFIRINOX and NR033 intermediate sensitivity (Figure 36B).

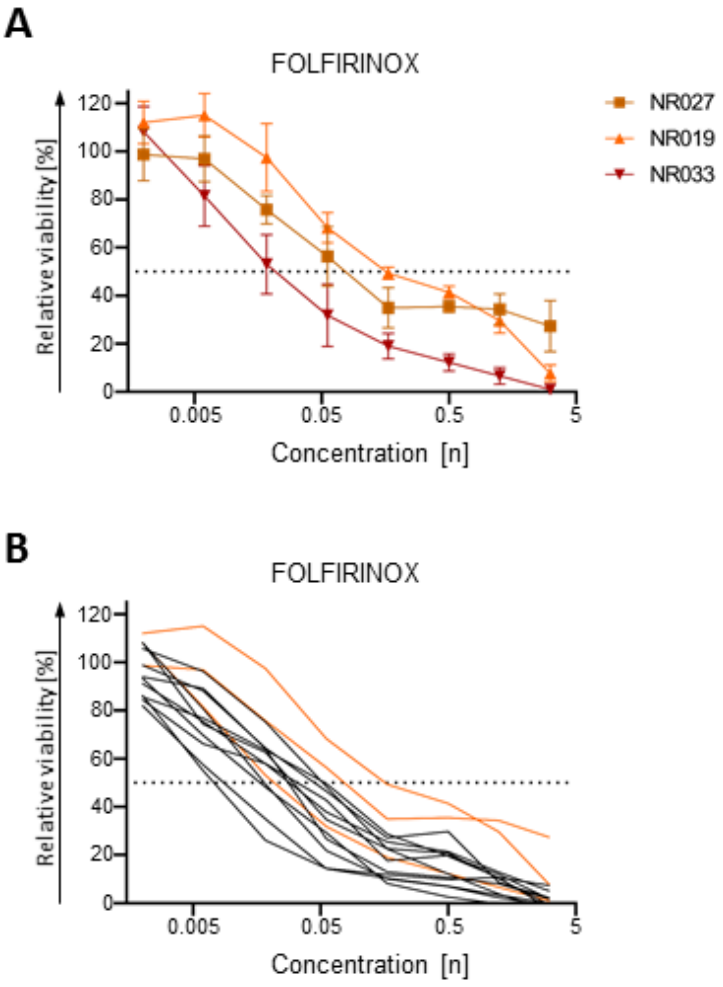

Figure 36 – FOLFIRINOX pharmacotyping PDAC PDOs of three NeoResponse patients. A) Dose-response curves of three PDAC PDO lines treated with different concentrations of FOLFIRINOX shows PDO line individual response patterns. Dose dependent viabilities were calculated by normalizing to the untreated negative control. **B)** Obtained drug sensitivity data from NR027, NR019 and ND033 (orange lines) were compared to the data from 11 CTx naïve PDAC PDO lines (black lines) pharmacotyped earlier to assess the FOLFIRINOX sensitivities from NR027, NR019 and ND033.

The tumor regression grade was assessed after surgical resection by board certified pathologists for the corresponding patients from NR019, NR027 and NR033. A major response to FOLFIRNOX therapy was seen for NR027, while the matching PDO line showed poor response to the same CTx treatment. For the FOLFIRINOX resistant PDO line NR019, a TRG2 (intermediate) was seen *in vivo* and NR033 only showed a minor (TRG1) response, while the respective PDO line harbored an intermediate response to the drug treatment.

Discussion

10.1 Full dose neoadjuvant chemotherapy in LA PDAC patients improves R- and N-status in case of successful surgical resection

In this study, clinical data from 59 patients with unresectable LA PDAC have been retrospectively analyzed to investigate the impact of severe side effect mediated dose adaption on neoCTx treatment outcome. Within the FOLFIRINOX cohort, 29.3% of individuals received an adapted dose, while 27.8% of patients in the Gem/nab-Pac group did not sustain full course therapy. Dose adaption rates might be even higher considering that in case of unsuccessful surgical resection or a switch to palliative care due to the occurrence of distant metastasis and/or tumor progression while receiving neoCTx, patients were not included in our analysis. Yet, our data is in line with a recently published retrospective multi-center study from Vary and colleagues assessing the RDI for the three single drug compounds of the FOLFIRINOX protocol in 243 PDAC patients which received the respective neoCTx[113]. Vary and colleagues reported single drug RDIs for irinotecan, oxaliplatin, 5-FU bolus and the 5-FU infusion of 81%, 79%, 75% and 85% respectively. In their study, a dose adaptation was already required in 34.6% of individuals after administration of the first treatment cycle. Dose adaptation was also necessary in a significant fraction of patients that received full course at cycle 1 during subsequent treatment cycles, resulting in a cumulative FOLFIRINOX multi drug RDI of 80.3% in the analyzed cohort. Within the scope of our retrospective analysis, we observed a significant impact of the neoCTx dose administered to PDAC patients prior surgery on the R-status. This finding revealed a negative effect of dose adaptation on patient therapy outcome, as surgical resection with tumor free margins (R0) improves median survival time and 5-year survival rate significantly[47,48]. The N-status, which also has strong prognostic value, is not impacted by dose adaptions but by the TRG[114]. As we identified a clear, yet not significant trend for improved response after full course neoCTx, the N status might get indirectly affected by dose adaptions. Besides these effects of dose adaptations, we observed improved R- and N-parameters in patients with TRG2 and/or TRG3 in comparison to the cohort with resectable PDAC disease. Potential benefits of neoCTx in patients with resectable PDAC are currently debated intensively. For patients with resectable PDAC, upfront surgery is the standard of care followed by adjuvant CTx to improve disease free survival and OS[115–118]. Yet, it is estimated that for 50% of patients undergoing surgical resection of the tumor an adjuvant CTx is not possible due to poor ECOG status[33,119].

A meta-analysis of 14 studies concluded that neoCTx followed by surgery showed superior survival compared to upfront surgery followed by adjuvant CTx in patients with resectable PDAC[120]. In addition, R- and N-status were improved in the neoCTx + surgery group compared to the upfront surgery cohort. However, adding patients that received neoCTx but did not undergo surgical resection revealed no

significant survival benefit. In esophageal cancer, a different type of gastrointestinal cancer, promising results have been reported when administering neoadjuvant radio-chemotherapy in patients with resectable disease[121,122]. As a result, some patients with resectable tumor receive neoadjuvant treatment prior to surgery.

Taken together, neoCTx dose adaption, which was observed in a significant proportion of LA PDAC patients, impacted both the R- and N-status. Yet, data from a larger patient cohort is required to investigate the influence of dose adaption on treatment outcome (TRG), as a clear trend towards worse response was seen. Considering that neoCTx might also be beneficial for patients with resectable PDAC in the future, biomarkers are needed that guide neoCTx protocols to prevent dose adaptation of treatment.

10.2 Organoids initiated from patient derived tumor specimens share molecular features with the respective tissue of origin

The focus of this study was the generation and characterization of a PDAC PDO living biobank as well as the identification of potential applications and limitations of organoids as a preclinical model. Between December 2016 and June 2021 tumor tissue sample from primary PDAC and distant metastasis have been collected, resulting in a biobank of nearly 90 PDO lines. PDAC PDO repositories have been reported in the meantime by other groups, i.e. the laboratory of Tuveson reported the largest one with 114 successfully established cell lines in 2018[123]. The laboratories of Sato and Clevers reported that 49 PDAC lines were generated from primary tumor samples and the Clevers lab managed to establish a 52 PDO line containing biobank, respectively [104,105]. Despite the Tuveson group, no reports on extensive PDO generation from PDAC metastasis have been published, which can be explained with difficulties of obtaining tissue samples from these respective lesions[123]. Surgical resection of PDAC metastases is not recommended as patients do not profit in terms of improved OS or PFS. Yet, we managed to establish PDAC PDOs from liver metastasis in 6 cases from which primary tumor PDOs were initiated in only one of these cases. To our knowledge, no group reported the comprehensive generation of PDAC organoids from neoCTx pretreated patients, which was feasible in 13 cases as part of this study. Interestingly, take rates for PDO initiation from pretreated patients correlated with the TRG, which might be explained by low numbers of viable tumor cells in tissue specimens from patients with major response to neoCTx. Success rates for PDO generation from CTx naïve patient tumor tissue increased with time and reached 70% for the last 10 samples processed. Our results were comparable to the studies of Tiriac and colleagues (78%), and Driehuis and colleagues (62%)[105,123]. However, definitions for successful PDO generation are not standardized, as we defined

growth beyond passage 10 and Tiriac and colleagues stable growth past passage 5 as criteria for PDO initiation. This also accounts for initiation rates for PDOs from EUS-FNA samples, which were, according to Tiriac similar with 87% and 62% for passages zero and five, respectively[124].

Within the scope of this study, the main reasons for PDO initiation failure are the quality of tissue specimen, the media composition, and the batch effects of the Matrigel. As seen for FNA samples were no organoids have been observed in some cases in passage zero, the cellularity of tissue samples is crucial too, especially for PDAC disease with high degree of desmoplasia and low content of epithelial tumor cells[125]. PDAC PDOs can be established from minimal starting material derived from EUS-FNA biopsies with even slightly higher take rates compared to surgical resection specimens. This leads to the assumption that the length of time needed until the samples gets processed might impact on PDO outgrowth. For EUS-FNA biopsies, the digestion of the tissue was initiated within 10 minutes after the sample has been taken. On the other hand, surgical specimens were usually de-vascularized for several hours before removed completely, followed by an examination by pathologists. This resulted in a long warm and cold ischemia time before processing of tumor specimens were initiated in our laboratory.

The current composition of the complex PDAC medium allows organoid growth in most cases, yet it might not contain all signal pathway inhibitors/activators and other substances required for PDO initiation of a subgroup of tumors. Individual tumors harbor unique genomic alterations, which may influence the composition of an optimal growth medium. As PDAC PDO libraries expanded, it has been noticed that a significant number of PDO lines did not rely on Wnt3a and Rspondin, contradicting the previous described dependency on both substances[91,104]. More research on optimized PDAC medium composition is necessary in the future, as it could increase the take rate of PDO generation.

Empirically significant differences between Matrigel batches have been observed, which also might impact on the growth behavior of PDOs. For liver organoids, it has been shown that the ECM composition and stiffness alters growth rates underlining the need for defined and/or synthetic organ specific ECMs[126]. In our study, contamination of cell cultures was rare and negligible. Furthermore, tumor size (T) and grade of differentiation (G) did not influence the chance for successful PDO outgrowth. Frequently cancer-associated-fibroblasts (CAFs) can be found PDO cultures at passage zero/passage one before disappearing while subsequently passaging the cell line. The separation of both cell population resulted in a small library of CAFs and matching PDAC PDO lines, allowing the generation of more complex *in vitro* co-culture models in the near future. Organoid-CAF co-cultures already have been established by other groups and were used for investigating the interplay between both cell populations *in vitro*[127,128].

Taken together, PDAC PDO initiation was feasible within 3 weeks in most cases, regardless of generated from surgical resections from CTx naïve or neoCTx patients, or from EUS-FNA samples.

However, within this timeframe, a purity of 100% PDAC tumor organoid was unlikely, which can be explained with the medium composition. In our study, EGF was added to the PDAC medium to allow outgrowth of rare *KRAS* non-mutated PDAC organoid lines. However, EGF is essential for expanding normal pancreatic organoids, which resulted in varying intensities of contamination with pancreatic organoids within the first 5-8 passages. It might be worthwhile to test different PDAC medium mixtures for early PDO cultures in the future that exclusively select for tumor organoids in early PDO lines, despite the more time-consuming cultivation process. As *KRAS* is mutated in 90% and *TP53* in 50% of PDAC, an early selection for tumor organoids could be feasible in most cases[18,129]. This could be considered for cultivating new PDAC PDO lines by withdrawal of EGF, and supplementing the media with nutlin-3, a synthetic agent that has cytotoxic properties in cell expressing wild type TP53[104].

The collection of the PDAC PDOs revealed various morphologies among the PDOs, most were exclusive tumor organoids. Cystic shaped PDOs with a hollow lumen were not necessarily contaminated with normal pancreatic organoids, as a cultivation was achieved for some of those cell lines for at least 30 passages and *KRAS* mutations were detected. Here, the validation of the *KRAS* status was primarily carried out via commercial Sanger sequencing as it is cost efficient, resulting in the identification of mutated *KRAS* in 45 PDO lines. Nonetheless, this sequencing method relies on high allele frequencies in the template for detection which is not often the case in early passage PDAC PDO lines due to contamination with pancreatic cells. More expensive methods with a high sequencing depth such as panel sequencing would be more suitable. Isolating DNA for sequencing from PDO lines past passage 10 could also result in a higher allele frequency of altered *KRAS*. Yet, both methods are cost intensive and/or time consuming. Despite *KRAS* sequencing, a further characterization of PDAC PDOs was conducted for a subset of organoid lines. IHC stainings of primary tumor tissue sections and the respective matching organoid line showed high molecular similarities. PDAC tumors with nucleus accumulating mutated TP53 gave rise to PDOs with the same phenotype.

This raised the question if molecular subtypes of PDAC were identical in the respective PDO line as this could result in an improved treatment of patients by encompassing these patients according to the molecular tumor properties in the near future. Although subtyping of PDAC is not routinely performed in the clinic, first data indicate a subtype specific response to systemic chemotherapy[14,72,82]. Furthermore, the predictive value of PDAC subtypes has been shown by multiple groups[72,81,82]. However, nearly all patients were treated with similar standard of care CTx even though PDAC is known to be a heterogeneous disease and response to systemic treatment is often limited[130]. According to Collisson and colleagues the three subtypes of PDAC, which are the quasi-mesenchymal, the exocrine-like and the classical subtype, were defined on mRNA expression analysis using microarray technology[72]. Based on these findings, Noll and colleagues established a protocol for the assessment of the PDAC subtypes using IHC staining of only two markers, KRT81 and HNF1A. As subtyping of PDAC

PDOs has not been conducted before and the originally described antibody for HNF1A was not anymore commercially available, we aimed to address both issues by identifying an alternative marker for HNF1a for PDAC subtyping in PDOs. Based on the PDAssinger gene set, we identified *CFTR* as a potential replacement for *HNF1A*. RT-qPCR revealed a high correlation between the gene expression of *HNF1A* and *CFTR* in a set of 23 analyzed PDAC PDO lines. IF staining of 7 PDAC organoid lines also showed either very strong or absent staining of CFTR, which allowed robust classification of the respective biomarker. Moreover, CFTR expression was mutually exclusive to the expression of KRT81 in most cases, which leads to the assumption that CFTR expression evaluation allows molecular PDAC subtyping according to Collisson and colleagues.[72]. Subsequently, subtyping was feasible in 9 out of 10 PDAC organoid lines and a high concordance (six out of seven samples) between the primary PDAC tumors and the corresponding organoid lines was observed. For one primary PDAC tumor a strong staining for KRT81 and CFTR was detected, while the corresponding PDO line was exclusively positive for KRT81. High expression of both markers has also been observed by others groups, yet a molecular subtyping is not possible for these rare cases[81,82]. A CFTR expression was not seen for the corresponding organoid line on mRNA and protein level, which might be explained with a restriction of clonality for this respective PDO line. It is possible, that the PDO line has been established from KRT81 positive PDAC tissue regions exclusively. Taken together, subtyping of PDAC via expression analysis of only two markers is feasible in most cases and rapidly assessed at low costs. Yet, microarray or mRNA sequencing data for the expression analysis of all PDAssinger genes within the PDO lines analyzed in this study are still needed. Furthermore, these findings need to be validated by subtyping more PDAC samples via KRT81 and CFTR expression levels determination, which could also proof the existence of an exocrine-like PDAC subtype. According to Moffitt, this subtype can be attributed to the contamination with healthy pancreatic tissue in samples that have been analyzed via microarray technology[130]. Based on sequencing of *KRAS* using next generation sequencing methods, we identified allele frequencies of nearly 50% in most cases indicative that the PDO lines are tumorigenic. Yet, the staining of CFTR resulted in a homogenous positivity of the whole organoid culture, strongly arguing for the existence of an exocrine-like PDAC subtype.

Prospective clinical trials are needed to evaluate whether molecular subtype specific treatment protocols may improve therapy outcomes in PDAC patients. The methodological requirements have been established by our study, as PDAC PDOs now can be initiated from FNA samples in most cases, followed by subtyping via IF staining of the PDO lines. This is of importance in the neoadjuvant setting, as EUS-FNA samples are of very limited material size, which normally does not allow routine IHC based subtyping.

In summary, we identified CFTR as a suitable replacement of HNF1A for molecular PDAC subtyping. We showed that subtyping of EUS-FNA derived PDAC PDOs is feasible and allows the classification of the corresponding primary tumor from minimal starting material.

10.3 Pharmacotyping of patient derived organoids as a strategy for individualized treatment in pancreatic ductal adenocarcinoma

Parameters considered for choice of systemic chemotherapy are often the patients´ age, co-morbidities and the ECOG status[14,33]. Yet, a standardized guideline for CTx treatment decision making is not in place and in most cases, patients receive either FOLFIRINOX or Gem/nab-Pac in the neoadjuvant setting with varying treatment outcome. In this study, potential applications of PDAC PDOs have been evaluated with the aim to improve treatment outcome by developing patient tailored treatment protocols. For this purpose, a 384-well plate based pharmacotyping platform has been established which allowed rapid pharmacotyping of PDO lines within 7 days. Only small amounts of starting material are required, and results were robust over several passages. Most importantly, the process could be automated which enables routine pharmacotyping of PDOs of any cancer entities in the near future.

Subsequent pharmacotyping of PDAC PDOs from CTx naïve patients resulted in an organoid line individual response pattern to commonly used chemotherapeutic single drugs. This data underlines the diversity of interpatient response, explained by unique genetic, epigenetic, metabolic and other features within individual tumors, that mediate resistance but also sensitivities to certain substances. Similar observations were made in multi-drug FOLFIRINOX and Gem/Pac drug assays *in vitro*. In our study, we identified two out of eleven CTx naïve PDO lines to harbor resistance to one poly-drug treatment, while being sensitive for the other protocol respectively. Additional three PDO lines showed either resistance or sensitivity to one drug combination and an intermediate response to the respected other regimen. As a result, in five out of eleven cases PDAC PDOs could have supported clinician decision making to choose the potentially more efficient therapy option. Considering that the randomized SWOG-S1505 revealed equal efficacies for the FOLFIRINOX and the Gem/nab-Pac regimen in the neoadjuvant setting in LA PDAC patients, PDOs could act as the urgently needed biomarker for guiding tailored neoCTx treatment decision in the future[42]. It is also estimated, that the neoCTx in PDAC treatment will become of more importance in the future, as several clinical trials showed that patients with localized resectable disease benefit from neoCTx that followed surgical resection compared to upfront surgery followed by adjuvant chemotherapy[120]. Treatment of patients with BR PDAC also might be improved by neoCTx prior surgery as R0 resection become more likely to achieve[131].

Pharmacotyping of neoCTx PDAC PDOs revealed a tendency for drug resistance to the chemotherapeutical regimen that have been administered to the respective patient from which the organoid line has been established from. This might be explained by the development of new resistance mediating alterations under selection pressure or the enrichment of already existing resistant clones within the tumor. Yet not all neoCTx PDAC PDO lines pharmacotyped exhibited reduced sensitivities to the respective treatment protocol. Consequently, PDOs could become of importance by assisting clinical decision making by choosing the most efficient adjuvant CTx in patients that already received a neoCTx. However, more neoCTx PDOs need to be analyzed to finally identify the impact of neoCTx on drug resistances in tumor cells.

Further improvements in PDAC therapy could be achieved by reconsidering the interplay of chemotherapeutical substances in multi-drug regimens. In the past, promising results have been achieved by introducing drug combination protocols in the treatment of patients with advanced cancer diseases[37,38,132–134]. Improved response rates often have been justified by additive or even synergistic drug interaction, which is absent in any mono-substance therapy. Palmer and colleagues, however, showed that superior drug combination efficacy can be explained with independent drug actions[135]. With increasing numbers of substances administered simultaneously, bypassing drug resistances within a genetically heterogeneous tumor becomes more likely. However, the superior efficacy of drug combination also increases the rate at which severe side effects are induced. As a result of that RDI reduction or treatment termination is required in many cases. As shown before, we observed a trend towards reduced response to neoCTx in patients that did not receive full course treatment. Furthermore, the R- and N-status were affected in case of administering adapted doses to LA PDAC patients. As inferior responses to neoCTx in patients that received adapted neoCTx have been reported for other tumor entities, we asked if PDAC PDOs could be used to increase the number of patients that sustain full course neoCTx[136–138]. Subsequently, we investigated the impact on drug combination efficacy after removing the most inefficient compound. For both regimens, FOLFIRINOX and Gem/Pac we showed no significant effect on the dose-response curve, when poor acting drugs have been removed from the treatment protocol. In one case (DD412), no change in efficacy was seen regardless of which substance has been excluded. This is in line with the observation that the PDAC organoid line did not respond well to all FOLFIRINOX compounds in single drug experiments.

Using PDOs to identify inefficient chemotherapeutical drugs, might result in the withdrawal of a given drug from the treatment schedule without impacting treatment efficacy. This in turn could result in less severe side effects under neoCTx and could improve quality of life for many patients with advanced cancers. Furthermore, this strategy could impact the number of patients that require neoCTx dose adaption and consequently might lead to higher rates of intermediate/major tumor regression grades and potentially better OS in LA PDAC patients. PDAC patients with good ECOG status that are scheduled

to receive adjuvant CTx could also benefit from PDO pharmacotyping, as successful post-surgery chemotherapy improve survival[43,44].

Taken together, the initiation of PDOs allows to stratify patients' individual drug responses within combination therapy, which in turn could lead to patient tailored chemotherapy protocols in the neoadjuvant and adjuvant setting. This potentially could result in improved long-term survival rates but also improved quality of life for patients undergoing systemic chemotherapy. Nevertheless, feasibility needs to be tested in a prospective clinical trial setting to show if and to what extent PDAC PDOs are able to predict patients´ response to systemic treatment, similarly what has been shown for colorectal cancer PDOs[106,139,140].

10.4 Tissue derived organoids as patient cancer avatars for response prediction in LA PDAC

In order to investigate, if PDOs can predict LA PDAC patients´ response to neoCTx the prospective NeoResponse trial was set up at the University Hospital Carl Gustav Carus Dresden. Subsequently, LA PDAC patients have been recruited from April 2018 on and three years later also from the "Städtisches Krankenhaus Dresden Friedrichstadt" to increase the number of patients enrolled for the trial.

In total 55 patients have been recruited from April 2018 until June 2021, from which two were enrolled at the "Städtisches Krankenhaus Dresden Friedrichstadt". Prior to trial initiation, it has been estimated that recruitment of 100 individuals is necessary to get sufficient data including patient TRG and PDO drug sensitivities from patients completing the study. The biggest hurdle was thought to be the PDAC PDO generation rate, which was set to 50%. However, the PDO take rate reached 80% over time and the main limitations have been the lack of tumor tissue samples which have not been derived in 31% of all cases. In total, PDOs from histologically confirmed LA PDAC patients were generated from only 38.2% of the patient cohort. As we have shown that dose adaptation impacts therapy outcome, patients with any neoCTx protocol modifications have been excluded from the analysis, which was not considered before initiating the clinical trial. Additionally, patients that switched from one multi-drug regimen to another after more than 1 cycle of neoCTx did not allow correlation analysis of *in vitro* and *in vivo* data, as assigning potential cytotoxic effects to a particular regimen was not possible.

As discussed before, PDO initiation from EUS FNA samples was feasible in most of cases within clinically relevant time frames with higher outgrowth rates and less time required as reported by others[95,124,141]. Strikingly, in some cases PDOs have been generated from a single biopsy, containing sufficient material for histopathological confirmation of PDAC disease by pathologists and organoid initiation, which meant no additional risk due to PDO generation. Repeated EUS FNA sampling was required in 7 cases

(12.7%) of patients, from which in one case tumor organoids successfully have been established from both samples. Repeated sampling for histopathological analysis is a common procedure in PDAC diagnosis and could be addressed using PDOs[142]. As neoCTx cannot be started without histological verification of the tumor disease, treatment initiation is delayed in these patients with unknown impact on therapy outcome and survival. Recently it was shown, that PDAC diagnosis is feasible by performing digital droplet PCR (ddPCR) for assessing the *KRAS* status on cell free DNA (cfDNA) derived from early PDO culture supernatant[143]. Both, PDO generation from EUS-FNA samples as well as mutation calling via ddPCR from cfDNA could shorten diagnosis times in PDAC.

Due to the low sample size of three FOLFIRINOX tested PDAC PDOs, correlation analysis of PDO and patient response was not possible. Yet, an overlap of patient TRG and organoid sensitivity was not seen, as a patient with a major response to neoCTx with FOLFIRINOX gave rise to a resistant PDO line. For the other two patients TRG1 and TRG2 was identified, while the PDO lines showed intermediate and poor response respectively. In a recent publication by Grossmann and colleagues, a strong correlation between PDAC organoid drug sensitivities and corresponding patient response to treatment was seen[141]. However, the sample size was relatively low (n= 12) and additional work is needed to finally assess the treatment outcome predictive capacity of PDAC organoids. Yet, the work of Grossmann and colleagues strongly indicates that response prediction in PDAC is feasible using PDOs which is in line with other prospective clinical trials such as the ones in colorectal cancer[106,139,140].

Related to the NeoResponse trial, pharmacotyping with drug combinations should be reconsidered as the empirically determined mixture ratio of all three drugs might result in an outcome bias. Single drug testing might be a more suitable approach as also indicated by other groups addressing similar scientific questions[141,144].

Despite these issues, a guideline for consistent PDO generation, characterization and pharmacotyping is urgently required, as each research group investigating the predictive value of PDOs as personalized patient avatars has its own quality standards. This accounts for the PDAC medium composition which differs within the PDAC PDO community for which clear clonal selective effects have been shown but also for the minimum required extent of PDO line characterization prior pharmacotyping[95,104,105,112,141,145]. Basic PDO characterization can be done on DNA level for identifying common known PDAC driver mutations[108] and protein level for example via IHC staining for molecular subtype assessment via Collisson, Moffit or Bailey or verification of epithelial and pancreatic markers[72,79,80]. Pharmacotyping is performed with varying protocols, which prevents merging of data from different groups as it would be too difficult or even impossible to interpret these results. Considering the high expenses for drug testing in a Matrigel based model system, standard protocols are highly recommended and needed.

In summary, the hurdles of the NeoResponse trial have been solved successfully, as (i) PDAC PDOs can be generated with high confidence, (ii) characterization of new PDAC PDO lines on DNA and protein levels is feasible and (iii) a robust drug testing platform has been established requiring only limited materials numbers of organoids as well as relative low amounts of Matrigel and cultivation medium. However, for evaluating the predictive value of PDAC PDOs concerning patients' neoCTx response, multiple sites recruitment of patients is needed.

Summary

Pancreatic cancer is the seventh leading cause of cancer related mortalities worldwide and incidences are increasing. The prognosis remains poor as the 5-year survival rate is below 10%. This can be partly explained by the silent progression of disease as most patients present with advanced disease at time of diagnosis. In turn, surgical resection, the only potential curative measure, is not possible in nearly 80% of cases due to the occurrence of distant metastasis and/or infiltration of major vessels in close proximity to the pancreas. In patients with localized but advanced disease, resectability can be achieved in some cases by initiation of a neoCTx. However, as neoCTx is commonly conducted by administering multi-drug treatments, severe side effects occur frequently, which require an adaption of drug doses administered.

In this study, we revealed the negative impact of these drug dose changes during neoCTx on the patients´ treatment outcome. R0 resections were significantly less frequently observed, and the N-status significantly impacted by the tumor regression grade, which in turn trended towards minor response in the cohort of patients that did not sustain full dose course prior surgery. In turn, treatment of LA PDAC could be improved by increasing the proportion of patients that undergo neoCTx without any changes of the treatment schedule. Patient-derived PDAC organoid could serve as an avatar of patients´ tumor disease on which optimal treatment protocols could be tested.

In this study, a large living PDAC PDO biobank successfully has been established from surgical resection specimens as well as EUS guided FNA samples. Subsequently, a new protocol for molecular subtyping of PDAC on organoids was established by assessing the expression level of KRT81 and CFTR, as a replacement for HNF1a, using IF staining. Strikingly, we observed identical PDAC subtypes in PDOs and their respective tissue of origin in nearly all cases. This observation allowed the assumption that PDOs could indeed be used as patient-individual avatars to identify treatment sensitivities and resistances, as they share fundamental molecular properties with the tissue they have been initiated from.

Extensive pharmacotyping was performed for many PDO lines by testing the response behavior to the multi-drug regimens FOLFIRINOX and Gem/Pac, as well as their respective single drug compounds. As a result, we observed diverse response patterns for each PDAC PDO line. A poor response to FOLFIRINOX did not necessarily imply a resistance to Gem/Pac. PDO pharmacotyping could guide treatment decision making in the foreseeable future. Moreover, when the non-efficient drug was removed, no changes of overall efficacy of treatment in PDOs was observed, implying that additional therapy improvements could be possible using this *ex vivo* model. This observation was true for both commonly used chemotherapy protocols, FOLFIRINOX and Gem/Pac and could result in less drug mediated side effects under (neo)adjuvant CTx without impacting treatment efficacy.

Yet, the main goal of this study was to assess if PDAC PDOs can be used to predict the neoCTx outcome of PDAC patients. All methods required to address this issue in a prospective clinical trial have been established as a protocol for PDAC PDOs initiation from minimal starting material has been established and subsequently improved resulting in take rates of up to 80%. To support this study, we successfully secured patient enrollment from a second clinical center, which will increase the number of recruited patients in the future. Unfortunately, at the time of writing this thesis, patient numbers were not sufficient to answer the question of the predictive value of PDAC PDOs in regard to the current standard of care.

Bibliography

1. Yuan, Q., Pan, A., Fu, Y. & Dai, Y. *Anatomy and physiology of the pancreas*. *Integrative Pancreatic Intervention Therapy* (INC, 2021). doi:10.1016/b978-0-12-819402-7.00001-2.
2. Shah, A., Fehmi, A. & Savides, T. J. Increased rates of duodenal obstruction in pancreatic cancer patients receiving modern medical management. *Dig. Dis. Sci.* **59**, 2294–2298 (2014).
3. Sung, H. *et al.* Global Cancer Statistics 2020: GLOBOCAN Estimates of Incidence and Mortality Worldwide for 36 Cancers in 185 Countries. *CA. Cancer J. Clin.* **71**, 209–249 (2021).
4. Gatta, G. *et al.* Cancer survival in Europe 1999-2007 by country and age: Results of EUROCARE-5 - A population-based study. *Lancet Oncol.* **15**, 23–34 (2014).
5. Ferlay, J., Partensky, C. & Bray, F. More deaths from pancreatic cancer than breast cancer in the EU by 2017. *Acta Oncol. (Madr).* **55**, 1158–1160 (2016).
6. Larsson, S. C. *et al.* Overall obesity, abdominal adiposity, diabetes and cigarette smoking in relation to the risk of pancreatic cancer in two Swedish population-based cohorts. *Br. J. Cancer* **93**, 1310–1315 (2005).
7. Patel, A. V. *et al.* Obesity, recreational physical activity, and risk of pancreatic cancer in a large U.S. cohort. *Cancer Epidemiol. Biomarkers Prev.* **14**, 459–466 (2005).
8. McCarty, M. F. Up-regulation of IGF binding protein-1 as an anticarcinogenic strategy: Relevance to caloric restriction, exercise, and insulin sensitivity. *Med. Hypotheses* **48**, 297–308 (1997).
9. Ben, Q. *et al.* Diabetes mellitus and risk of pancreatic cancer: A meta-analysis of cohort studies. *Eur. J. Cancer* **47**, 1928–1937 (2011).
10. Luo, W., Tao, J., Zheng, L. & Zhang, T. Current epidemiology of pancreatic cancer: Challenges and opportunities. *Chinese J. Cancer Res.* **32**, 705–719 (2020).
11. Babic, A. *et al.* Pancreatic cancer risk associated with prediagnostic plasma levels of leptin and leptin receptor genetic polymorphisms. *Cancer Res.* **76**, 7160–7167 (2016).
12. Greer, J. B., Lynch, H. T. & Brand, R. E. Hereditary pancreatic cancer: A clinical perspective. *Best Pract. Res. Clin. Gastroenterol.* **23**, 159–170 (2009).
13. Howes, N. & Neoptolemos, J. P. Risk of pancreatic ductal adenocarcinoma in chronic pancreatitis. *Gut* **51**, 765–766 (2002).
14. Park, W., Chawla, A. & O'Reilly, E. M. Pancreatic Cancer: A Review. *JAMA - J. Am. Med. Assoc.* **326**, 851–862 (2021).
15. Orth, M. *et al.* Pancreatic ductal adenocarcinoma: Biological hallmarks, current status, and future perspectives of combined modality treatment approaches. *Radiat. Oncol.* **14**, 1–20 (2019).

16. Kopp, J. L. *et al.* Identification of Sox9-Dependent Acinar-to-Ductal Reprogramming as the Principal Mechanism for Initiation of Pancreatic Ductal Adenocarcinoma. *Cancer Cell* **22**, 737–750 (2012).
17. Friedlander, S. Y. G. *et al.* Context-Dependent Transformation of Adult Pancreatic Cells by Oncogenic K-Ras. *Cancer Cell* **16**, 379–389 (2009).
18. Waters, A. M. & Der, C. J. KRAS: The critical driver and therapeutic target for pancreatic cancer. *Cold Spring Harb. Perspect. Med.* **8**, 1–17 (2018).
19. Hruban, R. H., Maitra, A., Kern, S. E. & Goggins, M. Precursors to Pancreatic Cancer. *Gastroenterol. Clin. North Am.* **36**, 831–849 (2007).
20. Maitra, A. *et al.* Multicomponent analysis of the pancreatic adenocarcinoma progression model using a pancreatic intraepithelial neoplasia tissue microarray. *Mod. Pathol.* **16**, 902–912 (2003).
21. Hanahan, D. & Weinberg, R. A. Hallmarks of cancer: the next generation. *Cell* **144**, 646–74 (2011).
22. Hanahan, D. Hallmarks of Cancer: New Dimensions. *Cancer Discov.* **12**, 31–46 (2022).
23. Kleeff, J. *et al.* Pancreatic cancer. *Nat. Rev. Dis. Prim.* **2**, 1–23 (2016).
24. Makohon-Moore, A. P. *et al.* Limited heterogeneity of known driver gene mutations among the metastases of individual patients with pancreatic cancer. *Nat. Genet.* **49**, 358–366 (2017).
25. Rhim, A. D. *et al.* EMT and dissemination precede pancreatic tumor formation. *Cell* **148**, 349–361 (2012).
26. Diaz, C. L., Cinar, P., Hwang, J., Ko, A. H. & Tempero, M. A. CA 19-9 Response: A Surrogate to Predict Survival in Patients with Metastatic Pancreatic Adenocarcinoma. *Am. J. Clin. Oncol. Cancer Clin. Trials* **42**, 898–902 (2019).
27. Goonetilleke, K. S. & Siriwardena, A. K. Systematic review of carbohydrate antigen (CA 19-9) as a biochemical marker in the diagnosis of pancreatic cancer. *Eur. J. Surg. Oncol.* **33**, 266–270 (2007).
28. Vincent, A., Herman, J., Schulick, R., Hruban, R. H. & Goggins, M. Pancreatic cancer. *Lancet* **378**, 607–620 (2011).
29. Hasan, S., Jacob, R., Manne, U. & Paluri, R. Advances in pancreatic cancer biomarkers. *Oncol. Rev.* **13**, 69–76 (2019).
30. O'Sullivan, B. *et al.* Understanding and Reasonable Expectations. **18**, 849–851 (2018).
31. Rochefort, M. M. *et al.* Impact of tumor grade on pancreatic cancer prognosis: Validation of a novel TNMG staging system. *Ann. Surg. Oncol.* **20**, 4322–4329 (2013).
32. Demir, I. E. *et al.* R0 Versus R1 Resection Matters after Pancreaticoduodenectomy, and Less after Distal or Total Pancreatectomy for Pancreatic Cancer. *Ann. Surg.* **268**, (2017).
33. Müller, P. C. *et al.* Neoadjuvant Chemotherapy in Pancreatic Cancer: An Appraisal of the Current

High-Level Evidence. *Pharmacology* 143–153 (2020) doi:10.1159/000510343.

34. Seufferlein, T. *et al.* Optimizing the management of locally advanced pancreatic cancer with a focus on induction chemotherapy: Expert opinion based on a review of current evidence. *Cancer Treat. Rev.* **77**, 1–10 (2019).
35. Perri, G., Prakash, L. & Katz, M. H. G. Defining and Treating Borderline Resectable Pancreatic Cancer. *Curr. Treat. Options Oncol.* **21**, 1–11 (2020).
36. Burris, H. A. *et al.* Improvements in survival and clinical benefit with gemcitabine as first- line therapy for patients with advanced pancreas cancer: A randomized trial. *J. Clin. Oncol.* **15**, 2403–2413 (1997).
37. Conroy, T. *et al.* FOLFIRINOX versus Gemcitabine for Metastatic Pancreatic Cancer. *N. Engl. J. Med.* **364**, 1817–1825 (2011).
38. Von Hoff, D. D. *et al.* Increased Survival in Pancreatic Cancer with nab-Paclitaxel plus Gemcitabine. *N. Engl. J. Med.* **369**, 1691–1703 (2013).
39. Conroy, T. *et al.* FOLFIRINOX versus Gemcitabine for Metastatic Pancreatic Cancer. *N. Engl. J. Med.* **364**, 1817–1825 (2011).
40. Suker, M. *et al.* FOLFIRINOX for locally advanced pancreatic cancer: a systematic review and patient-level meta-analysis. *Lancet Oncol.* **17**, 801–810 (2016).
41. Rae Cho, Huapyong Kang, Jung Hyun Jo, Hee Seung Lee, Moon Jae Chung, J. Y. P. & Seung Woo Park, Si Young Song, Chansik An, Mi-Suk Park, S. B. World Journal of Pediatrics. *World J Pediatr* **7**, (2011).
42. Sohal, D. *et al.* SWOG S1505: Results of perioperative chemotherapy (peri-op CTx) with mfolfirinox versus gemcitabine/nab-paclitaxel (Gem/nabP) for resectable pancreatic ductal adenocarcinoma (PDA). *J. Clin. Oncol.* **38**, 4504 (2020).
43. Flaum, N., Hubner, R. A., Valle, J. W., Amir, E. & McNamara, M. G. Adjuvant chemotherapy and outcomes in patients with nodal and resection margin-negative pancreatic ductal adenocarcinoma: A systematic review and meta-analysis. *J. Surg. Oncol.* **119**, 932–940 (2019).
44. DePeralta, D. K. *et al.* Completion of adjuvant therapy in patients with resected pancreatic cancer. *Hpb* **22**, 241–248 (2020).
45. Murphy, J. E. *et al.* Total neoadjuvant therapy with FOLFIRINOX followed by individualized chemoradiotherapy for borderline resectable pancreatic adenocarcinoma: A phase 2 clinical trial. *JAMA Oncol.* **4**, 963–969 (2018).
46. Jang, J. Y. *et al.* Oncological Benefits of Neoadjuvant Chemoradiation With Gemcitabine Versus Upfront Surgery in Patients With Borderline Resectable Pancreatic Cancer: A Prospective, Randomized, Open-label, Multicenter Phase 2/3 Trial. *Ann. Surg.* **268**, 215–222 (2018).
47. Strobel, O. *et al.* Pancreatic cancer surgery. *Ann. Surg.* **265**, 565–573 (2017).

48. van Roessel, S. *et al.* Pathological Margin Clearance and Survival After Pancreaticoduodenectomy in a US and European Pancreatic Center. *Ann. Surg. Oncol.* **25**, 1760–1767 (2018).

49. Baliyan, V., Kordbacheh, H., Parakh, A. & Kambadakone, A. Response assessment in pancreatic ductal adenocarcinoma: role of imaging. *Abdom. Radiol.* **43**, 435–444 (2018).

50. Ferrone, C. R. *et al.* Radiological and surgical implications of neoadjuvant treatment with FOLFIRINOX for locally advanced and borderline resectable pancreatic cancer. *Ann. Surg.* **261**, 12–17 (2015).

51. Verbeke, C., Löhr, M., Severin Karlsson, J. & Del Chiaro, M. Pathology reporting of pancreatic cancer following neoadjuvant therapy: Challenges and uncertainties. *Cancer Treat. Rev.* **41**, 17–26 (2015).

52. Le Scodan, R. *et al.* Histopathological response to preoperative chemoradiation for resectable pancreatic adenocarcinoma: The French Phase II FFCD 9704-SFRO trial. *Am. J. Clin. Oncol. Cancer Clin. Trials* **31**, 545–552 (2008).

53. Miller, A. R. *et al.* Preoperative chemoradiation and pancreaticoduodenectomy for adenocarcinoma of the pancreas. *Hepatogastroenterology.* **45**, 624–633 (1998).

54. White, R. R. *et al.* Significance of histological response to preoperative chemoradiotherapy for pancreatic cancer. *Ann. Surg. Oncol.* **12**, 214–221 (2005).

55. Washington, K. *et al.* Protocol for the Examination of Specimens From Patients With Carcinoma of the Exocrine Pancreas Procedures • Partial Pancreatectomy • Pancreaticoduodenectomy (Whipple Resection) • Total Pancreatectomy Previous contributors. (2012).

56. Hartman, D. J. & Krasinskas, A. M. Assessing treatment effect in pancreatic cancer. *Arch. Pathol. Lab. Med.* **136**, 100–109 (2012).

57. Mellon, E. A. *et al.* Predictors and survival for pathologic tumor response grade in borderline resectable and locally advanced pancreatic cancer treated with induction chemotherapy and neoadjuvant stereotactic body radiotherapy. *Acta Oncol. (Madr).* **56**, 391–397 (2017).

58. Zhang, Y. K., Wang, Y. J., Gupta, P. & Chen, Z. S. Multidrug Resistance Proteins (MRPs) and Cancer Therapy. *AAPS J.* **17**, 802–812 (2015).

59. Maréchal, R. *et al.* Deoxycitidine kinase is associated with prolonged survival after adjuvant gemcitabine for resected pancreatic adenocarcinoma. *Cancer* **116**, 5200–5206 (2010).

60. Erkan, M. Understanding the stroma of pancreatic cancer: Co-evolution of the microenvironment with epithelial carcinogenesis. *J. Pathol.* **231**, 4–7 (2013).

61. Duluc, C. *et al.* Pharmacological targeting of the protein synthesis mTOR /4E- BP 1 pathway in cancer-associated fibroblasts abrogates pancreatic tumour chemoresistance . *EMBO Mol. Med.* **7**, 735–753 (2015).

62. Lesina, M., Wörmann, S. M., Neuhöfer, P., Song, L. & Algül, H. Interleukin-6 in inflammatory and malignant diseases of the pancreas. *Semin. Immunol.* **26**, 80–87 (2014).
63. Adamska, A. *et al.* Molecular and cellular mechanisms of chemoresistance in pancreatic cancer. *Adv. Biol. Regul.* **68**, 77–87 (2018).
64. Principe, D. R. *et al.* The Current Treatment Paradigm for Pancreatic Ductal Adenocarcinoma and Barriers to Therapeutic Efficacy. *Front. Oncol.* **11**, 1–25 (2021).
65. Sparreboom, A. *et al.* Limited oral bioavailability and active epithelial excretion of paclitaxel (Taxol) caused by P-glycoprotein in the intestine. *Proc. Natl. Acad. Sci. U. S. A.* **94**, 2031–2035 (1997).
66. Peters, G. J. *et al.* Induction of thymidylate synthase as a 5-fluorouracil resistance mechanism. *Biochim. Biophys. Acta - Mol. Basis Dis.* **1587**, 194–205 (2002).
67. Longley, D. B. & Johnston, P. G. Molecular mechanisms of drug resistance. *J. Pathol.* **205**, 275–292 (2005).
68. Beretta, G. L. *et al.* Increased levels and defective glycosylation of MRPs in ovarian carcinoma cells resistant to oxaliplatin. *Biochem. Pharmacol.* **79**, 1108–1117 (2010).
69. Mishima, M., Samimi, G., Kondo, A., Lin, X. & Howell, S. B. The cellular pharmacology of oxaliplatin resistance. *Eur. J. Cancer* **38**, 1405–1412 (2002).
70. Shirota, Y. *et al.* ERCC1 and thymidylate synthase mRNA levels predict survival for colorectal cancer patients receiving combination oxaliplatin and fluorouracil chemotherapy. *J. Clin. Oncol.* **19**, 4298–4304 (2001).
71. Gourdier, I. *et al.* Drug specific resistance to oxaliplatin is associated with apoptosis defect in a cellular model of colon carcinoma. *FEBS Lett.* **529**, 232–236 (2002).
72. Collisson, E. A. *et al.* Subtypes of pancreatic ductal adenocarcinoma and their differing responses to therapy. *Nat. Med.* **17**, 500–503 (2011).
73. Maximiano, S., Magalhães, P., Guerreiro, M. P. & Morgado, M. Trastuzumab in the Treatment of Breast Cancer. *BioDrugs* **30**, 75–86 (2016).
74. Collisson, E. A., Bailey, P., Chang, D. K. & Biankin, A. V. Molecular subtypes of pancreatic cancer. *Nat. Rev. Gastroenterol. Hepatol.* **16**, 207–220 (2019).
75. Planchard, D. *et al.* Dabrafenib plus trametinib in patients with previously untreated BRAFV600E-mutant metastatic non-small-cell lung cancer: an open-label, phase 2 trial. *Lancet Oncol.* **18**, 1307–1316 (2017).
76. Ledermann, J. *et al.* Olaparib Maintenance Therapy in Patients With Platinum-Sensitive Relapsed Serous Ovarian Cancer. *Obstet. Gynecol. Surv.* **69**, 594–596 (2014).
77. Waddell, N. *et al.* Whole genomes redefine the mutational landscape of pancreatic cancer. *Nature* **518**, 495–501 (2015).

78. Badea, L., Herlea, V., Dima, S. O., Dumitrascu, T. & Popescu, I. Combined gene expression analysis of whole-tissue and microdissected pancreatic ductal adenocarcinoma identifies genes specifically overexpressed in tumor epithelia. *Hepatogastroenterology.* **55**, 2016–2027 (2008).
79. Moffitt, R. A. *et al.* Virtual microdissection identifies distinct tumor- and stroma-specific subtypes of pancreatic ductal adenocarcinoma. *Nat. Publ. Gr.* **47**, 1168–1178 (2015).
80. Bailey, P. *et al.* Genomic analyses identify molecular subtypes of pancreatic cancer. *Nature* **531**, 47–52 (2016).
81. Noll, E. M. *et al.* CYP3A5 mediates basal and acquired therapy resistance in different subtypes of pancreatic ductal adenocarcinoma. *Nat. Med.* **22**, 278–287 (2016).
82. Muckenhuber, A. *et al.* Pancreatic ductal adenocarcinoma subtyping using the biomarkers hepatocyte nuclear factor-1A and cytokeratin-81 correlates with outcome and treatment response. *Clin. Cancer Res.* **24**, 351–359 (2018).
83. Clevers, H. Modeling Development and Disease with Organoids. *Cell* **165**, 1586–1597 (2016).
84. Corrò, C., Novellasdemunt, L. & Li, V. S. W. A brief history of organoids. *Am. J. Physiol. - Cell Physiol.* **319**, C151–C165 (2020).
85. Valentine, T. & Swarm, R. Solid tumors produce extracellular matrices . This is particularly apparent in the case of chondrosarcomas where tumor cells exist in lacunar spaces surrounded by extracellular matrix . The matrix produced by normal cartilage cells protein core and form. **145**, 204–220 (1977).
86. Sato, T. *et al.* Single Lgr5 stem cells build crypt-villus structures in vitro without a mesenchymal niche. *Nature* **459**, 262–265 (2009).
87. Barker, N. *et al.* Lgr5+ve Stem Cells Drive Self-Renewal in the Stomach and Build Long-Lived Gastric Units In Vitro. *Cell Stem Cell* **6**, 25–36 (2010).
88. Stange, D. E. *et al.* XDifferentiated Troy+ chief cells act as reserve stem cells to generate all lineages of the stomach epithelium. *Cell* **155**, 357 (2013).
89. Artegiani, B. & Clevers, H. Use and application of 3D-organoid technology. *Hum. Mol. Genet.* **27**, R99–R107 (2018).
90. Huch, M. *et al.* Unlimited in vitro expansion of adult bi-potent pancreas progenitors through the Lgr5/R-spondin axis. *EMBO J.* **32**, 2708–2721 (2013).
91. Boj, S. F. *et al.* Organoid models of human and mouse ductal pancreatic cancer. *Cell* **160**, 324–338 (2015).
92. Merker, S. R., Weitz, J. & Stange, D. E. Gastrointestinal organoids: How they gut it out. *Dev. Biol.* **420**, 239–250 (2016).
93. Broutier, L. *et al.* Culture and establishment of self-renewing human and mouse adult liver and pancreas 3D organoids and their genetic manipulation. *Nat. Protoc.* **11**, 1724–1743 (2016).

94. Sato, T. *et al.* Long-term expansion of epithelial organoids from human colon, adenoma, adenocarcinoma, and Barrett's epithelium. *Gastroenterology* **141**, 1762–1772 (2011).

95. Tiriac, H. *et al.* Organoid profiling identifies common responders to chemotherapy in pancreatic cancer. *Cancer Discov.* CD-18-0349 (2018) doi:10.1158/2159-8290.CD-18-0349.

96. Driehuis, E. *et al.* Pancreatic cancer organoids recapitulate disease and allow personalized drug screening. *PNAS* (2019) doi:10.1073/pnas.1911273116.

97. Romero-Calvo, I. *et al.* Human organoids share structural and genetic features with primary pancreatic adenocarcinoma tumors. *Mol. Cancer Res.* **17**, 70–83 (2019).

98. Dekkers, J. F. *et al.* A functional CFTR assay using primary cystic fibrosis intestinal organoids. *Nat. Med.* **19**, 939–945 (2013).

99. Schwank, G. *et al.* Functional repair of CFTR by CRISPR/Cas9 in intestinal stem cell organoids of cystic fibrosis patients. *Cell Stem Cell* **13**, 653–658 (2013).

100. Lamers, M. M. *et al.* SARS-CoV-2 productively infects human gut enterocytes. *Science (80-.).* **369**, 50–54 (2020).

101. Bartfeld, S. & Clevers, H. Organoids as model for infectious diseases: Culture of human and murine stomach organoids and microinjection of helicobacter pylori. *J. Vis. Exp.* **2015**, 1–9 (2015).

102. Duque-Correa, M. A., Maizels, R. M., Grencis, R. K. & Berriman, M. Organoids – New Models for Host–Helminth Interactions. *Trends Parasitol.* **36**, 170–181 (2020).

103. Yui, S. *et al.* Functional engraftment of colon epithelium expanded in vitro from a single adult Lgr5 + stem cell. *Nat. Med.* **18**, 618–623 (2012).

104. Seino, T. *et al.* Human Pancreatic Tumor Organoids Reveal Loss of Stem Cell Niche Factor Dependence during Disease Progression. *Cell Stem Cell* **22**, 454-467.e6 (2018).

105. Driehuis, E. *et al.* Pancreatic cancer organoids recapitulate disease and allow personalized drug screening. *Proc. Natl. Acad. Sci. U. S. A.* **116**, 26580–26590 (2019).

106. Vlachogiannis, G. *et al.* Patient-derived organoids model treatment response of metastatic gastrointestinal cancers. *Science (80-.).* **926**, 920–926 (2018).

107. Sachs, N. *et al.* A Living Biobank of Breast Cancer Organoids Captures Disease Heterogeneity. *Cell* **172**, 373-386.e10 (2018).

108. Hayashi, H. *et al.* Utility of assessing the number of mutated KRAS, CDKN2A, TP53, and SMAD4 genes using a targeted deep sequencing assay as a prognostic biomarker for pancreatic cancer. *Pancreas* **46**, 335–340 (2017).

109. Hellemans, J., Mortier, G., De Paepe, A., Speleman, F. & Vandesompele, J. qBase relative quantification framework and software for management and automated analysis of real-time quantitative PCR data. *Genome Biol.* **8**, (2008).

110. Hennig, A. *et al.* Detecting drug resistance in pancreatic cancer organoids guides optimized chemotherapy treatment. *J. Pathol.* (2022) doi:10.1002/path.5906.
111. Georgakopoulos, N. *et al.* Long-term expansion, genomic stability and in vivo safety of adult human pancreas organoids. *BMC Dev. Biol.* **20**, 1–20 (2020).
112. Hennig, A. *et al.* CFTR Expression Analysis for Subtyping of Human Pancreatic Cancer Organoids. *Stem Cells Int.* **2019**, 1–8 (2019).
113. Vary, A. *et al.* FOLFIRINOX relative dose intensity and disease control in advanced pancreatic adenocarcinoma. *Ther. Adv. Med. Oncol.* **13**, 1–12 (2021).
114. Karjol, U. *et al.* Lymph Node Ratio as a Prognostic Marker in Pancreatic Cancer Survival: A Systematic Review and Meta-Analysis. *Cureus* **12**, 1–9 (2020).
115. Conroy, T. *et al.* FOLFIRINOX or Gemcitabine as Adjuvant Therapy for Pancreatic Cancer. *N. Engl. J. Med.* **379**, 2395–2406 (2018).
116. Oba, A. *et al.* Neoadjuvant Treatment in Pancreatic Cancer. *Front. Oncol.* **10**, 1–10 (2020).
117. Neoptolemos, J. P. *et al.* Comparison of adjuvant gemcitabine and capecitabine with gemcitabine monotherapy in patients with resected pancreatic cancer (ESPAC-4): a multicentre, open-label, randomised, phase 3 trial. *Lancet* **389**, 1011–1024 (2017).
118. Trial, A. R. C. & Roll, L. vs Observation in Patients Undergoing Curative-Intent Resection of Pancreatic Cancer. **297**, 267–277 (2007).
119. Mackay, T. M. *et al.* The risk of not receiving adjuvant chemotherapy after resection of pancreatic ductal adenocarcinoma: a nationwide analysis. *Hpb* **22**, 233–240 (2020).
120. Lee, Y. S., Lee, J. C., Yang, S. Y., Kim, J. & Hwang, J. H. Neoadjuvant therapy versus upfront surgery in resectable pancreatic cancer according to intention-to-treat and per-protocol analysis: A systematic review and meta-analysis. *Sci. Rep.* **9**, 1–8 (2019).
121. van Hagen, P. *et al.* Preoperative Chemoradiotherapy for Esophageal or Junctional Cancer. *N. Engl. J. Med.* **366**, 2074–2084 (2012).
122. Shapiro, J. *et al.* Neoadjuvant chemoradiotherapy plus surgery versus surgery alone for oesophageal or junctional cancer (CROSS): Long-term results of a randomised controlled trial. *Lancet Oncol.* **16**, 1090–1098 (2015).
123. Tiriac, H. *et al.* Organoid profiling identifies common responders to chemotherapy in pancreatic cancer. *Cancer Discov.* **8**, 1112–1129 (2018).
124. Tiriac, H. *et al.* Successful creation of pancreatic cancer organoids by means of EUS-guided fine-needle biopsy sampling for personalized cancer treatment. *Gastrointest. Endosc.* **87**, 1474–1480 (2018).
125. Mahadevan, D. & Von Hoff, D. D. Tumor-stroma interactions in pancreatic ductal adenocarcinoma. *Mol. Cancer Ther.* **6**, 1186–1197 (2007).

126. Sorrentino, G. *et al.* Mechano-modulatory synthetic niches for liver organoid derivation. *Nat. Commun.* **11**, (2020).

127. Öhlund, D. *et al.* Distinct populations of inflammatory fibroblasts and myofibroblasts in pancreatic cancer. *J. Exp. Med.* jem.20162024 (2017) doi:10.1084/jem.20162024.

128. Tsai, S. *et al.* Development of primary human pancreatic cancer organoids, matched stromal and immune cells and 3D tumor microenvironment models. *BMC Cancer* **18**, 1–13 (2018).

129. Aguirre, A. J. *et al.* Real-time genomic characterization of advanced pancreatic cancer to enable precision medicine. *Cancer Discov.* **8**, 1096–1111 (2018).

130. Biankin, A. V. & Maitra, A. Subtyping Pancreatic Cancer. *Cancer Cell* **28**, 411–413 (2015).

131. Janssen, Q. P., O'Reilly, E. M., van Eijck, C. H. J. & Groot Koerkamp, B. Neoadjuvant Treatment in Patients With Resectable and Borderline Resectable Pancreatic Cancer. *Front. Oncol.* **10**, 1–13 (2020).

132. Mokhtari, R. B. *et al.* Combination therapy in combating cancer SYSTEMATIC REVIEW: COMBINATION THERAPY IN COMBATING CANCER BACKGROUND. *Oncotarget* **8**, 38022–38043 (2017).

133. Al-Batran, S. E. *et al.* Perioperative chemotherapy with fluorouracil plus leucovorin, oxaliplatin, and docetaxel versus fluorouracil or capecitabine plus cisplatin and epirubicin for locally advanced, resectable gastric or gastro-oesophageal junction adenocarcinoma (FLOT4): a ra. *Lancet* **393**, 1948–1957 (2019).

134. de Gramont, A. *et al.* Leucovorin and fluorouracil with or without oxaliplatin as first-line treatment in advanced colorectal cancer. *J. Clin. Oncol.* **18**, 2938–2947 (2000).

135. Palmer, A. C. & Sorger, P. K. Combination Cancer Therapy Can Confer Benefit via Patient-to-Patient Variability without Drug Additivity or Synergy. *Cell* **171**, 1678-1691.e13 (2017).

136. Crawford, J. *et al.* Relative dose intensity of first-line chemotherapy and overall survival in patients with advanced non-small-cell lung cancer. *Support. Care Cancer* **28**, 925–932 (2020).

137. Qi, W. *et al.* The effect of reduced RDI of chemotherapy on the outcome of breast cancer patients. *Sci. Rep.* **10**, 1–13 (2020).

138. Kirino, S. *et al.* Relative dose intensity over the first four weeks of lenvatinib therapy is a factor of favorable response and overall survival in patients with unresectable hepatocellular carcinoma. *PLoS One* **15**, 1–11 (2020).

139. Ooft, S. N. *et al.* Patient-derived organoids can predict response to chemotherapy in metastatic colorectal cancer patients. *Sci. Transl. Med.* **11**, 1–10 (2019).

140. Yao, Y. *et al.* Patient-Derived Organoids Predict Chemoradiation Responses of Locally Advanced Rectal Cancer. *Cell Stem Cell* **26**, 17-26.e6 (2020).

141. Grossman, J. E. *et al.* Organoid Sensitivity Correlates with Therapeutic Response in Patients with

Pancreatic Cancer. *Clin. Cancer Res.* clincanres.4116.2020 (2021) doi:10.1158/1078-0432.ccr-20-4116.

142. Kitano, M. *et al.* Impact of endoscopic ultrasonography on diagnosis of pancreatic cancer. *J. Gastroenterol.* **54**, 19–32 (2019).

143. Dantes, Z. *et al.* Implementing cell-free DNA of pancreatic cancer patient–derived organoids for personalized oncology. *JCI Insight* **5**, (2020).

144. Beutel, A. K. *et al.* A prospective feasibility trial to challenge patient–derived pancreatic cancer organoids in predicting treatment response. *Cancers (Basel).* **13**, 1–18 (2021).

145. Huang, L. *et al.* Ductal pancreatic cancer modeling and drug screening using human pluripotent stem cell- and patient-derived tumor organoids. *Nat. Med.* **21**, 1364–1371 (2015).

Appendix

Supplementary Table 1 – PDAC patient cohort

Patient #	Age (at day of surgery)	Sex	T	N	R	G
1	60	m	3	1	0	3
2	64	f	2	2	0	3
3	78	m	2	2	0	3
4	66	f	2	1	0	3
5	68	f	2	2	0	3
6	80	m	3	2	1	3
7	72	f	2	0	0	2
8	61	m	3	1	0	2
9	70	m	3	1	0	3
10	54	f	2	1	0	2
11	63	f	2	0	0	2
12	67	f	2	1	1	2
13	71	f	3	2	0	2
14	71	m	3	1	0	2
15	58	m	3	2	0	3
16	61	f	3	1	0	2
17	80	f	3	2	1	3
18	71	m	3	1	0	3
19	62	m	3	2	1	2
20	56	f	2	0	0	3
21	63	f	3	1	0	3
22	64	m	2	2	0	3
23	70	m	2	1	0	2
24	72	m	2	1	1	3
25	67	f	2	2	1	3
26	66	f	2	1	0	3
27	57	m	1	0	0	3
28	78	m	2	1	0	2
29	76	m	3	0	0	3
30	77	m	2	2	1	2
31	77	f	2	1	0	2
32	69	f	2	2	1	3
33	78	m	2	1	0	3
34	79	f	2	2	1	2
35	78	f	2	1	0	2
36	67	f	3	2	1	3
37	82	m	2	0	0	2

38	74	m	2	1	Rx	3
39	62	m	3	0	Rx	3
40	64	m	2	1	0	3
41	57	f	2	1	0	3
42	66	f	3	2	Rx	3
43	78	m	1	1	1	2
44	65	m	2	2	1	3
45	83	m	2	1	0	2
46	55	m	2	2	0	3
47	79	f	2	1	0	2
48	58	f	3	0	0	2
49	62	m	3	2	Rx	3
50	49	f	3	2	0	2
51	57	f	2	1	0	2
52	76	f	2	2	0	3
53	80	f	3	1	0	2
54	80	m	2	0	0	2
55	69	m	3	1	0	2
56	57	m	2	2	0	2
57	81	f	2	2	0	3
58	84	f	2	1	0	3
59	76	m	3	2	0	2
60	72	f	1	0	0	3
61	60	m	2	1	0	2
62	76	m	2	1	0	2
63	70	f	3	1	0	2
64	35	f	2	1	1	2
65	67	m	3	2	Rx	3
66	72	m	3	0	0	3

Rx: Not clearly determinable

Supplementary Table 2 – LA PDAC patient cohort

#	Age (at date of surgery)	Sex	N	R	neoCTx regimen	Dose	TRG
1	52	m	1	0	FOLFIRINOX	full course	3
2	43	f	2	0	FOLFIRINOX	full course	1
3	65	m	0	Rx	FOLFIRINOX	full course	1
4	78	f	0	1	Gem/nab-Pac	full course	1
5	62	m	1	0	FOLFIRINOX	adapted	1
6	62	m	1	0	FOLFIRINOX	full course	3
7	77	m	0	0	Gem/nab-Pac	adapted	1
8	62	m	2	0	FOLFIRINOX	full course	2
9	59	f	2	0	FOLFIRINOX	full course	1
10	63	m	2	Rx	FOLFIRINOX	full course	2
11	68	f	0	0	FOLFIRINOX	full course	2
12	55	m	0	0	FOLFIRINOX	full course	2
13	62	f	1	0	FOLFIRINOX	adapted	1
14	77	f	1	0	Gem/nab-Pac	full course	1
15	61	m	0	0	FOLFIRINOX	full course	3
16	69	m	1	0	FOLFIRINOX	adapted	1
17	67	f	0	1	FOLFIRINOX	adapted	1
18	72	f	0	0	Gem/nab-Pac	adapted	1
19	65	f	1	1	FOLFIRINOX	adapted	1
20	70	m	0	1	FOLFIRINOX	adapted	2
21	59	f	2	0	Gem/nab-Pac	adapted	1
22	62	m	2	0	FOLFIRINOX	full course	2
23	50	m	0	0	FOLFIRINOX	adapted	2
24	51	m	1	0	FOLFIRINOX	full course	1
25	65	m	2	0	FOLFIRINOX	full course	2
26	78	f	1	0	Gem/nab-Pac	full course	1
27	75	f	1	0	Gem/nab-Pac	full course	1
28	58	f	0	0	FOLFIRINOX	full course	2
29	67	m	1	0	FOLFIRINOX	full course	1
30	62	m	0	1	FOLFIRINOX	full course	2
31	63	f	2	1	FOLFIRINOX	full course	1
32	62	m	1	0	FOLFIRINOX	full course	1
33	51	f	0	0	(FOLFIRINOX) & Gem/nab-Pac	full course	2
34	48	f	2	0	FOLFIRINOX	full course	2
35	72	f	1	0	Gem/nab-Pac	full course	1
36	66	f	0	0	FOLFIRINOX	adapted	3
37	57	f	0	1	FOLFIRINOX	adapted	1
38	66	f	1	0	FOLFIRINOX	full course	1

39	71	m	1	0	FOLFIRINOX	adapted	1
40	57	f	0	0	FOLFIRINOX	full course	3
41	47	m	1	Rx	Gem/nab-Pac	full course	2
42	49	m	2	1	FOLFIRINOX	adapted	1
43	79	m	1	0	Gem/nab-Pac	adapted	1
44	73	m	1	Rx	Gem/nab-Pac	full course	2
45	76	f	0	0	FOLFIRINOX	full course	3
46	62	m	1	0	Gem/nab-Pac	full course	3
47	66	f	1	Rx	FOLFIRINOX	adapted	1
48	64	m	0	Rx	FOLFIRINOX	full course	1
49	63	f	0	0	FOLFIRINOX	full course	3
50	61	f	1	0	FOLFIRINOX	full course	3
51	68	f	0	0	FOLFIRINOX	full course	2
52	65	f	2	0	FOLFIRINOX	full course	1
53	60	f	1	1	FOLFIRINOX	full course	1
54	81	f	0	0	Gem/nab-Pac	full course	2
55	64	f	1	0	FOLFIRINOX	full course	1
56	71	f	1	0	Gem/nab-Pac	full course	2
57	73	f	1	0	Gem/nab-Pac	full course	1
58	68	m	0	0	Gem/nab-Pac	full course	2
59	80	m	0	1	Gem/nab-Pac	adapted	2

Rx: Not clearly determinable

FOLFIRINOX: 5-FU + folinic acid + oxaliplatin + irinotecan

Gem/nab-Pac: gemcitabine + nanoparticle albumin-bound paclitaxel

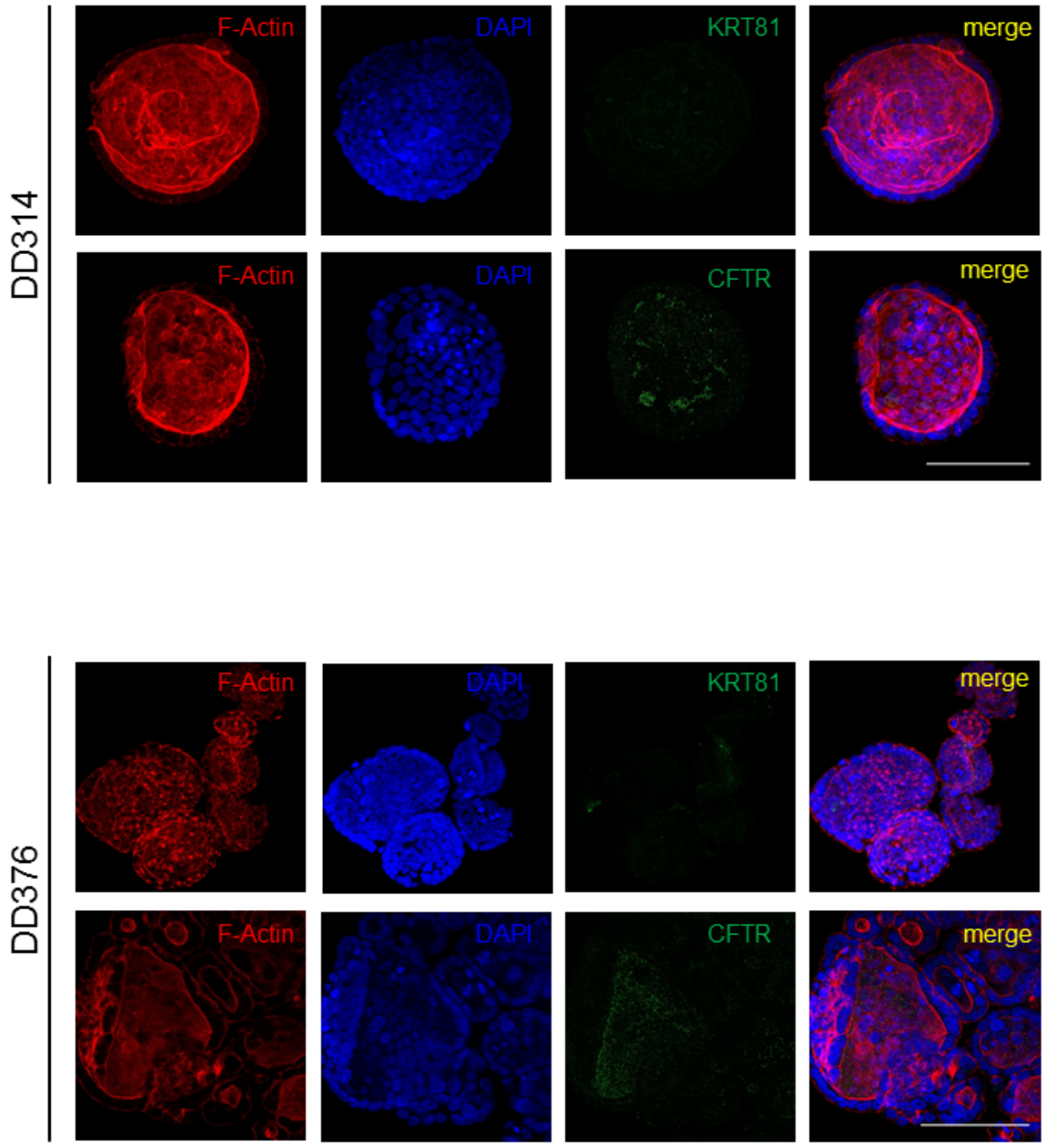

Supplementary Figure 1 – IF staining of CFTR and KRT81 on human PDAC organoids. The CFTR and KRT81 expression analysis was performed on eight additional PDAC organoids (DD314, DD376, DD394, DD439, DD442, NR002, NR005 and NR006) for assessing the molecular PDAC subtype according to Collisson[72]. DAPI and Phalloidin stained cell nuclei and F-actin respectively. Scale bars represents 200 µm. Stainings have been performed and imaged by Laura Wolf. IF staining figures have been taken from Hennig *et al.* 2019[112] with permission from Stem Cells International.

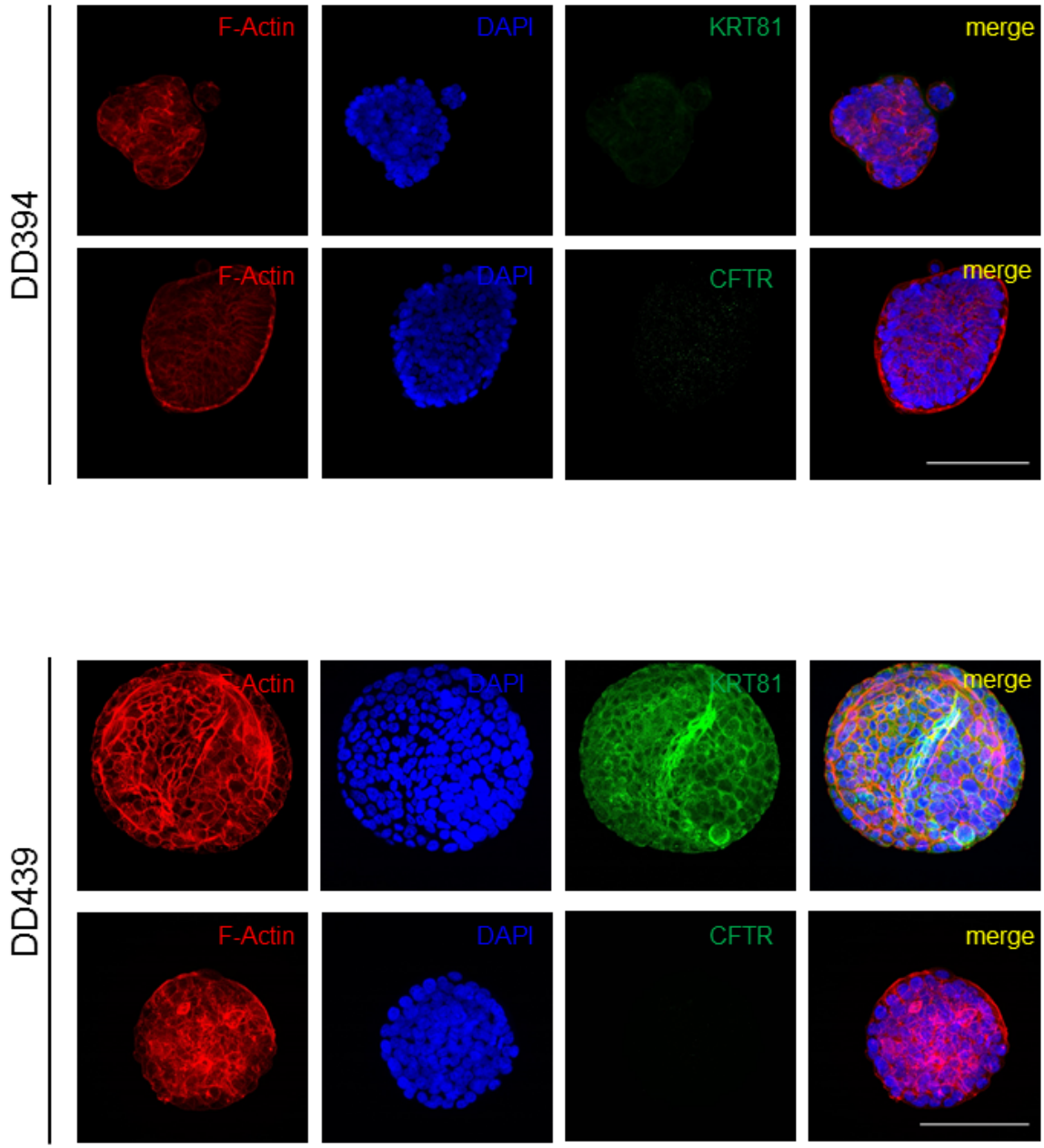

(Supplementary Figure 1 continued)

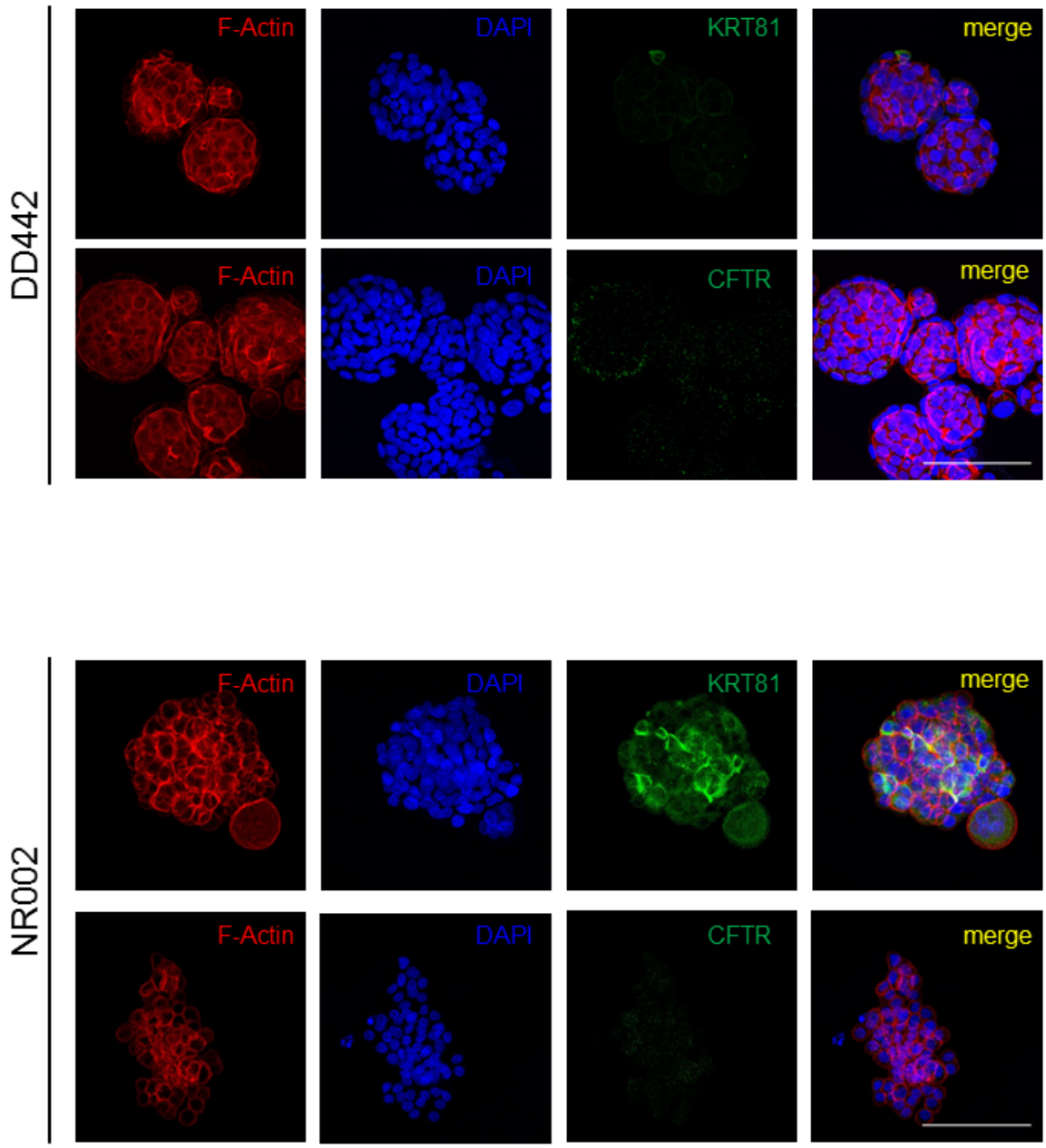

(Supplementary Figure 1 continued)

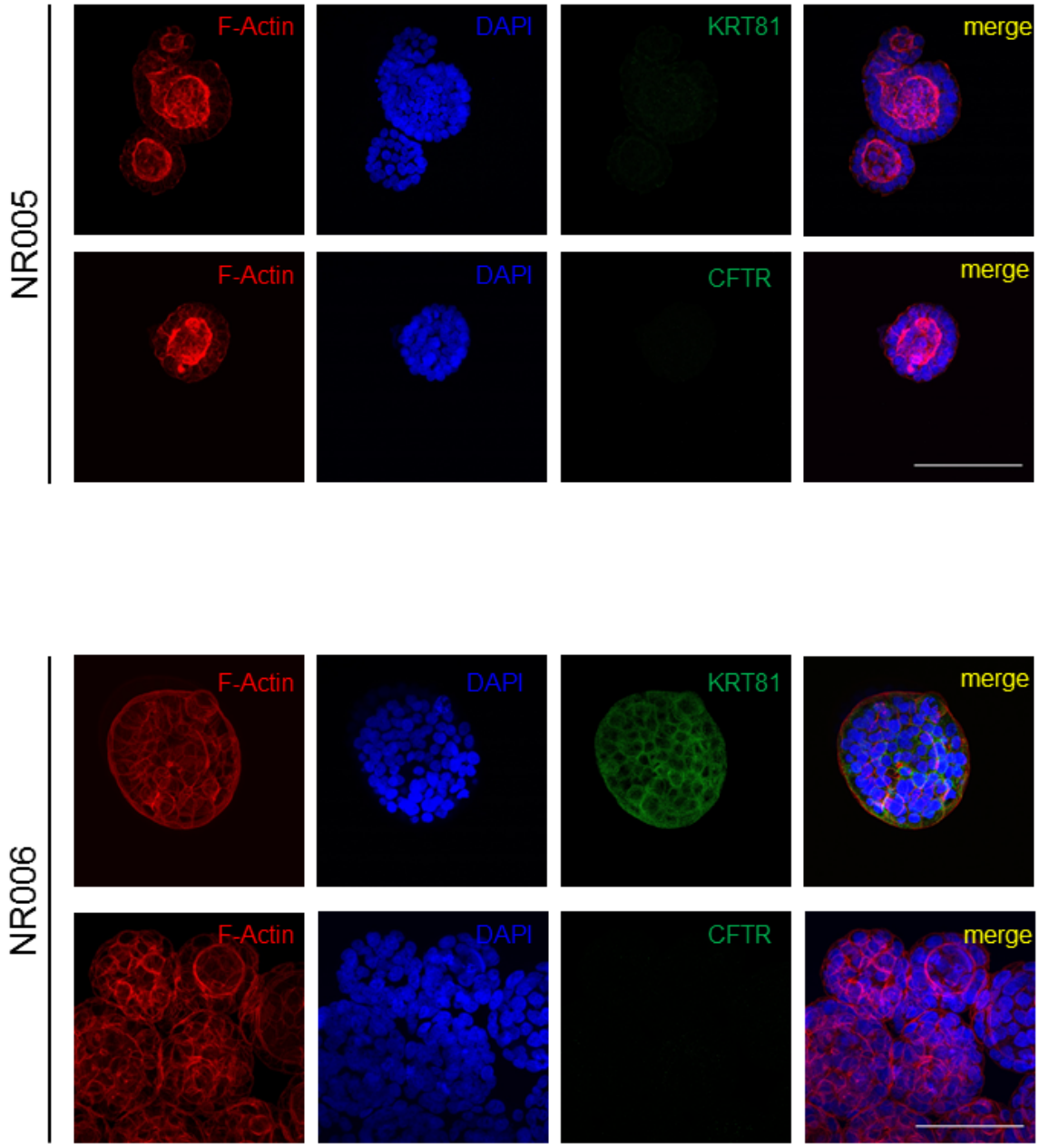

(Supplementary Figure 1 continued)

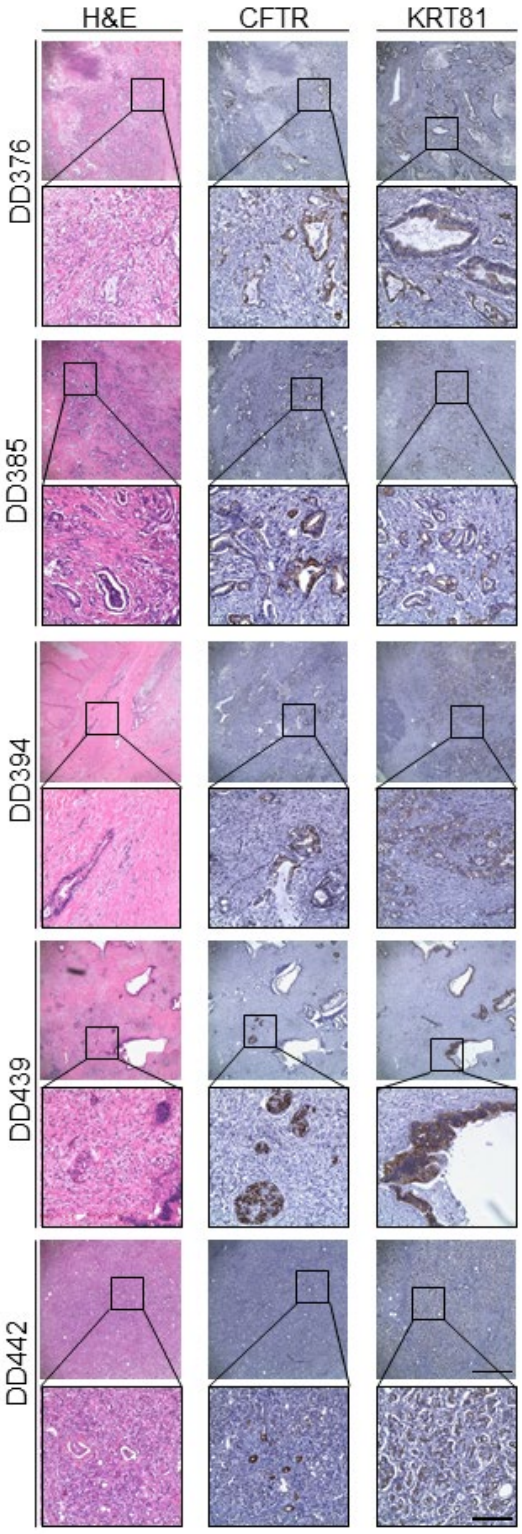

Supplementary Figure 2 - CFTR and KRT81 expression analysis in primary PDAC tissue sections. IHC stainings of CFTR and KRT81 on corresponding primary tumor tissue sections of 5 additional PDAC organoids lines have been performed for determining the molecular subtype according to Collisson *et al.* and Noll *et al.*[72,81]. Scale bars represents 200 µm. Images have been taken from Hennig *et al.* 2019[112] with permission from Stem Cells International.

Danksagung

Mein Dank gilt all denjenigen, die mich während meiner Doktorandenzeit unterstützt und begleitet haben.

Mein besonderer Dank gilt PD Dr. Daniel Stange und Prof. Dr. Thilo Welsch, die mir eine Vielzahl herausfordernder und umso spannender Projekte anvertrauten. Beide haben mich, obwohl enorm in den Klinikalltag eingebunden, stets durch ihr Wissen und ihren Rat unterstützt und mir gleichzeitig viel Freiraum zum Weiterentwickeln meiner Fähigkeiten als Wissenschaftler gewährt.

Ich danke Prof. Dr. Christian Dahmann und Prof. Dr. Maximilian Reichert für das Begutachten meiner Doktorarbeit, sowie allen weiteren Mitgliedern der Promotionskommission, Prof. Dr. Christoph Neinhuis, Prof. Dr. Thorsten Mascher und Prof. Dr. Sebastian Zeissig.

Ich danke Dr. Franziska Baenke und Dr. Therese Seidlitz für all die Unterstützung, durch ihr Wissen und ihre Erfahrungen als Wissenschaftlerinnen.

Ich danke meinen ehemaligen Kollegen der AG Stange, allen voran Susi, Trixi, Heike, Tim, Juliane, Kathi, Dylan und Kristin für die gute Zusammenarbeit, die herzliche Atmosphäre, die vielen Kuchenrunden und die vielen schönen Momente die mir in Zeiten, in denen einem die Wissenschaft viel Kraft, Nerven und Ausdauer abverlangten, halfen.

Ich danke Dr. Anna Klimova für die Unterstützung bei der Beantwortung aller biostatistischer Fragen, die während der Bearbeitung der Projekte aufkamen.

Ich danke den Mitarbeitern der Medizinischen Klinik 1 und dem Institut für Pathologie des Universitätsklinikums Dresden für die erfolgreiche Zusammenarbeit in den vergangenen Jahren.

Mein ganz besonderer Dank gilt meiner Familie und meinen Freunden, die mich vom ersten Tag des Studiums bis heute unterstützt und begleitet haben. Insbesondere möchte ich mich bei meinem Bruder Andre bedanken.

Erklärung entsprechend §5.5 der Promotionsordnung

Hiermit versichere ich, dass ich die vorliegende Arbeit ohne unzulässige Hilfe Dritter und ohne Benutzung anderer als der angegebenen Hilfsmittel angefertigt habe; die aus fremden Quellen direkt oder indirekt übernommenen Gedanken sind als solche kenntlich gemacht. Die Arbeit wurde bisher weder im Inland noch im Ausland in gleicher oder ähnlicher Form einer anderen Prüfungsbehörde vorgelegt.
Die Dissertation wurde im Zeitraum vom 01.12.2016 bis 30.11.2021 verfasst und von PD Dr. Daniel E. Stange, Klinik und Poliklinik für Viszeral-, Thorax- und Gefäßchirurgie am Universitätsklinikum Carl Gustav Carus Dresden, betreut.

Meine Person betreffend erkläre ich hiermit, dass keine früheren erfolglosen Promotionsverfahren stattgefunden haben. Ich erkenne die Promotionsordnung der Fakultät Biologie, Technische Universität Dresden an.
Ich erkenne die Promotionsordnung der Fakultät für Mathematik und Naturwissenschaften, Technische Universität Dresden an.

_____

Datum, Unterschrift